

## INFORMATION TO USERS

This manuscript has been reproduced from the microfilm master. UMI films the text directly from the original or copy submitted. Thus, some thesis and dissertation copies are in typewriter face, while others may be from any type of computer printer.

**The quality of this reproduction is dependent upon the quality of the copy submitted.** Broken or indistinct print, colored or poor quality illustrations and photographs, print bleedthrough, substandard margins, and improper alignment can adversely affect reproduction.

In the unlikely event that the author did not send UMI a complete manuscript and there are missing pages, these will be noted. Also, if unauthorized copyright material had to be removed, a note will indicate the deletion.

Oversize materials (e.g., maps, drawings, charts) are reproduced by sectioning the original, beginning at the upper left-hand corner and continuing from left to right in equal sections with small overlaps.

Photographs included in the original manuscript have been reproduced xerographically in this copy. Higher quality 6" x 9" black and white photographic prints are available for any photographs or illustrations appearing in this copy for an additional charge. Contact UMI directly to order.

Bell & Howell Information and Learning  
300 North Zeeb Road, Ann Arbor, MI 48106-1346 USA  
800-521-0600

UMI<sup>®</sup>



# SYSTEM IDENTIFICATION, ADAPTIVE CONTROL AND FORMATION DRIVING OF FARM TRACTORS

A DISSERTATION  
SUBMITTED TO THE DEPARTMENT OF AERONAUTICS AND  
ASTRONAUTICS  
AND THE COMMITTEE ON GRADUATE STUDIES  
OF STANFORD UNIVERSITY  
IN PARTIAL FULFILLMENT OF THE REQUIREMENTS  
FOR THE DEGREE OF  
DOCTOR OF PHILOSOPHY

Andrew Karl Wilhelm Rekow

March 2001

UMI Number: 3002036

UMI<sup>®</sup>

---

UMI Microform 3002036

Copyright 2001 by Bell & Howell Information and Learning Company.

All rights reserved. This microform edition is protected against  
unauthorized copying under Title 17, United States Code.

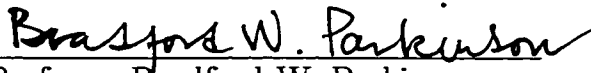
---

Bell & Howell Information and Learning Company  
300 North Zeeb Road  
P.O. Box 1346  
Ann Arbor, MI 48106-1346

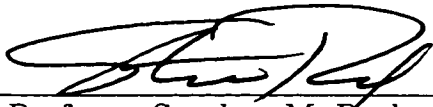
© Copyright 2001 by Andrew Karl Wilhelm Rekow

All Rights Reserved

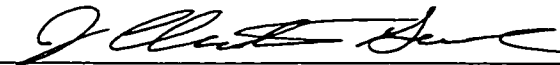
I certify that I have read this thesis and that in my opinion it is fully adequate, in scope and in quality, as a dissertation for the degree of Doctor of Philosophy.

  
\_\_\_\_\_  
Professor Bradford W. Parkinson  
(Principal Advisor)

I certify that I have read this thesis and that in my opinion it is fully adequate, in scope and in quality, as a dissertation for the degree of Doctor of Philosophy.

  
\_\_\_\_\_  
Professor Stephen M. Rock

I certify that I have read this thesis and that in my opinion it is fully adequate, in scope and in quality, as a dissertation for the degree of Doctor of Philosophy.

  
\_\_\_\_\_  
Professor Christian Gerdes

Approved for the University Committee on Graduate  
Studies:

  
\_\_\_\_\_  
Dean of Graduate Studies



# Abstract

Great increases in agricultural productivity and profitability can be gained by increasing the navigational control accuracy of a farm tractor. To maximize accuracy in the presence of environmental uncertainties, a novel technique for on-line parameter identification has been developed. This method combines the Extended Kalman Filter (EKF) and the Least Mean Square (LMS) algorithms and is used to identify key parameters which describe the dynamics of a farm tractor. This algorithms provides a 15:1 improvement in computational efficiency over the traditional EKF, while offering comparable convergence rates and noise rejection properties. Experimental data on a full-sized John Deere tractor shows a 25 percent improvement in lateral accuracy when using the adaptive controller versus a fixed controller over identical trajectories.

In addition to parameter identification, farmers require formation driving capability for routine operations. Multiple farm vehicles work cooperatively together to accomplish a common goal. Several formation driving algorithms were developed for these varying requirements. An experimental implementation of a fully autonomous farm vehicle following a human operated lead vehicle demonstrated an accuracy of 10 centimeters in the in-track direction and 10 centimeters in the cross track direction.





# Dedication

To my wife and her infinite patience.



# Acknowledgments

No project of this size is ever accomplished alone. There were many, many people who contributed in both technical and less tangible capacities. I owe special gratitude to my advisor, Professor Brad Parkinson, for his guidance, leadership and especially for his enthusiasm and backing for the GPS tractor project.

I also owe a great deal of thanks to my colleagues in the project. Dr. Mike O'Connor for his contagious optimism and Dr. Tom Bell for his unbelievable problem solving abilities. Also, to Dave Bevely for his real-world practicality and experience. I certainly could not have completed this work without the significant contributions made by each of these three outstanding people.

Special thanks also go to Gabe Elkaim for all the ideas that were bounced over the cubicle walls. Not only is Gabe a great technical warehouse, he is also a good friend.

A great deal of credit goes to the folks at Deere and Company. A special thanks goes to Bob Mayfield for his enthusiasm and willingness to work with the "Tractor Boys." His vision for the future of agriculture has been a great shaping factor in the work I've done.

The largest round of thanks goes out to my family. For my parents, Marlin and Dianne for their constant belief in my abilities and convincing me that anything, even

this, is possible. Lastly, to my wife, Dena, for her patience, love, support and her willingness to put our lives on hold while I pursued my education.

# Contents

|   |            |
|---|------------|
| <b>Abstract</b>                                       | <b>v</b>   |
| <b>Dedication</b>                                     | <b>vii</b> |
| <b>Acknowledgments</b>                                | <b>ix</b>  |
| <br>  |            |
| <b>I System Identification and Adaptive Control</b>   | <b>1</b>   |
| <br>  |            |
| <b>1 Introduction</b>                                 | <b>3</b>   |
| 1.1 GPS Overview . . . . .                            | 4          |
| 1.1.1 Differential GPS . . . . .                      | 4          |
| 1.2 The Autofarming Concept . . . . .                 | 9          |
| 1.2.1 Vehicle Navigation Hardware . . . . .           | 10         |
| 1.2.2 Previous Work in Automatic Guidance . . . . .   | 12         |
| 1.2.3 Accuracy Requirements for Autofarming . . . . . | 14         |
| 1.3 Problem Statement . . . . .                       | 17         |
| 1.4 Major Contributions . . . . .                     | 20         |
| <br>  |            |
| <b>2 Vehicle Modeling</b>                             | <b>23</b>  |

|          |   |           |
|----------|---|-----------|
| 2.1      | Steering Actuator Model . . . . .                                       | 23        |
| 2.2      | Vehicle Steering Dynamics Model . . . . .                               | 26        |
| 2.3      | Vehicle Longitudinal Dynamics Model . . . . .                           | 30        |
| 2.4      | Full Vehicle Estimation Model . . . . .                                 | 32        |
| 2.5      | Variations in the O'Connor Parameters . . . . .                         | 33        |
| 2.5.1    | $P_2$ . . . . .   | 34        |
| 2.5.2    | $P_3$ . . . . .   | 34        |
| 2.5.3    | $P_4$ . . . . .   | 35        |
| 2.5.4    | $P_5$ . . . . .   | 35        |
| 2.6      | Expected Variation in the Parameters . . . . .                          | 36        |
| 2.6.1    | Forward Speed, $V_x$ . . . . .  | 36        |
| 2.6.2    | Vehicle Leverarms, $l_1$ , $l_2$ and $c$ . . . . .                      | 37        |
| 2.6.3    | Tire Cornering Stiffnesses, $C_{\alpha_f}$ and $C_{\alpha_r}$ . . . . . | 38        |
| 2.6.4    | Moment of Inertia, $I_z$ . . . . .                                      | 38        |
| 2.6.5    | O'Connor Parameters Under Varying Conditions . . . . .                  | 38        |
| 2.6.6    | Simulated Performance With Mismodeled O'Connor Parameters               | 39        |
| <b>3</b> | <b>Real Time Parameter Identification Methods</b>                       | <b>43</b> |
| 3.1      | The Philosophy of Parameter Identification . . . . .                    | 44        |
| 3.2      | The LMS Algorithm . . . . .   | 45        |
| 3.2.1    | Model Updating . . . . .  | 46        |
| 3.2.2    | Convergence of the LMS algorithm . . . . .                              | 48        |
| 3.3      | The EKF Algorithm . . . . .   | 51        |
| 3.4      | The Keller Method . . . . .   | 56        |
| 3.5      | The LMS/EKF method . . . . .  | 59        |

|           |   |            |
|-----------|---|------------|
| 3.5.1     | Practical Computational Advantages of the LMS/EKF algorithm | 61         |
| 3.5.2     | A Simple LMS/EKF Example . . . . .                          | 62         |
| <b>4</b>  | <b>Vehicle Parameter Identification Methods</b>             | <b>67</b>  |
| 4.1       | Steering Actuator Identification . . . . .                  | 68         |
| 4.1.1     | Actuator Parameter Gradient Estimation . . . . .            | 73         |
| 4.1.2     | Actuator Model Stability . . . . .                          | 74         |
| 4.2       | Vehicle Steering Dynamics Identification . . . . .          | 77         |
| 4.2.1     | O'Connor Parameter Identification . . . . .                 | 77         |
| 4.2.2     | Stability Of Parameters . . . . .                           | 84         |
| 4.3       | Vehicle Longitudinal Dynamics Identification . . . . .      | 88         |
| 4.3.1     | Longitudinal Parameter Identification . . . . .             | 88         |
| 4.3.2     | Longitudinal Parameter stability . . . . .                  | 90         |
| 4.4       | Vehicle Parameter Identifiability . . . . .                 | 92         |
| 4.5       | Parameter Identification Computation . . . . .              | 95         |
| 4.6       | Parameter Identification With Realistic Paths . . . . .     | 97         |
| <b>5</b>  | <b>Simulation and Field Tests</b>                           | <b>103</b> |
| 5.1       | Simulation . . . . .  | 103        |
| 5.1.1     | Actuator Identification . . . . .                           | 103        |
| 5.1.2     | Tractor Identification . . . . .                            | 106        |
| 5.2       | Experimental Results . . . . .                              | 110        |
| <b>II</b> | <b>Formation Driving</b>                                    | <b>117</b> |
| <b>6</b>  | <b>Introduction</b>   | <b>119</b> |



|          |   |            |
|----------|---|------------|
| 6.1      | Classes of Similar Problems . . . . .                       | 119        |
| 6.2      | Previous Work in Formation Driving . . . . .                | 121        |
| 6.3      | Problem Statement . . . . .                                 | 123        |
| <b>7</b> | <b>Formation Driving Algorithms</b>                         | <b>127</b> |
| 7.1      | Dynamic Models . . . . .                                    | 127        |
| 7.1.1    | Estimator Model . . . . .                                   | 128        |
| 7.1.2    | Regulator Model . . . . .                                   | 129        |
| 7.1.3    | Sensor Network and Communications . . . . .                 | 130        |
| 7.2      | Formation Lateral Position Regulation . . . . .             | 132        |
| 7.2.1    | The Carrot on the Stick . . . . .                           | 132        |
| 7.2.2    | The Virtual Tether and Line, “Tractor on a Stick” . . . . . | 134        |
| 7.2.3    | The Cookie Crumb Trail . . . . .                            | 135        |
| 7.2.4    | Lateral Formation Control Along Arcs . . . . .              | 136        |
| 7.3      | Formation Longitudinal Position Regulation . . . . .        | 139        |
| 7.4      | Formation Driving Trajectory Types . . . . .                | 141        |
| <b>8</b> | <b>Collision Avoidance</b>                                  | <b>145</b> |
| 8.1      | Fuzzy Logic . . . . .                                       | 145        |
| 8.1.1    | Fuzzy Membership Functions . . . . .                        | 147        |
| 8.1.2    | Fuzzy Rules . . . . .                                       | 149        |
| 8.2      | The No Fly Zone . . . . .                                   | 149        |
| 8.3      | The Fuzzy Box Controller . . . . .                          | 150        |
| 8.4      | The Dynamic Fuzzy Box Controller . . . . .                  | 154        |

|           |   |            |
|-----------|---|------------|
| <b>9</b>  | <b>Formation Driving Experimental Results</b> | <b>159</b> |
| 9.1       | Position Regulation Performance . . . . .     | 160        |
| 9.2       | Collision Avoidance Simulations . . . . .     | 165        |
| <b>10</b> | <b>Conclusions</b>                            | <b>169</b> |
| 10.1      | Conclusions . . . . .                         | 169        |
| 10.2      | Future Work . . . . .                         | 172        |
| 10.3      | Closing . . . . .                             | 175        |
| <b>A</b>  | <b>Vehicle Configuration</b>                  | <b>177</b> |
| A.1       | John Deere Model 7800 . . . . .               | 177        |
| A.2       | John Deere Model 8400 . . . . .               | 178        |
| A.3       | Sensor and Actuator Hardware . . . . .        | 180        |
| A.4       | Formation Driving Master Vehicle . . . . .    | 183        |

# List of Tables

|     |  |     |
|-----|--|-----|
| 1.1 | Standard GPS Error Model . . . . .   | 5   |
| 2.1 | Expected Physical Parameters for John Deere 8400 Tractor . . . . .                                   | 37  |
| 2.2 | Parameter Variations Under Several Operational Condition . . . . .                                   | 39  |
| 2.3 | Lateral Performance with Mismodeled O'Connor Parameters . . . . .                                    | 41  |
| 3.1 | Damping in the Eigendirections of R for the Weight Vector . . . . .                                  | 51  |
| 3.2 | The dc2d Algorithm . . . . .   | 58  |
| 4.1 | Primary Parameter Influences on Measurement Errors . . . . .   | 81  |
| 4.2 | Floating Point Operations Count for PP-EKF and LMS/EKF Algorithms                                    | 96  |
| 5.1 | Lateral Error Comparison On Curved Trajectory . . . . .  | 112 |
| 6.1 | Automated Highway System History . . . . .   | 121 |
| 8.1 | The Fuzzy Inference System . . . . .   | 150 |
| 8.2 | Fuzzy Controller Conflict Resolution Commands for Desired Point on<br>Right side of Master . . . . . | 153 |
| 8.3 | Dynamic Box Dimension Coefficients . . . . .   | 155 |

# List of Figures

|     |  |    |
|-----|--|----|
| 1.1 | Vehicle Navigation System Configuration . . . . .  | 11 |
| 1.2 | Cultivator Clearance Dimensions . . . . .  | 14 |
| 1.3 | Probability of Cultivator Incursions . . . . .   | 16 |
| 2.1 | Steering Valve Calibration Data for the 8400 . . . . .   | 24 |
| 2.2 | Deadzone Model Signal Flow . . . . .   | 25 |
| 2.3 | Vehicle State Definitions . . . . .  | 27 |
| 2.4 | Tire Cornering Stiffness . . . . .   | 28 |
| 2.5 | Tractor Dimension Definition . . . . .   | 29 |
| 2.6 | On Road Gear speed Calibration . . . . .   | 31 |
| 2.7 | Lateral Performace with Mismodeled O'Connor Parameters . . . . .   | 42 |
| 3.1 | Spring mass system used in LMS/EKF example . . . . .   | 63 |
| 3.2 | Learning Curves for the Spring Mass System Example . . . . .   | 65 |
| 4.1 | Steering Actuator . . . . .  | 68 |
| 4.2 | Deadzone Parameter Definition . . . . .  | 70 |
| 4.3 | Parameter Identification Cost Trade off with $p_2 = -0.2$ , $p_3 = 3.5$ ,<br>$p_4 = 1.8$ and $p_5 = 1.7$ . . . . . | 94 |
| 4.4 | Parameter Identification Cost Trade off with Yaw Rate Measurement  | 96 |
| 4.5 | Signal to noise ratio for tractor yaw rate, $\Omega$ . . . . .   | 98 |

|      |   |     |
|------|---|-----|
| 4.6  | Signal to noise ratio for tractor steer angle, $\delta$ . . . . .   | 99  |
| 4.7  | Signal to noise ratio for tractor slew rate, $\omega$ . . . . .   | 100 |
| 5.1  | Truth system for Actuator Identification Simulation . . . . .   | 104 |
| 5.2  | Deadband Learning curves for Actuator Identification Simulation . .   | 104 |
| 5.3  | Dynamics Estimate Convergence for Actuator Identification Simulation  | 105 |
| 5.4  | Deadband Learning curves for Actuator Identification Simulation with<br>Poor Initial Guess . . . . .                                    | 106 |
| 5.5  | Dynamics Estimate Convergence for Actuator Identification Simula-<br>tion with Poor Initial Guess . . . . .                             | 107 |
| 5.6  | Short Term Comparison of EKF and LMS/EKF parameter identifica-<br>tion performance on simulated tractor under noise free conditions . . | 108 |
| 5.7  | Long Term Comparison of EKF and LMS/EKF parameter identifica-<br>tion performance on simulated tractor under noise free conditions . .  | 108 |
| 5.8  | Short Term Comparison of EKF and LMS/EKF parameter identifica-<br>tion performance on simulated tractor with sensor noise . . . . .     | 109 |
| 5.9  | Long Term Comparison of EKF and LMS/EKF parameter identifica-<br>tion performance on simulated tractor with sensor noise . . . . .      | 109 |
| 5.10 | Experimental Vehicle with 6 Row Cultivator Attached . . . . .   | 111 |
| 5.11 | Curved Path System Identification Trajectory . . . . .  | 111 |
| 5.12 | Curved Path System Identification Performance . . . . .   | 112 |
| 5.13 | Figure 8 Sysid Trajectory used in Parameter Estimation . . . . .  | 114 |
| 5.14 | Learning Curves from Data of 5 Nov 1999 . . . . .   | 115 |
| 6.1  | A Combine Unloading Grain Into a Grain Cart Pulled by a Tractor in<br>South Texas . . . . .   | 124 |

|     |   |     |
|-----|---|-----|
| 6.2 | Cooperative Row-Skipping Trajectories . . . . .   | 125 |
| 6.3 | A Pair of Cotton Pickers Cooperating to Harvest Cotton in California's<br>Central Valley . . . . .                    | 125 |
| 7.1 | Radio Modem Communication Configuration . . . . .   | 131 |
| 7.2 | Carrot on the Stick Geometry . . . . .  | 133 |
| 7.3 | Geometry for Arc Formation Driving Reference State Generation . .   | 137 |
| 7.4 | A Typical Trajectory Set to Transfer Grain from a Combine to a Grain<br>Truck Using Formation Algorithms . . . . .    | 143 |
| 8.1 | Fuzzy Kanizsa Square . . . . .  | 146 |
| 8.2 | Fuzzy Truth Example . . . . .   | 148 |
| 8.3 | Fuzzy Membership Function Examples . . . . .  | 148 |
| 8.4 | Fixed Box No Fly Zone Dimensions . . . . .  | 151 |
| 8.5 | Fuzzy and Linear Controller Authority versus Collision Imminence . .  | 156 |
| 8.6 | Dynamic Box No Fly Zone Dimensions . . . . .  | 156 |
| 8.7 | Dynamic Box Dimensions . . . . .  | 157 |
| 9.1 | Trajectories driven with slave vehicle maintaining position 5 meters to<br>the right of the master vehicle . . . . .  | 160 |
| 9.2 | Formation position errors for desired position of five meters to the right<br>of the master vehicle . . . . .         | 161 |
| 9.3 | Trajectories driven with slave vehicle maintaining position ten meters<br>to the rear of the master vehicle . . . . . | 162 |
| 9.4 | Formation position errors for desired position of ten meters to the rear<br>of the master vehicle . . . . .           | 163 |

|     |   |     |
|-----|---|-----|
| 9.5 | How Small Heading Errors Translate Into Large Linear Errors with<br>Large Leverarms . . . . . | 164 |
| 9.6 | Anticollision simulation trajectories . . . . .   | 166 |
| A.1 | John Deere Model 7800 Test Tractor . . . . .  | 178 |
| A.2 | John Deere Model 8400 Test Tractor . . . . .  | 179 |
| A.3 | John Deere Model 8400 Test Tractor Antenna Configuration . . . . .                            | 180 |
| A.4 | John Deere Model 8400 Test Tractor Steer Angle Sensor . . . . .                               | 181 |
| A.5 | John Deere Model 8400 Test Tractor Guidance Computer . . . . .                                | 182 |
| A.6 | Formation Driving Master Vehicle Test Tractor . . . . .                                       | 183 |

**Part I**

**System Identification and Adaptive  
Control**





# CHAPTER 1

## Introduction

As a student in the department of Aeronautics and Astronautics at Stanford University I am often asked the question “What’s a rocket scientist doing working on farm tractors?” The answer is that my chosen field has much to offer today’s average farmer. The days of the ox jaw scythe are long gone. We are entering the age of the automated farm. Today’s farmers are employing such technology as radar crop monitoring [MHQK98] and optical robotic weed control technology [LSG99] in an effort to minimize operating costs and maximize his profitability. It is therefore of little surprise that there exists an intense interest in the availability of a highly accurate method to control farm tractors. There has also been an eager acceptance of the Global Positioning System for navigation by the agricultural community. This is due to its’ ease of use, flexibility, potential for extremely high accuracy, reliability and profitability.

The work presented in this dissertation is an extension of previous work that combines the previous two ideas and moves towards a practical system that enables extreme precision guidance for a farm tractor. It attempts to maximize the accuracy achieved by accounting for the variable conditions encountered by a farm tractor.

## 1.1 GPS Overview

The Global Positioning System (GPS) is simply the latest, and most accurate in a long line of radio navigation methods.[PJ96], [KF97], [For91] The system consists nominally of 24 orbiting satellites. Each satellite contains an extremely accurate atomic clock, continually broadcasting radio transmissions towards the surface of the earth. The data signals transmitted consist of information reflecting from where the signal was transmitted and also the exact time of transmission for each signal. A user with the appropriate equipment and know-how can measure the time of arrival for each signal and calculate a distance to each satellite. From these range measurements, the user can quickly triangulate their position. This particular practice is known as “Stand Alone GPS” in reference to the fact that the only user equipment required is a single GPS receiver. This is the basic service for which GPS was designed and is still its most common use.

### 1.1.1 Differential GPS

The accuracy of Stand Alone GPS ranges from on the order of 10 meters to more than 100 meters.<sup>1</sup> This accuracy is certainly sufficient for general navigational uses such as in general aircraft navigation or a soldier in the field. It is insufficient for many other applications such as autonomous control of land vehicles or low visibility

---

<sup>1</sup>The U.S.D.O.D previously imposed an intentional error, referred to as Selective Availability (SA), on the signal available to the general public. This was done in an attempt to discourage the use of GPS as a weapon by enemies of the United States. The net effect of SA was a degradation of accuracy to approximately 100 meters for non-authorized users. The U.S. military and its allies have always had access to the heavily encrypted signal which yields accuracies on the order of 10 meters. Selective availability was disabled on May 1, 2000 yielding 10 meter performance for civil as well as military users.

Table reproduced from [Par96]

| Error Source                              | 1 $\sigma$ Error, m (no SA) |        |       | 1 $\sigma$ Error, m (SA on) |        |       |
|---|-----------------------------|--------|-------|-----------------------------|--------|-------|
|   | Bias                        | Random | Total | Bias                        | Random | Total |
| Ephemeris data                            | 2.1                         | 0.0    | 2.1   | 2.1                         | 0.0    | 2.1   |
| Satellite Clock                           | 2.0                         | 0.7    | 2.1   | 20.0                        | 0.7    | 20.0  |
| Ionosphere                                | 4.0                         | 0.5    | 4.0   | 4.0                         | 0.5    | 4.0   |
| Troposphere                               | 0.5                         | 0.5    | 0.7   | 0.5                         | 0.5    | 0.7   |
| Multipath                                 | 1.0                         | 1.0    | 1.4   | 1.0                         | 1.0    | 1.4   |
| Receiver Measurement                      | 0.5                         | 0.2    | 0.5   | 0.5                         | 0.2    | 0.5   |
| User Equivalent range error               | 5.1                         | 1.4    | 5.3   | 20.5                        | 1.4    | 20.6  |
| Vertical 1 $\sigma$ errors - VDOP = 2.5   |                             |        | 12.8  |                             |        |       |
| Horizontal 1 $\sigma$ errors - HDOP = 2.0 |                             |        | 10.2  |                             |        |       |

Table 1.1: Standard GPS Error Model

aircraft landings. As a result, various methods have been developed to improve this accuracy.

Table 1.1 outlines the major contributors of errors to a position solution. Other than the intentional degradation, the largest contributors to civil accuracy are the uncertainty in satellite position (in both time and space) and atmospheric perturbations. For two receivers located near one another, the majority of these errors are common to both receivers. Both receivers measure the exact same Satellite clock errors and nearly identical Ephemeris, Ionospheric and Tropospheric errors. When one works the problem backwards, in other words, one takes measurements from a known location, the cumulative effect of all these errors can be directly measured. Once these errors are known for a specific location they can be applied and subtracted out from the measurements taken at another nearby location.

### **Code Phase Differential GPS**

A common method of differential GPS is referred to as code phase differential GPS (DGPS.) Part of the signal coming down from the satellites is a digital code. In code phase GPS the time of arrival of a particular bit-front is measured utilizing two independent receivers. One of these receivers is at a known location and is referred to as the base or reference station. This base station subtracts the measured range to the satellite from the expectation for each measurement and relays this error to the second, mobile receiver. The second receiver, at the unknown location then applies these corrections to it's own measurements and thus obtains a significantly more accurate position measurement than it could alone. In doing this, common mode errors such as ephemeris and atmospheric errors can be subtracted out, leaving predominately receiver noise.

Due to fundamental limitations in this technique, the accuracy of this method is approximately 1 to 2 meters. These limits stem from the receivers ability to track the incoming signal to higher precision as well as signal noise (especially multipath) corrupting the measurements.

A significant disadvantage to many applications utilizing this method is the need for a second receiver to provide reference data. This requirement increases both the cost and complexity for any system. In many applications, however, the increase in accuracy more than offsets the increased cost of a reference station.

### **Wide Area Differential GPS**

The U.S. Federal Aviation Administration is currently developing the Wide Area Augmentation System. (WAAS)[EWP<sup>+</sup>96] This system is a direct assault on the

requirement of having a physical, local reference station. WAAS consists of a large number of federally operated reference stations spread across North America. These stations monitor the transmissions of the GPS signal and feed data into a central location. At the command center, this information is rapidly processed and the corrections are curve fit to cover the entire nation. This information will then be relayed through several geosynchronously orbiting satellites back down to the users. This method provides a virtual reference station everywhere within the coverage area. This method is expected to be operational by the year 2002 providing roughly equal accuracy as local code phase differential methods.

### **Carrier Phase Differential GPS**

The highest accuracy GPS method available today is Carrier Phase Differential GPS. [PE96] Rather than measuring the time of arrival of the bit front from the satellite, this method measures the difference in phase in the carrier signal at a given instant between the reference station and the user. This measurement can be made to be much more accurate than can the time of arrival measurement from a bit front. This increase in accuracy allows for position accuracy approaching 2 to 3 centimeters.

The difficulty associated with this particular technique is that the initial phase measurement can only be measured from 0 to 360 degrees. In all likelihood there is some integer number of carrier signal wavelengths between the user and the reference station which must somehow be determined in order to make the required measurement. This dilemma is referred to as the integer ambiguity. Several methods exist for determining these integers ranging from initializing at a known location, a brute force search of all the possible integer combinations to reducing the search space by

widelaning or allowing enough time for sufficient satellite geometry change to estimate the integers.

All of these methods are merely for determining the initialization integers. Once these have been obtained they can be stored and the relative phase of the two receivers can be tracked past 0 and 360 degrees. Subsequent measurements then enjoy the highly accurate precision carrier wave differential GPS offers. As new satellites come into view, the integer ambiguity can be immediately resolved utilizing the precise position measurement.

This method also suffers from the requirement of an independent reference station. To the author's knowledge no plans currently exist for a carrier phase equivalent to WAAS. However, with the rapid advancement of GPS technology currently enjoyed, this requirement becomes a small price to pay for such high accuracy.

The measurement that reflects the 2 cm accuracy is the relative vector from the reference station to the roving antenna. The absolute position of the roving antenna is no more precise than that of the reference station. If, however, three or more antennas are mounted to a rigid body, the relative positions of all three antennas can be very accurately measured utilizing this technique. With the relative positions of three or more points on a rigid body known, it is a simple matter of geometry to calculate the three dimensional orientation (roll, pitch and yaw) of that body. CDGPS attitude systems can also quickly initialize integers thanks to the fixed and known baselines between antennas. [Coh92], [BIMG98]

## 1.2 The Autofarming Concept

The term “Autofarming” is a general term used to describe a class of techniques that combine GPS and agricultural vehicles. These applications include things such as

- **Driver Guidance Assistance:** This is where the position information is displayed to the operator who then guides the vehicle. No attempt to drive the vehicle automatically is made.
- **Automatic Row Guidance:** In this application straight rows are automatically driven. The operator then takes over at the end of each row and performs the U-turns and row approach.
- **Automatic Curve Guidance:** This is identical to Automatic Row Guidance with an extension to curved paths.
- **Automatic Farming** where the farmer is still in the vehicle but the trajectory planning and steering and vehicle operation is handled automatically. The operator functions mainly in a supervisory role to assure safety.
- **Autonomous Farming** where the vehicle is performing tasks without direct human management.

Each of these requires an accurate measurement of vehicle position. GPS is able to provide this measurement. Each of these also requires varying degrees of increased safety. The Driver Guidance Assistance needs only a minor increase to safety over unassisted operation in the form of making sure the operator keeps his eye on the field and not the display. Automatic Row Guidance and Farming require a higher level of



safety awareness. One must be cautious for things such as the operator's falling asleep or misunderstanding the operational mode of the controller. This problem is most similar to an aircraft autopilot flying itself into the ground because the pilot thought the autopilot was in altitude hold mode rather than rate of descent hold mode.

Autonomous Farming requires the strictest safety procedures. The vehicle must be at all times aware of its position and the position of obstacles around it. It must also be able to identify what constitutes a dangerous situation and react appropriately to minimize that danger.

### 1.2.1 Vehicle Navigation Hardware

The basic component of the vehicle navigation system that will be presented in following chapters consisted of the GPS receiver. In the work revisited in this thesis this receiver consisted of a carrier phase differential receiver with a ground based reference receiver. This positioning system was capable of making measurements to within 2 cm ( $1\sigma$ ). This position measurement reflected the position of one of the four antennas mounted on the roof of the cab. The antennas were mounted on the roof of the cab to achieve good visibility to the maximum number of satellites.

In a realistic setting it is not the roof of the cab that is to be controlled but rather some other point, a projection straight down from the center of the rear axle for instance. Also, because the antenna was mounted so high (roughly 3m above the ground) very small roll and pitch changes translated into measurable position changes at the top of the cab when the position of the vehicle itself (measured at the tires) had not changed significantly. These two factors dictated that some form of attitude measurement system be utilized. With the measurement of roll, pitch

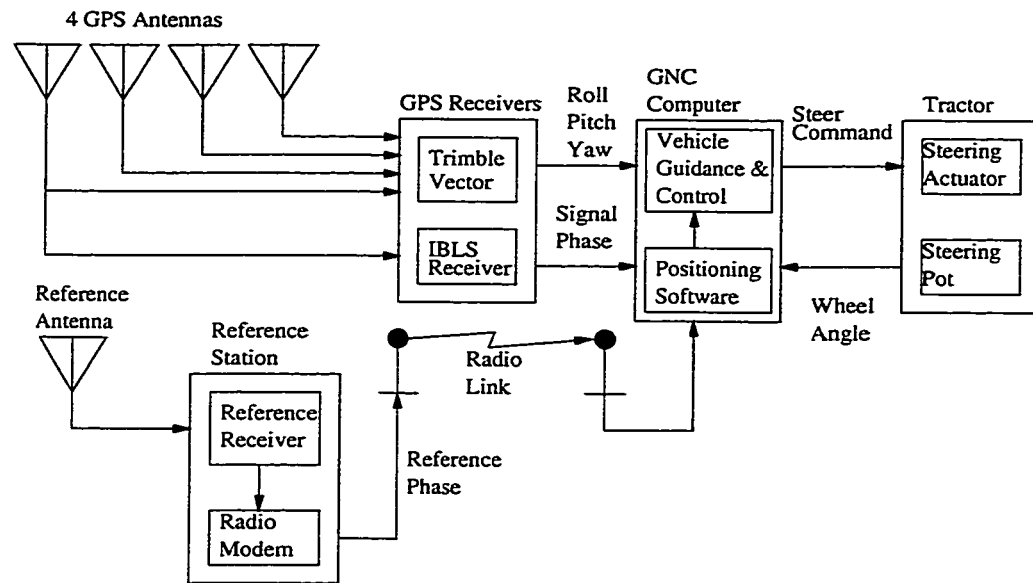


Figure 1.1: Vehicle Navigation System Configuration

and yaw a projection from the antenna position measurement to a measurement of a control point position could be made. In the experimental vehicles utilized in this work this measurement was made also via GPS. A Trimble Vector system tied to the four antennas mounted on the roof of the cab provided attitude measurements.

Because there is such a lag between the input (steer angle slew rate) and the output (vehicle position) it was convenient, from a control system's point of view, to add a measurement of the steer angle. This allowed for much more accurate vehicle state estimation and consequently much tighter control. In the experimental vehicles, this measurement was achieved utilizing a linear potentiometer fixed between the tractor frame and the steering joint.

A significant fraction of farm tractors are tracked vehicles rather than wheeled vehicles. These vehicles steer by developing a speed differential between the left and

the right tracks. Rather than commanding a steer angle slew rate to generate a steer angle which in turn generates a yaw rate, a differential speed on the treads is directly commanded, forgoing the need for a steer angle measurement.

### 1.2.2 Previous Work in Automatic Guidance

To date, most research in Autofarming has focused on the navigation problem. This problem is expressed as two very simple questions:

1. Where am I? (The positioning problem)

and

2. Now that I know where I am, how do I get to where I need to be?

(The control problem)

Prior to the appearance of GPS, most work attempted to emulate how a human operator did his job and focused on optical systems for positioning. Various techniques were tried and implemented using pattern recognition. [T<sup>+</sup>85], [RS87]. With the advent of a relatively low cost, zero drift position sensor in the guise of GPS, the focus has quickly changed to allow this new technology to assist in the problem. Several groups are concurrently working this type of research. Some notable projects include *Trimble Navigation* and their light bar. This bar takes differential GPS position and interfaces it to a light bar indicator mounted in the cab. This light bar displays the lateral error from the tractor's position and that of a preprogrammed set of rows. The operator attempts to steer so the left/right light remains centered much as a pilot flying a VOR tries to keep the needle centered. [WB98]

Australia's *Mailer Family and AgSystems Pty Ltd* use CDGPS for autonomously tracking straight rows. [Mai97], [Joh97], [Nas97] This product has resulted in a

commercial product known as the BEELINE Navigator. This system is an after-market add-on steering assist that has the capability of tracking a straight row to within 2 cm. The primary attitude sensor for the BEELINE Navigator is a six-axis inertial measurement unit. Unfortunately, the inertial system in this product tends to drift requiring periodic stops to reset the bias estimates.

Japan's Institute of Agricultural Machinery Department of the Bio-oriented technology Research Advancement Institution (IAM-BRAIN) have been developing and comparing different types of positioning and navigation systems. The researchers at IAM-BRAIN have been exploring the performance of GPS as compared to optical and magnetic systems. One system uses a combination of buried wires, lasers and optical tracking techniques to guide a tractor autonomously over the field. [N<sup>+</sup>97a], [N<sup>+</sup>97b]

Previous Work at Stanford University originated with Michael O'Connor's automatic golf cart. O'Connor developed the basic vehicle models and control algorithms used for the John Deere / Stanford tractor. In addition he showed that small variations in roll could induce a measurable position change in the antenna position and that these could provide potentially destabilizing disturbances unless accounted for with a leverarm correction. O'Connor also developed and implemented accurate row-tracking algorithms on flat terrain. [O'C97] Thomas Bell extended O'Connor's work by developing algorithms for arcs, spirals and ultimately arbitrary curves. He also developed algorithms to provide accurate control over sloped terrain and contours. [Bel99]

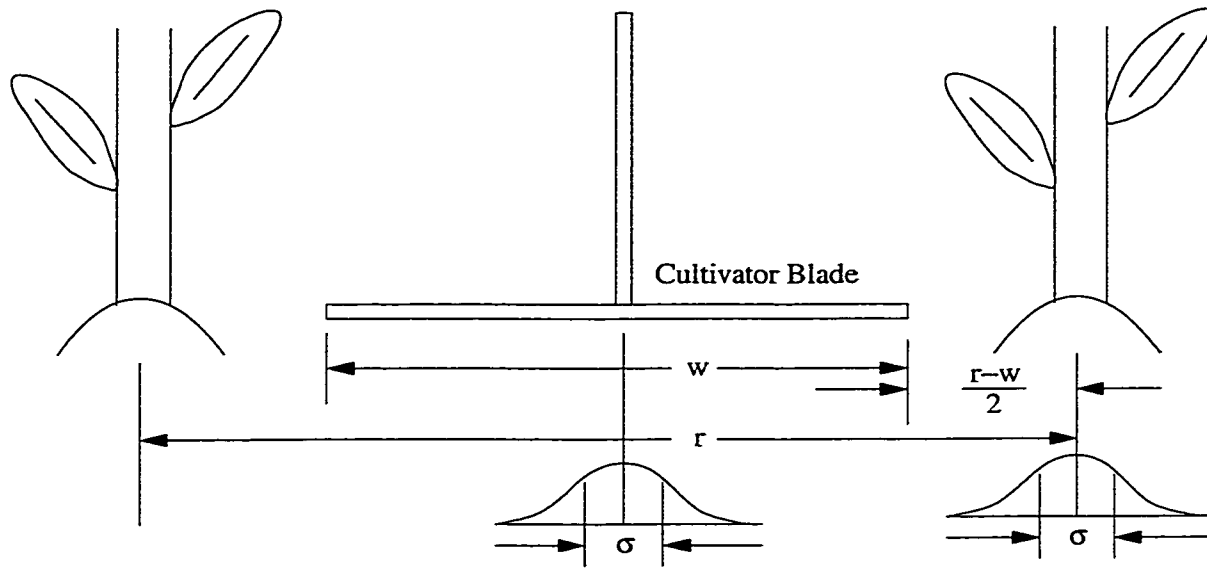


Figure 1.2: Cultivator Clearance Dimensions

### 1.2.3 Accuracy Requirements for Autofarming

The critical test of any autofarming system is cultivation. Mechanical cultivation consists of pulling a cutting blade through the soil between the rows of plants with the intention of cutting weeds out at the roots. With the high cost and ecologic impact of chemical cultivation, mechanical cultivation has been on the increase in recent years. For obvious reasons, mechanical cultivation is a more ecologically attractive process than chemical. Additionally, with the advent of autofarming systems, the requirement for highly skilled operators who can precisely guide the tractor through the rows without removing crop is being reduced. This reduction in operator overhead strengthens the case for mechanical cultivation. These arguments are only valid if the autofarming system is accurate enough that it does not periodically wander through rows of crop and reduce yield.

With mechanical cultivation, not only is the accuracy of the cultivation pass of importance, but so is the pass in which the seeds were planted. As shown in Figure 1.2 there is some inherent uncertainty in both the positions of the plants and of the cultivator. It could be argued that the two most accuracy critical operations, planting and cultivation, would be executed under automatic steering. Therefore, the standard deviation in the plant locations and cultivator locations should be approximately equal. It can also be assumed that at a single point in the field both these operations exhibit Gaussian error distributions and are uncorrelated. With these assumptions, the probability distribution for the spacing between the edge of the cultivator and the crop can be described by the equation

$$p(x) = \frac{1}{\sqrt{2\pi}} e^{-\frac{(x - \frac{r-w}{2})^2}{4\sigma^2}} \quad (1.1)$$

where

$\sigma$  is the standard deviation of a single pass,

$r$  is the row spacing and

$w$  is the cultivator blade width.

Equation (1.1) allows the calculation of the probability of cultivator incursions (PoCI.) The PoCI is simply the area of the probability curve which reflects an overlap of the cultivator and a plant. The total probability can be approximated to a great deal of accuracy by

$$\int_{-\infty}^0 p(x)dx + \int_{r-w}^{\infty} p(x)dx = 2 \int_{-\infty}^0 p(x)dx \quad (1.2)$$

Equation (1.2) was evaluated for 30 inch rows and three different sizes of cultivator

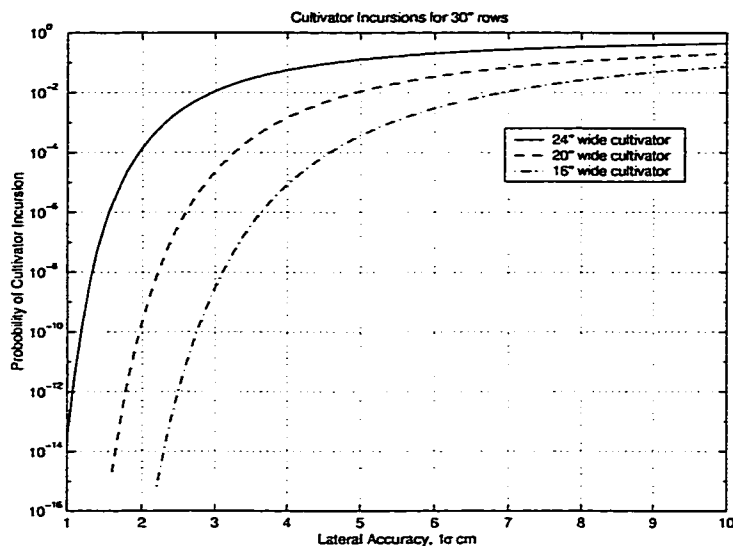


Figure 1.3: Probability of Cultivator Incursions

blades and displayed in figure 1.3. This plot illustrates the great benefits achieved by improving the lateral control from 2.5 cm to 1.5 cm. Though one centimeter may not appear to be a significant change in the location for a 30,000 pound machine, that one centimeter means the difference between a PoCI of 0.2% and one of 0.00003% with a 24 inch cultivator. On a  $\frac{1}{2}$  mile by  $\frac{1}{4}$  mile (80 acre) field, this translates into the difference between 7000 square feet of destroyed crop as opposed to just a single square foot. Under ideal conditions, 1.5 centimeter accuracy on vehicle control is certainly possible. With a smooth field, well modeled vehicle dynamics and tight control 1.5 centimeters is an excellent goal for accuracy.

## 1.3 Problem Statement

Agriculture is an industry that operates with high overhead and low margins. Any technology that could be introduced to improve efficiency can greatly assist in the reduction of cost and the increase in profitability in the production of food. One such technology may be the accurate guidance of tractors using GPS. If farmers could guide their tractors exactly over a designated spot year after year and without the need for good visibility it could open up other possibilities such as underground irrigation systems or around the clock operation.

A promising benefit of highly accurate control is the significant reduction of row overlap. The ability to put the edge of the implement exactly on the edge of the last row could save a significant amount of time, labor and fuel. By Agsystems' calculations, a single operation on a 182 Ha (450 acre) field requires effectively farming 204 Ha, an extra 12% when row overlap is not controlled. [Ano99] This translates into 2.5 extra hours in the field on every run and approximately \$4,400 (Australian) lost every year. This extra money is wasted on every operation and, over the course of a single season, accrues to a significant amount of money.

Recent work in automatic control of farm tractors [O'C97], [Bel99] has shown the feasibility of automatically steering of farm tractors. Other recent work has shown that these controllers are very sensitive to changing conditions. [RBBP99] The behavior of farm tractors is subject to many influences such as soil conditions, vehicle configuration, vehicle ballast, implement configuration and others. All these factors influence the vehicle dynamics in often inconvenient and unpredictable ways.

These changing conditions exhibit themselves as changes in the steering dynamics of the tractors. The lateral behavior of the tractor can vary quite significantly without



dramatic deterioration of closed loop performance during straight row operation. This is simply because the tractor is not moving in the lateral direction. However, when tracking curved paths, the energy in the lateral states greatly increases. The tractor must turn to track these trajectories and therefore the lateral behavior becomes more important. The more accurately these changes can be assessed, the more accurately the desired trajectory can be tracked.

In order to achieve optimal performance, the behavior of the vehicle must be well understood and well modeled by the control system. In an automotive setting, these dynamics can be predicted by careful analysis of vehicle mass, geometry, tires and configuration. For the most part the road conditions do not vary to the degree with which they do in a corn field<sup>2</sup>. These variations affect the behavior of the vehicle. A skilled driver can usually quickly and effectively adapt to these variations. Additionally the basic configuration of the tractor must often be changed in order to maximize the efficiency of the particular daily task. Such modifications include adding or removing dual rear tires, using differential lock or adding ballast. In addition to the operator introduced modifications, the soil properties in the field are changing almost daily. These changes greatly influence the way the tires interact with the soil and the handling of the vehicle. Any automatic steering system should, somehow, be able to adapt to the varying conditions encountered in a realistic setting. The vehicle control system must also be able to adapt to these changes either by pre-calibration or the ability to learn in the field. In an agricultural setting pre-calibration is not always possible or practical. With these needs and the accuracy requirements outlined in section 1.2.3 in mind, one is left with the need for a control system that can monitor

---

<sup>2</sup>All due respect goes to those of us who have spent a winter or more driving in the chillier regions of the world with roads covered by snow and ice

it's own performance and optimize itself for changing conditions.

There are two approaches to providing a controller able to adapt to variations in conditions. The first is an off-line identification and robust control approach.[EOBP96] This would be undesirable in a practical setting for two main reasons. Operational conditions can vary over time spans on the order of several minutes as the tractor moves from one region of the field to another. Furthermore, the time and complexity of performing calibration runs is not desirable in an operational setting. The farmer in the field is expecting a turn-key application and he will not tolerate taking an hour out of every morning to calibrate his tractor.

The second approach to responding to changes in operational conditions is to perform system identification in real time. During operation, the system monitors its own performance and adjusts itself to best fit the observations made. This allows the control system to calibrate itself during operation without direct user interaction. This was the approach adopted for this work.

To implement the real time identification, several important physical parameters were singled out for identification. This approach differs from many classical system identification algorithms which treat the identified system as a "Black Box" such as the maximum likelihood and observer/Kalman identification algorithms. A black box model is one in which signals come in one end and system responses come out on the other. What goes on internally is of secondary importance as long as the modeled output matches the experimental response. As a result, it is difficult to incorporate any a-priori knowledge into the design or extract any physical interpretation from the system. One can only define very basic system configurations such as the number of states or the number of inputs. The definition of what these states are or how they

interact cannot be defined. While this may be an attribute when little is known about the system itself, this was deemed a liability when work began on this project due to the relatively detailed knowledge of the basic structure of the vehicle dynamics. A black box model is also often more apt to fall prey to unmodeled, poorly modeled or ill-conditioned noise. In addition to this, these models often result in excessive numbers of unknowns that have little relation to a physical model. These factors influenced the author's decision to implement parameter identification over system identification.

## 1.4 Major Contributions

The emphasis of this research is to provide the foundation for controlling vehicles in and out of formation with high accuracy. Consequently, the work was divided into two areas: Parameter Identification/Adaptive Control and Formation Driving/Co-operative Control. An introduction to the formation driving problem will be outlined in chapter 6. In this research the emphasis has been on the specialized application of GPS guided farm tractors. Much of this work can quite easily be adapted to other wheeled vehicles or other systems. The major contributions developed are

- The development of a technique to identify a system with both dynamics and an input deadzone in real time. Originally this was developed in order to control the actuator fitted to the experimental vehicle. This algorithm however can immediately be applied to any other system that can be modeled with a similar structure as presented in section 2.1.

- The development of a technique to identify system parameters in real time without extending the system states in a Kalman filter to include those parameters. This technique was also further refined to the specialized case of a farm tractor with position, attitude and steer angle sensors. A general form of this method is presented in section 3.5. This algorithm provided a significant decrease in computation complexity when compared to a Physical Parameter - Extended Kalman Filter (PP-EKF) for the identification of the O'Connor parameters.
- The experimental verification and implementation of the LMS/EKF parameter identification algorithm.
- The experimental demonstration of the benefits of using an adaptive scheme over a fixed controller on a farm tractor.
- The determination of a cost / benefit relationship for identifying the O'Connor parameters. It is shown that the most difficult parameters to identify happen to be the least critical to identify the most precisely.
- The development of algorithms that allow formation driving and co-operative control of two or more farm tractors.
- The experimental verification of algorithms allowing formation driving of two farm tractors.
- The illustration of the ability to hold position to a master vehicle utilizing only position information from the master vehicle. Both lateral and longitudinal accuracy utilizing this method were shown to be approximately 10cm.

- The development of anti-collision algorithms that allow tighter formations than traditionally allowed by other methods. Traditional anti-collision algorithms were developed for aircraft applications where vehicles were never allowed to get near enough to each other that the relative orientation of the vehicle affects the boundaries. In an agricultural environment the vehicles may need to work in very close proximity to each other. As a result methods that took the relative headings of the vehicles into account were necessary.

## CHAPTER 2

# Vehicle Modeling

The general approach employed for modeling of the tractor in this dissertation was to break the entire system into smaller, more manageable pieces. The longitudinal dynamics (forward and reverse) were treated as decoupled from those in the lateral (left and right) directions. Similarly the steering valve was modeled as a separate sub-system of the overall steering dynamics.

### 2.1 Steering Actuator Model

Steering the experimental vehicle was done with a hydraulic actuator driving the wheel angle. This actuator consisted of a hydraulic valve opened and adjusted by a pair of push-pull solenoids. An input pulse width modulated voltage induced current flow through the solenoids and commanded the valve position which in turn resulted in a controlled flow to the steering cylinders. The resulting mapping from pulse width modulated signal to steering tire slew rate exhibited a substantial non-linearity. This non-linearity consisted of two parts both apparent in Figure 2.1. The first non-linearity exhibited was a saturation in the actuator limiting slew rate at

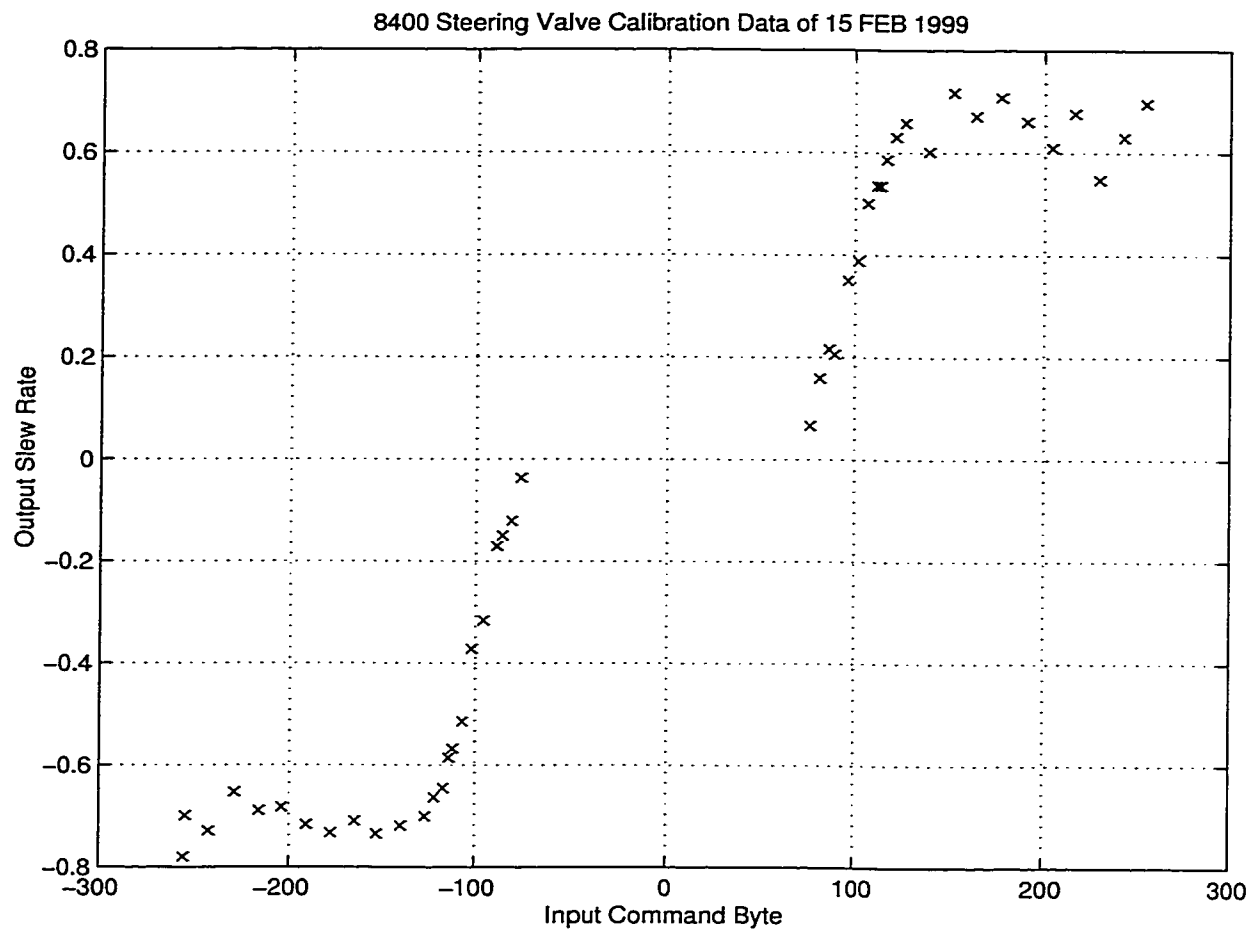


Figure 2.1: Steering Valve Calibration Data for the 8400

approximately 0.65 rad/sec (about  $37^\circ/\text{sec}$ ). The second is a substantial deadzone encompassing over half the useful range of the valve.

The steering response also exhibited some dynamic response and was modeled as a slight lag between requested slew rate and the resulting steady state slew rate. This effect was much more subtle and difficult to calibrate than were the saturation and the deadzone.

The saturation of the actuator was easily dealt with by including a saturation limit

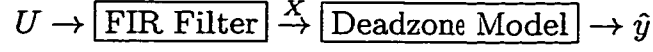


Figure 2.2: Deadzone Model Signal Flow

of 0.65 rad/sec to the model. The dynamics and the deadzone were more difficult to model. The goal of this modeling was to ultimately produce an inverse controller such that a requested slew rate could be achieved easily. The model chosen consisted of a FIR filter to model the slew dynamics cascaded into a deadzone model (see Figure 2.2). The order of these models was important to simplify the on-line identification of these models outlined in section 4.1. The estimate of the plant response was evaluated as

$$X = W^T U$$

$$\hat{y} = \begin{cases} m_1(X - b_1) & \text{if } X > b_1, \\ m_2(X + b_2) & \text{if } X < -b_2, \\ 0 & \text{if } -b_2 \leq X \leq b_1. \end{cases} \quad (2.1)$$

where

$W$  is the weight vector of the FIR filter,

$U$  is the input vector (off a tap delay line),

$X$  is the FIR filter output representing the dynamic response,

$m_1, m_2$  are the slopes of the upper and lower deadband regions respectively and

$b_1, b_2$  are the boundaries for the upper and lower deadband regions.



## 2.2 Vehicle Steering Dynamics Model

The vehicle steering model was a modified version of the steering model developed by Wong[Won93] and further refined by O'Connor[O'C97]. The Wong model accounts for all tire forces and the vehicle inertia. The O'Connor model simplified the very complex tire/soil interactions by assuming small lateral tire slips and linearizing the behavior. This allowed the vehicle dynamics to be modeled as several first order lags. The O'Connor model assumed the vehicle was moving only about a straight line and only one lateral dimension (the lateral error) was included. The model utilized in O'Connor's work made the slight generalization to planar motion in the East and North directions. When neglecting the lateral velocity of the control point, the resulting model was

$$\begin{aligned}
 \dot{E} &= V_x \sin \Psi - \Omega_z p_2 \cos \Psi \\
 \dot{N} &= V_x \cos \Psi + \Omega_z p_2 \sin \Psi \\
 \dot{\Psi} &= \Omega_z \\
 \dot{\Omega}_z &= -p_3 \Omega_z + p_4 V_x \tan \delta \\
 \dot{\delta} &= \omega \\
 \dot{\omega} &= p_5 (u - \omega)
 \end{aligned} \tag{2.2}$$

Where

$E$  is the east position of the control point,

$N$  is the north position of the control point,

$\Psi$  is the true heading of the vehicle,

$\Omega_z$  is the yaw rate of the vehicle,

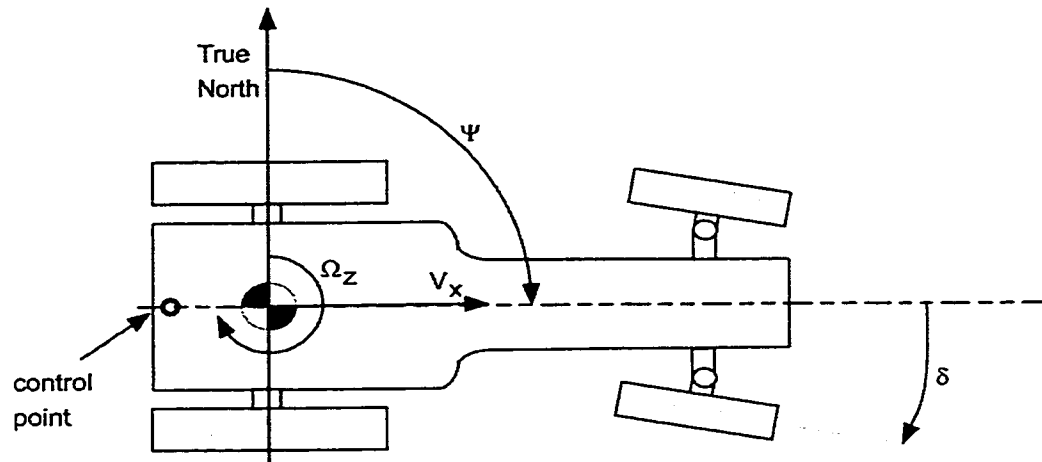


Figure 2.3: Vehicle State Definitions

$\delta$  is the effective steer angle of the vehicle,

$\omega$  is the slew rate of the front wheels,

$p_2$  is the influence of  $\Omega_z$  on lateral velocity,

$p_3$  is the yaw damping,

$p_4$  is the steering effectiveness and

$p_5$  is the lag in the steering actuator.

A graphical representation of how these states are measured is depicted in fig 2.3. A positive heading ( $\Psi$ ) was measured clockwise from true north, a positive yaw rate ( $\Omega_z$ ) was in the direction of increasing heading and a positive steer angle ( $\delta$ ) was in the direction that would induce the vehicle to turn to the right.

The parameters  $p_2$  through  $p_5$ <sup>1</sup> are referred to as the O'Connor parameters as they were introduced by O'Connor in his thesis work.[O'C97] Parameter  $p_2$  can be

<sup>1</sup>The parameter  $p_1$  was defined as the derivative of the lateral velocity with respect to small heading changes. It was theoretically and experimentally shown by O'Connor to be unity. For this reason it is omitted from this dissertation.

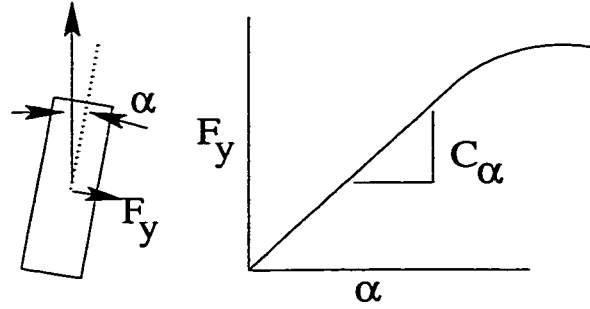


Figure 2.4: Tire Cornering Stiffness

interpreted as the influence of yaw rate on the lateral velocity. Parameters  $p_3$  and  $p_4$  are the time lag associated with the steering response and the yaw acceleration from a given forward speed and steer angle respectively. Finally,  $p_5$  is the time lag inherent in the steering valve.

These parameters are derived in [O'C97] by analyzing the forces introduced at the tires. They very compactly encompass the complex interactions between vehicle and operating conditions. When decomposed, these parameters have the following physical interpretations:

$$\begin{aligned}
 p_2 &\approx c \\
 p_3 &\approx \frac{2(C_{\alpha r} l_2^2 + C_{\alpha f} l_1^2) - 2(l_2 - c)(C_{\alpha r} l_2 - C_{\alpha f} l_1)}{I_z V_x} \\
 p_4 &\approx \frac{2C_{\alpha f} l_1}{I_z} \\
 p_5 &\approx \frac{1}{\tau_{steering}}
 \end{aligned} \tag{2.3}$$

where

$C_{\alpha f}$  and  $C_{\alpha r}$  are the proportionality constants from tire sideslip to tire force (known as

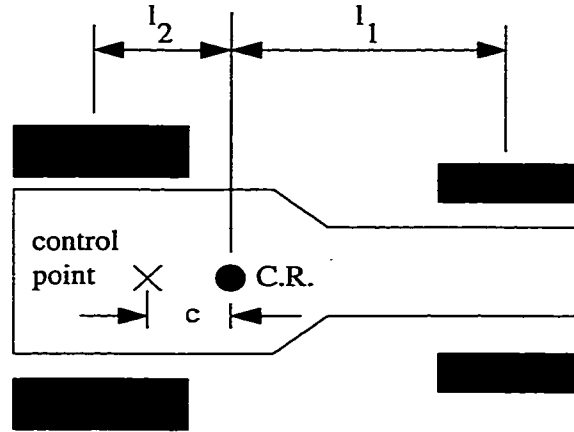


Figure 2.5: Tractor Dimension Definition

the tire cornering stiffness, Figure 2.4), these parameters also encompass the tire/soil interaction

$c$  denotes the distance from the control point to the center of rotation<sup>2</sup>,

$l_1$  denotes the distance from the front tire to the axis of rotation (Figure 2.5),

$l_2$  denotes the distance from the rear tire to the axis of rotation and

$I_z$  is the moment of inertia in the yaw axis.

The derivation of these relations are covered extensively in chapter 5 of [O'C97]. Several assumptions are made in order to simplify the analysis. The first assumption is that only the first order terms of the non-linearities are important. This assumption includes a small angle approximation for the tire lateral slip angles. When the higher order terms are neglected, the longitudinal and lateral dynamics can be approximated

---

<sup>2</sup>The center of rotation is defined as the point with zero lateral velocity. (i.e. the point whose velocity vector is tangent to the trajectory) It is not the point about which the entire vehicle is turning. Because of tire forces, the center of rotation is not necessarily at the center of mass. In an imaginary vehicle with infinite tire stiffness and infinite traction, and thus no lateral tire slip, the center of rotation, as defined here, would be located at the center of the rear axle.

as decoupled. A second assumption is that the lateral velocity of the entire vehicle (the difference between the velocity vector and the heading vector) was very small. It was shown in chapter 3 of [Bel99] that in a practical sense, very little would be lost in making this assumption. Small low frequency (as compared to the steering dynamics) lateral velocities could be compensated for by estimating a heading sensor bias state.

## 2.3 Vehicle Longitudinal Dynamics Model

On a conventional geared vehicle the ratio of engine RPM to vehicle speed remains relatively constant for each gear. The factors influencing this ratio are the mechanical gear ratio, the effective tire radius and the amount of slip the tire experiences in the longitudinal direction. The amount of slip the tire experiences is in turn dependent on many more factors including road surface, inflation pressure, normal and tractive loads, tire composition and construction and many others.[Gil92] To simplify these complex interactions, the transmission was modeled as

$$V_x = \kappa_g \omega_{engine} \quad (2.4)$$

where

$V_x$  is the forward speed of the vehicle,

$\kappa_g$  is the effective gear ratio for gear  $g$  and

$\omega_{engine}$  is the engine speed.

A calibration for the test vehicle is presented in fig 2.6. This calibration was run on a dry road and with no implement. This calibration will change substantially when

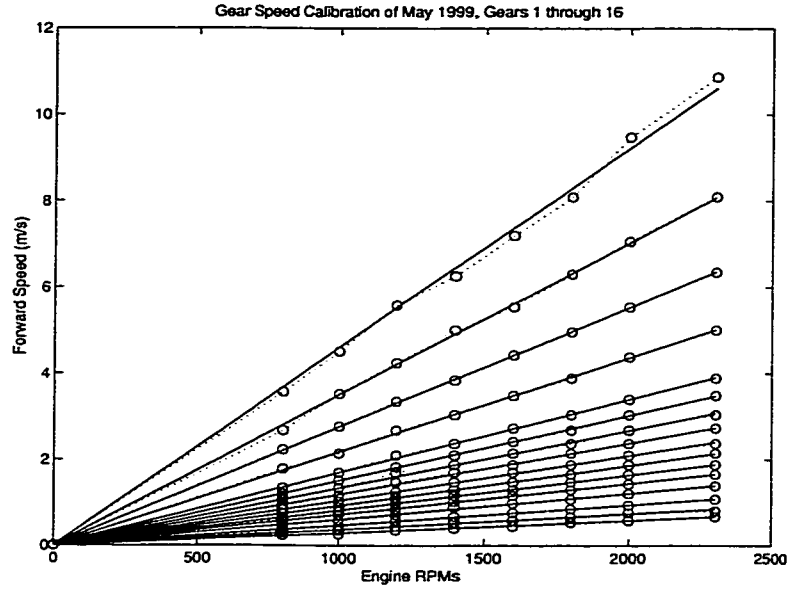


Figure 2.6: On Road Gear speed Calibration

the tractor is operated while pulling a load on a loose field.

Along with the gearing, there was a certain amount of lag associated with the engine RPM response. This lag becomes more pronounced in the higher gears when the engine could transmit less torque to the tires and thus has less accelerating force. This lag was modeled for each gear as

$$\dot{\omega}_{engine} = \frac{1}{\tau_g}(\omega_{command} - \omega_{engine}) \quad (2.5)$$

where

$\tau_g$  is the time lag associated with gear  $g$  and

$\omega_{command}$  is the desired steady state engine speed.

Differentiating equation (2.4) and combining (2.5) results in

$$\dot{V}_x = -\frac{1}{\tau_g}V_x + \frac{\kappa_g}{\tau_g}\omega_{command} \quad (2.6)$$

for a fixed gear. This yielded a simple input ( $\omega_{command}$ ) to output ( $V_x$ ) differential equation that could be made to have a very convenient closed form controller solution. This solution will be presented in section 7.3

## 2.4 Full Vehicle Estimation Model

The preceding models' primary use was for the parameter identification methods presented in Chapter 4. These methods relied on an estimated state. This state was generated using a Kalman filter that modeled the full planar dynamics of the tractor. In addition to the states presented in Sections 2.2 and 2.3, there were bias states in the heading measurement and the steer angle measurement. These inclusion of these biases is a direct result of the work done by O'Connor and Bell [Bel99] in order to account for crab angles<sup>3</sup> induced from side-slopes and asymmetric loads.

---

<sup>3</sup>A crab angle is defined as the angle between the vehicle's heading and velocity. When there is no sideslip, the crab angle is zero

The resulting model with inputs  $u_{steer}$  and  $\omega_{command}$  is

$$\dot{X} = \begin{bmatrix} \dot{E} \\ \dot{N} \\ \dot{\Psi} \\ \dot{\Omega} \\ \dot{\delta} \\ \dot{\omega} \\ \dot{\Psi}_{bias} \\ \dot{\delta}_{bias} \\ \dot{V}_x \end{bmatrix} = \begin{bmatrix} V_x \sin \Psi - p_2 \Omega \cos \Psi \\ V_x \cos \Psi + p_2 \Omega \sin \Psi \\ \Omega \\ -p_3 \Omega + p_4 V_x \delta \\ \omega \\ p_5 (u_{steer} - \omega) \\ 0 \\ 0 \\ \frac{1}{\tau_g} (\kappa_g \omega_{command} - V_x) \end{bmatrix} + noise \quad (2.7)$$

## 2.5 Variations in the O'Connor Parameters

In this work the O'Connor parameters characterized the steering dynamics of the vehicle. they are derived from the physical mechanics of vehicle motion.

For vehicles that remain consistent in their configuration, these parameters can be estimated with reasonable accuracy once and assumed to remain constant. Farm tractor and off-road vehicles in general can experience great variations in running conditions. Furthermore, these vehicles are typically industrial vehicles rather than personal transportation and are almost always working and consequently experience a wide range of operating loads. It is reasonable to expect that these factors will affect the behavior of the vehicle.



### 2.5.1 $P_2$

$P_2$  (units: length) represents the influence that a yaw rate has on lateral velocity. It is the measure of the leverarm from the axis of rotation to the control point projected to the ground plane. For a vehicle exhibiting perfect Ackerman steering and no lateral slip in any of the tires,  $p_2$  is simply the distance from the mid point of the rear axle to the control point. With the small rear tire slip assumption made in the O'Connor model this parameter is very nearly this distance.

The implements pulled by tractors often impose large lateral and vertical loads. Some of these implements, such as a hitched ripper, resist turning while others, such as a towed disk, will actually provide a steady state turning torque. These force based rather than kinematic influences have the effect of moving the axis of rotation. Heavy implements can also significantly move the center of gravity which also influences the distance to the control point.

The amount that this axis can move is influenced by how much force the implement exerts and also how the tractor is configured. For example a hitched ripper will most likely move the axis of rotation on a well ballasted tractor with excellent traction on all four tires much less than it will on a tractor with less efficient traction.

### 2.5.2 $P_3$

$P_3$  (units: 1/time) is most easily interpreted as the lag associated with yaw rate changes. This parameter is influenced by various factors. One obvious factor is the moment of inertia of the tractor itself. When a large, heavy implement is attached to the hitch this can significantly increase the moment of inertia of the vehicle. Another factor that influences this parameter is the lateral cornering stiffness of the tires. Just

as in an automobile, stiffer tires offer a quicker, more responsive feel. The stiffer tire provides a more rigid path for the tire forces to transmit their energy to the main mass of the vehicle. As a result, lateral tire traction also plays an important role in the value of  $p_3$ .

### 2.5.3 $P_4$

This parameter (units: 1/time \* length) is often referred to as the steering effectiveness. This parameter is affected by wheelbase length, moment of inertia of the tractor as well as the cornering stiffness and traction of the tires. It is very sensitive to weight distribution and traction variations. When the weight of the tractor is evenly distributed and the front tires are properly loaded they are more able to bite and turn the vehicle resulting in less lateral slip and making the no slip assumption a more valid estimate. When lightly loaded, such as when a heavy implement is hitched to the rear end, the front tires are less able to grab and provide a turning force to pull the front end of the tractor around.

### 2.5.4 $P_5$

This is the time lag (units 1/tim) in the steering actuation. This parameter is arguably the least variable of all the O'Connor parameters but the most difficult to analyze theoretically. It is primarily dependent on the hydraulic system and the transport delay of the valve system. There is also a finite amount of inertia in the valving, hydraulic fluid and the turning mechanics themselves that must be overcome before a full slew rate is achieved. Despite the fact that it is very slowly varying, as will be shown in Section 4.4, it is one of the most important parameters to identify.

This is due to the fact that any error in this parameter can be integrated several times before the error is detected at either the heading or the position estimates.

## 2.6 Expected Variation in the Parameters

There exists little experimental data as to the values of several of the contributing characteristics of the O'Connor Parameters in Equation (2.3). The cornering stiffness,  $C_\alpha$  of the tires utilized cannot be tested in the laboratory. The tires used in farm vehicles are simply too large to fit on the laboratory test equipment. Consequently, the information available is predominately theoretical, estimations or extrapolations from experiments on small scale models [CDN71], [Pac72]. In Owen and Bernard, [OB82], the ratio between the front and rear steering stiffnesses was obtained via careful modeling. The front tires of the vehicle utilized had the characteristics of small truck tires and a value of 65093 N/rad (250 lb/deg) was estimated for these tires. This estimate and the ratio between front and rear yielded a stiffness of 263756 N/rad (1013 lb/deg) for the rear tires.

The values expected for a John Deere 8400 tractor are as follows. These values were obtained through a discussion with a Deere engineer and are only approximate.

### 2.6.1 Forward Speed, $V_x$

The useful working speed of a farm tractor typically ranges from approximately  $1\frac{1}{2}$  m/s (3.35 mph) during precision operation to approximately 9 m/s (20 mph) during spraying operations. High speed operation ( $> 5$  m/s) is a subject of continuing

| Parameter                  | min            | nominal | max  |
|----------------------------|----------------|---------|------|
| $v_x$ (m/sec)              | $1\frac{1}{2}$ | 2.5     | 9    |
| $l_1$ (m)                  | 1.75           | 2       | 2.25 |
| $l_2$ (m)                  | 0.75           | 1       | 1.25 |
| $C_{\alpha_f}$ (N/deg)     | 200            | 2000    | 2200 |
| $C_{\alpha_r}$ (N/deg)     | 2000           | 2500    | 3000 |
| $I_z$ (kg m <sup>2</sup> ) | 5500           | 6000    | 9000 |

Table 2.1: Expected Physical Parameters for John Deere 8400 Tractor

research. Preliminary results indicate that the above model is inadequate to capture the true behavior of the vehicle. The above model greatly simplifies the tire dynamics which become increasingly more significant as speeds increase. Until a more refined model of vehicle dynamics is available, the speeds examined will be kept below 5 m/s.

### 2.6.2 Vehicle Leverarms, $l_1$ , $l_2$ and $c$

The vehicle leverarms describe the physical dimensions of the tractor and are illustrated in Figure 2.5.  $L_1$  and  $l_2$  describe how much torque the front and rear tires introduce for a given lateral load. As the center of gravity moves fore and aft, these distances change accordingly. The wheelbase of the vehicle does not change and therefore the sum of  $l_1$  and  $l_2$  is constant. The distance to the control point,  $c$ , also may vary with changes in the position of the center of gravity. The location of the center of gravity is influenced by ballast and implement. During typical operation, the center of gravity may move fore or aft by as much as 250 mm.

### 2.6.3 Tire Cornering Stiffnesses, $C_{\alpha_f}$ and $C_{\alpha_r}$

The cornering stiffness of a tire describes how much side force the tire produces for a given sideslip angle. This parameter was the most difficult to estimate accurately as it not only encompasses the mechanical properties of the tires, but the tire-soil interaction. Conversations with John Deere engineers lead to estimates of 2000 N/deg for the front tires and 2500 N/deg for the rear. These values were for an unloaded tractor on dry pavement. Cornering stiffnesses are sensitive to tire load and inflation pressure. As the load on the tire decreases, traction decreases and the stiffness goes down. This is important when a heavy implement is hitched to the rear of the tractor unloading the front tires. With these in mind, the cornering stiffness for the front tires were estimated to vary from 200 N/deg to 2000 N/deg and the rear tires were estimated to remain constant at 2500 N/deg.

### 2.6.4 Moment of Inertia, $I_z$

The moment of inertia along the yaw axis for the tractor alone was estimated to be approximately 5500 kg m<sup>2</sup>. This is the minimum value the moment will reach. As implements are hitched or ballast is added to the vehicle the moment will increase. The maximum moment was expected to be reached when heavily ballasted and the vehicle is carrying a heavy implement and was 9000 kg m<sup>2</sup>.

### 2.6.5 O'Connor Parameters Under Varying Conditions

The parameters described in the above sections were assigned reasonable values for a range of varying conditions and the resulting O'Connor parameters were tabulated in Table 2.2. To represent the effect of a implement being pulled through the ground,

| Condition                | $v_x$ | $l_1$ | $l_2$ | $C_{\alpha_f}$ | $C_{\alpha_r}$ | $C_{\alpha_h}$ | $I_z$ | $p_2$ | $p_3$ | $p_4$ |
|--------------------------|-------|-------|-------|----------------|----------------|----------------|-------|-------|-------|-------|
| Unloaded                 | 2     | 2     | 1     | 2000           | 2500           | 0              | 5500  | -0.3  | 2.1   | 1.45  |
| Transport<br>Heavy Impl. |       |       |       |                |                |                |       |       |       |       |
| ... Poor Ballast         | 5     | 2.25  | 0.75  | 500            | 2500           | 0              | 8000  | -0.05 | 0.17  | 0.28  |
| ... Good Ballast         | 5     | 2.1   | 0.9   | 1000           | 2500           | 0              | 9000  | -0.2  | 0.28  | 0.47  |
| Working<br>Heavy Impl.   |       |       |       |                |                |                |       |       |       |       |
| ... Poor Ballast         | 1.5   | 2.25  | 0.75  | 200            | 2500           | 2000           | 8000  | -0.05 | 0.85  | 0.11  |
| ... Good Ballast         | 1.5   | 2.1   | 0.9   | 800            | 2500           | 2000           | 9000  | -0.2  | 1.61  | 0.47  |
| Working<br>Light Impl.   | 1.5   | 2     | 1     | 2000           | 2500           | 1000           | 6000  | -0.3  | 3.14  | 1.33  |
| Spraying                 | 4     | 2     | 1     | 2000           | 2500           | 0              | 6500  | -0.3  | 0.89  | 1.23  |

Table 2.2: Parameter Variations Under Several Operational Condition

a cornering stiffness,  $C_{\alpha_h}$ , representing the hitched implements lateral torque was introduced as in [O'C97]. This force acted one meter behind the rear axle. The steering lag parameter,  $p_5$  was not tabulated as it is not affected by running conditions.

The resulting parameters in Table 2.2 give a rough expected range for the O'Connor parameters.

### 2.6.6 Simulated Performance With Mismodeled O'Connor Parameters

Several simulations were executed with various combinations of running conditions outlined in Table 2.2. In these simulations, there existed a mismatch between the vehicle operating conditions and the modeled state. The combinations simulated are outlined in Table 2.3

In addition to the mismatched model dynamics, a robust controller designed and

presented by Elkaim [EOBP97] was included. This robust controller was intended to be velocity invariant and insensitive to changing conditions. It was designed using the Observer Kalman Identification (OKID) system identification technique incorporating data from speeds ranging from 2.25 mph through 6.5 mph and conditions including unencumbered, pulling a disker and pulling a ripper. All data were combined to provide a single fourth order best fit model and an robust LQR controller to utilize under all conditions.

As expected, when the state of the tractor is well modeled, the performance of the controller is quite satisfactory. As shown in Figure 2.7, no errors exceed 5 cm in 10,000 time steps. When the state of the tractor is mismodeled the lateral error distribution error is significantly wider. One case of mismodeled parameters, Case 3, proved to be unstable. Even the relative moderate difference between a tractor configured for spraying and one modeled as empty was enough to significantly reduce the controller performance. The robust controller performed worse than the mismodeled controller. This is not entirely surprising as the robust controller was designed to provide assured stability rather than high bandwidth regulation performance.

The apparent sensitivity of the closed loop controller performance to variations in running conditions and the expectation that one tractor should be versatile enough to perform all these operations provides strong support for the utilization of some form of adaptive control. Recall in Section 1.2.3 improving the accuracy of the closed loop system from 2.5cm to 1.5cm translated into a 7000:1 improvement in crop losses. (And arguably farmer happiness) The high level of understanding of the vehicle dynamics as well as the ability to bound the model parameters suggests the use of parameter identification over system identification. As will be shown in the following chapters,

| Case | Vehicle State                            | Model State                              | lateral error ( $1\sigma$ ) |
|------|--|--|-----------------------------|
| 1    | Working, Heavy Impl.<br>Poorly Ballasted | Working, Heavy Impl.<br>Poorly Ballasted | 1.5 cm                      |
| 2    | Working, Heavy Impl.<br>Poorly Ballasted | Empty                                    | 2.4 cm                      |
| 3    | Working, Heavy Impl.<br>Poorly Ballasted | Robust OKID [EOBP97]                     | 2.5 cm                      |
| 4    | Empty                                    | Working, Heavy Impl.<br>Poorly Ballasted | unstable                    |
| 5    | Empty                                    | Empty                                    | 1.4 cm                      |
| 6    | Empty                                    | Spraying                                 | 2.2 cm                      |

Table 2.3: Lateral Performance with Mismodeled O'Connor Parameters

the parameter identification approach was a path that proved to be very successful in increasing system performance during experimentation.



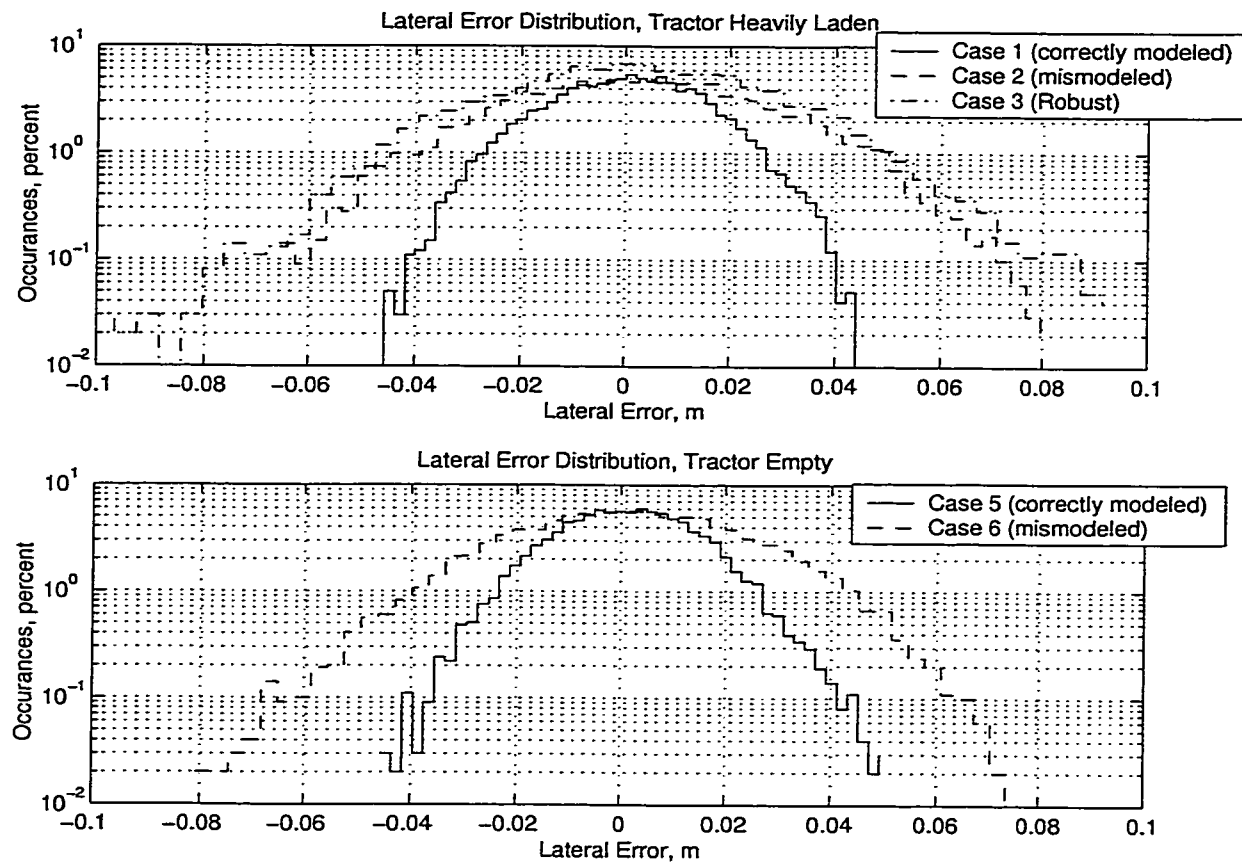


Figure 2.7: Lateral Performance with Mismodeled O'Connor Parameters

## CHAPTER 3

# Real Time Parameter Identification Methods

There are many methods of system identification and adaptive control in use today.[Kel93], [EOBP96], [WW96], [WS85], [Goo82], [Lju87] These methods can be subdivided into two main categories: On-line (Real Time) and Off-line(Post-Processing). Off-line system identification is most effectively used for designing a fixed gain controller for an unknown time invariant system. The system in question is usually time invariant and latency in the identified model is not a primary concern. Post-processing the data typically allows for a more accurate model as non-causal information can be incorporated into the identification process and smoothing filter techniques can be incorporated. In addition, because these methods do not require real-time execution, much more computationally complex algorithms can be quite satisfactorily implemented.

On-line parameter identifications methods, however, are typically more constrained than off-line methods. On-line identification is often used as an approach to adaptive control. These methods are advantageous for rapidly changing models where using

a fixed controller design will fail to meet the required performance objectives. Real time information about the dynamics of the system allows the control system to be adjusted dynamically in response to changes. These methods must be run in real time and provide timely information about the dynamics of the system. These constraints often limit the computational complexity as a solution must be evaluated within the given time frame. Powerful computers alleviate this problem somewhat. Regardless of this, it is still often more desirable to require lower processing power.

In the context of the work presented in this dissertation, on-line identification methods are utilized exclusively. The main focus was to address the issue of the changing dynamics of farm tractors during realistic operation. These dynamics may change with time constants on the order of days as different implements are attached and the overall field conditions change, or on the order of minutes or seconds as local soil conditions vary and interact with the vehicle.

It is not an extremely bold assertion to say that telling a farmer what he should have been doing yesterday is of very little value as compared to telling farmer what he could be doing right now to help optimize his operations. It is therefore necessary to optimize the operation of an automatic tractor control system in real time rather than with post-processing type approaches.

### **3.1 The Philosophy of Parameter Identification**

The advantage of parameter identification is that it reduces a large complex set of unknowns into a small number of (ideally) easily identifiable parameters. For instance, Sidman [Rov87] reduces a large, complex transfer function associated with a flexible robot arm to one parameterized by a single parameter, the payload mass.

This type of simplification allows the engineer to incorporate much more physical intuition and help constrain the form of the model to match the physics of the system. It also allows for monitoring and bounding of the identified model. If, for instance, noisy measurements and an extremely bad initial model yielded an estimate of a parameter that represented the mass of an item to be negative, the error can easily be identified. To deal with this, the engineer could put constraints on the estimated mass to discourage divergence.

## 3.2 The LMS Algorithm

The Least Mean Square (LMS) algorithm was developed in the late 1950's by Bernard Widrow and Ted Hoff.[WW96][WS85] This algorithm attempts to minimize a quadratic cost function, the expected square of the error between predictions and observations. It is a steepest descent type algorithm where the adaptation is directed in the steepest direction of the error paraboloid. The strength of this algorithm comes from its computational efficiency. Rather than exactly calculating the gradient, it makes an approximation at every epoch. The price that is paid for this increased computational efficiency is increased noise in the identified parameters. This noise may be somewhat alleviated but at the cost of slower convergence.

### 3.2.1 Model Updating

The LMS traditional algorithm requires the system to be representable by an output that is a linear function of an input vector:

$$\hat{y}_k = X_k^T W_k \quad (3.1)$$

where

$\hat{y}_k$  is the model output,

$X_k^T$  is the input vector and

$W_k$  is the weighting vector each at epoch  $k$  (the unknown system impulse response.)

The error is then defined as the difference between the desired model output and the actual model output. The desired output may be a specified frequency response if designing a filter or it can be the measured response of a dynamic system if a model of that system is desired.

$$\varepsilon_k = y_k^{des} - \hat{y}_k = y_k^{des} - X_k^T W_k \quad (3.2)$$

Finally, the error surface is defined as

$$\zeta = E [\varepsilon_k^2] \quad (3.3)$$

The update for the weight vector moves the weight vector down the error surface by adjusting the weights in a manner consistent with the gradient of  $\zeta$  with respect

to  $W_k$

$$W_{k+1} = W_k - \mu \nabla_{W_k} \quad (3.4)$$

When  $\nabla_{W_k}$  is known exactly this method reduces to Newton's method [WS85]. The weight vector simply moves down the steepest part of the error paraboloid at a speed proportional to the magnitude of the gradient and to the learning coefficient,  $\mu$ . The further from the minimum it is, the steeper the gradient and the faster the convergence. As the weight vector approaches the minimum of the paraboloid the weight vector is adjusted by smaller and smaller steps asymptotically approaching the minimum. The difficulty encountered when applying Newton's method is that  $\nabla_{W_k}$  is seldom known exactly. It is difficult and computationally expensive to calculate  $\nabla_{W_k}$  exactly. The “trick” of the LMS algorithm is to approximate  $\nabla_{W_k}$

$$\nabla_{W_k} = \frac{\partial \zeta}{\partial W_k} \frac{\partial E[\varepsilon_k^2]}{\partial W_k} \approx \frac{\partial \varepsilon_k^2}{\partial \varepsilon_k} \frac{\partial \varepsilon_k}{\partial W_k} = -2\varepsilon_k X_k \quad (3.5)$$

By setting

$$\hat{\nabla}_{W_k} = -2\varepsilon_k X_k \quad (3.6)$$

the LMS algorithm estimates the gradient with great computational efficiency. The

expected value of  $\hat{\nabla}_{W_k}$  is  $\nabla_{W_k}$

$$\begin{aligned}
 E \left[ \hat{\nabla}_{W_k} \right] &= -2E \left[ \varepsilon_k X_k \right] \\
 &= -2E \left[ y_k^{des} X_k - X_k X_k^T W_k \right] \\
 &= \nabla_{W_k}
 \end{aligned} \tag{3.7}$$

This approximated gradient is, as shown above, an unbiased estimate of the true gradient.

### 3.2.2 Convergence of the LMS algorithm

There does not currently exist a generalized proof of the convergence of the LMS algorithm. Despite this, there have been many proofs stating that the LMS algorithm will undoubtedly converge if specific conditions are met. [WS85], [WW96], [Hay84], [TJL87] These proofs constrain the spectral properties of the input, measurements and the speed of convergence. All these proofs illustrate that the more aggressive the learning rate becomes, the faster the parameters are identified but the less stable the identification becomes. To show this without generating an inconvenient recursive equation a change of coordinates in the weight space is necessary. The new space is translated, as it is in [WS85], to be zero at the minimum of the error paraboloid.

$$V_k = W_k - W_k^* \tag{3.8}$$

with  $W_k^*$  being the choice of weights which minimizes  $\zeta$ .<sup>1</sup> The update law for the weight vector in the new coordinate system (assuming  $W_{k+1}^* = W_k^*$ ) becomes

$$\begin{aligned} V_{k+1} &= W_{k+1} - W_{k+1}^* \\ &= W_k + 2\mu\varepsilon_k \mathbf{X}_k - W_k^* \\ &= V_k + 2\mu\varepsilon_k X_k \end{aligned} \tag{3.9}$$

The expected value for the next weight vector is therefore

$$\begin{aligned} E[V_{k+1}] &= E[V_k] + 2\mu E[\varepsilon X_k] \\ &= E[V_k] + 2\mu (E[y_k^{des} \mathbf{X}_k] - E[X_k X_k^T W_k]) \end{aligned} \tag{3.10}$$

The final step in solving for the stability of the LMS algorithm is to allow for some simplified notation and solve for  $W^*$

$$\begin{aligned} P &= E[y_k^{des} X_k] \\ R &= E[X_k X_k^T] \\ W^* &= \min \zeta = R^{-1} P \end{aligned} \tag{3.11}$$

---

<sup>1</sup>The subscript  $k$  on  $W_k^*$  is included in Equation (3.8) to account for the possibility of a time varying minimum.



Substituting Equation (3.11) into (3.10) yields the following

$$\begin{aligned}
 E[V_{k+1}] &= E[V_k] + 2\mu(P - RE[W_k]) \\
 &= E[V_k] + 2\mu(P - RE[W_k - W_k^*] - RW_k^*) \\
 &= E[V_k] + 2\mu(P - RE[V_k] - R(R^{-1}P)) \\
 &= E[V_k] - 2\mu RE[V_k] \\
 &= (I - 2\mu R) E[V_k] \\
 &= (I - 2\mu R)^k V_0
 \end{aligned} \tag{3.12}$$

Equation (3.12) shows us that stability is assured if all the eigenvalues of  $(I - 2\mu R)$  lie within the unit circle. This specification is met when

$$\frac{1}{\lambda_{max}} > \mu > 0 \tag{3.13}$$

where  $\lambda_{max}$  is the largest eigenvalue of  $R$ . The dynamics of the convergence in each eigendirection has similar behavior to that of the direction associated with  $\lambda_{max}$ . Table 3.1 shows the damping behavior in a single eigendirection as a function of the learning coefficient. In addition to showing stability, it has been shown that the weight vector converges to a state that will minimize  $\zeta$ , the minimum expected error.

The stability of the LMS is constrained by the  $\lambda_{max}$ , yet the long term rate of convergence is determined by  $\lambda_{min}$ . This is not a concern for well behaved systems with closely matched eigenvalues. Stability and convergence times may become a problem for systems with a large spread in eigenvalue magnitudes. These systems exhibit error paraboloids that are very long and narrow. The model of the system

|                      |  |
|----------------------|--|
| Stable (Convergent)  | $\frac{1}{\lambda} > \mu > 0$                  |
| Overdamped           | $\frac{1}{2\lambda} > \mu > 0$                 |
| Critically Damped    | $\mu = \frac{1}{2\lambda}$                     |
| UnderDamped          | $\frac{1}{\lambda} > \mu > \frac{1}{2\lambda}$ |
| Unstable (Divergent) | $\frac{1}{\lambda} \leq \mu$ or $\mu \leq 0$   |

Table 3.1: Damping in the Eigendirections of R for the Weight Vector

converges in a very polymodal fashion. The errors in the steep directions converge very rapidly and the model state spends a long time slowly moving down the shallow “valley” of the paraboloid.

The strength of the LMS algorithm lies in its computational simplicity. It arrives at this simplicity by taking a large number of small steps to converge eventually on the correct estimate. It is an excellent method for identifying relatively slow moving parameters but will track rapidly changing parameters poorly.

### 3.3 The EKF Algorithm

The extended Kalman filter (EKF) is the non-linear version of the Kalman filter<sup>2</sup>. Both types of Kalman filters are methods to account for not only the unperturbed dynamics of the system but also for the uncertainty induced by both environmental perturbations (process noise) and measurement errors. The EKF follows the same basic steps as the Kalman filter. However, whereas the Kalman filter is optimal in generating an estimate of the states in the system, the EKF loses this optimality by linearizing the measurement correction.[Ste94a] The EKF offers the added advantage

---

<sup>2</sup>The linear Kalman Filter is a famous and very well known algorithm to provide optimal filtering of noisy sensors and process disturbances. If the reader is unfamiliar with the Kalman Filter they are encouraged to reference [Ste94a].

of estimating both the system state and the uncertainty of those states at the same time as the unknown system parameters. This is useful when designing a control system to take advantage of the latest system model. The cost of this information is a much larger system to be manipulated.

Many factors may contribute to the non-linearity of the system to be observed. A few of these factors include fundamental non-linearities in the dynamics, dependence on unknown parameters and others. This work concentrates on system non-linearities and unknown parameters.

The EKF requires a state space format. The system to be used is described as

$$\begin{aligned}\dot{x}(t) &= f(x, u, w, t) \\ y(t) &= h(x, u, v, t) \\ E[w(t)w(t)^T] &= R\delta(t), E[v(t)v(t)^T] = Q\delta(t), E[v(t)w(t)^T] = 0\end{aligned}\tag{3.14}$$

where

$x$  is the state to be estimated,

$f$  is the function describing the dynamics of the system,

$u$  is the system inputs,

$y$  is the system measurement,

$h$  is the function describing each of the measurements in the system,

$w$  is the process noise vector,

$v$  is the measurement noise vector and

$\delta$  is the impulse function.

The noises,  $w$  and  $v$  must be zero mean noises. If they have a non-zero mean, the

noise can be broken into a bias (the DC levels) which are accounted for in  $f$  and  $h$  and the zero mean which will be referred to as simply  $w$  and  $v$  below.

In the discrete time implementation, the actual filtering occurs in two steps. First, the time propagation step utilizes the previous best estimate of the state, the known input and the most likely value for the unknown process noise. The equations of motion are projected forward in time to the time of the measurement. This step accounts for the finite time between the successive measurements, the movement of the system and the uncertainty injected by the process noise.

$$\begin{aligned} X_{k+1}^{(-)} &= X_k^{(+)} + \int_{t_k}^{t_{k+1}} f(X(\tau), u(\tau), E[w(\tau)], \tau) d\tau \\ P_{k+1}^{(-)} &= P_k^{(+)} + \int_{t_k}^{t_{k+1}} (F(\tau)P(\tau) + P(\tau)F^T(\tau) + Q(\tau)) d\tau \end{aligned} \quad (3.15)$$

where

$$\begin{aligned} F &= \left. \frac{\partial f}{\partial x} \right|_{x=x_k}, \quad G = \left. \frac{\partial f}{\partial u} \right|_{x=x_k} \\ P &= E \left[ (\hat{x} - x_{actual})^T (\hat{x} - x_{actual}) \right] \end{aligned} \quad (3.16)$$

There are various methods for evaluating the integrals above. The two most notable methods are a closed form integration of the continuous equations of motion over the interval  $t_k$  to  $t_{k+1}$ , or a finite length Taylor series approximation of the integral. With a zero order hold on the input these yield a linearized system where

$$\begin{aligned} X_{k+1}^{(-)} &= F_k X_k^{(+)} + G_k u_k \\ P_{k+1}^{(-)} &= F_k P_k^{(+)} F_k^T + Q_k \end{aligned} \quad (3.17)$$

The second step of the algorithm is the measurement update. This step results from linearizing the system about the current estimated state and applying the same measurement update as the Kalman filter.

$$\begin{aligned}
H_{k+1} &= \frac{\partial h(t_{k+1})}{\partial x(t_{k+1})} \\
K_{k+1} &= P_{k+1}^{(-)} H_{k+1}^T \left[ H_{k+1} P_{k+1}^{(-)} H_{k+1}^T + R_{k+1} \right]^{-1} \\
X_{k+1}^{(+)} &= X_{k+1}^{(-)} + K_{k+1} \left[ z_{k+1} - h \left( X_{k+1}^{(-)} \right) \right] \\
P_{k+1}^{(+)} &= [I - K_{k+1} H_{k+1}] P_{k+1}^{(-)}
\end{aligned} \tag{3.18}$$

This is the step in which the EKF loses its optimality. The update gains are a function of the system model, which is dependent on the state. Errors in the state estimate induce errors in the state model which result in a sub-optimal measurement update. There exist several methods to make the update more optimal, typically by making multiple iterative updates [KH97], [HKKP95]. Because of their high computational requirements these methods will not be outlined in this dissertation.

The EKF quite naturally lends itself to physical parameter (PP) identification. The PP-EKF simply augments the standard states with the unknown parameters ( $p$ ).

$$X_k^E = \begin{bmatrix} X_k \\ \hat{p} \end{bmatrix} \tag{3.19}$$

During state propagation, the state estimate is propagated in the normal fashion

while the parameter estimate is held constant

$$X_{k+1}^{E(-)} = \begin{bmatrix} X_{k+1}^{(-)} \\ \hat{p}_{k+1} \end{bmatrix} = \begin{bmatrix} F_k X_k^{(+)} + G_k u_k \\ \hat{p}_k \end{bmatrix} \quad (3.20)$$

Several gradients are then calculated. The actual method for evaluating these gradients will be discussed in detail in Section 3.4.

$$F_k^p \equiv \frac{\partial F_k}{\partial p}, G_k^p \equiv \frac{\partial G_k}{\partial p}, H_k^p \equiv \frac{\partial H_k}{\partial p} \quad (3.21)$$

$$\begin{aligned} F_k^E &\equiv \frac{\partial f(X_k^E, u_k)}{\partial X_k^E} \Big|_{X=X_k^{E(+)}} = \begin{bmatrix} F_k & F_k^p X_k^{(+)} + G_k^p u_k \\ 0 & I \end{bmatrix} \\ H_k^E &\equiv \frac{\partial h(X, u(t_k))}{\partial X} \Big|_{X=X_k^{E(+)}} = \begin{bmatrix} H_k & H_k^p X_k^{(+)} \end{bmatrix} \end{aligned} \quad (3.22)$$

From this point on, the PP-EKF algorithm proceeds identically as the EKF described earlier with  $F^E$  and  $H^E$  taking the role of  $F$  and  $H$ .

There are several advantages and disadvantages to using the PP-EKF algorithm. First, this method offers essentially a variable step size convergence, which results in relatively rapid initial convergence followed by reasonable noise rejection. This is true only with an accurate noise model. A poor noise model causes instabilities and periodically results in divergence of the estimator. Secondly, the PP-EKF algorithm is a full state space algorithm. The estimated states can be incorporated readily into an optimal control scheme. This comes at the cost of implementing matrix algebra in software or hardware. Lastly, the PP-EKF offers a measure of the uncertainty of

any state or parameter at every epoch. This results in increased computation and complexity as these covariances must be calculated along with the system states. The validity of the covariances on the parameters is often questionable. Often it is very difficult to provide a realistic disturbance model for the parameters. Consequently, often the process noises associated with the parameters are hand tweaked until the estimator provides satisfactory performance. In doing this adjustment, the covariance of the parameter estimates becomes a very crude approximation indeed.

### 3.4 The Keller Method

In his thesis, [Kel93], Keller extensively explores the EKF for physical parameter identification. Several interesting techniques are explored and developed such as a recursive algorithm for calculating the gradient of the discrete time state propagation matrix with respect to continuous time physical parameters. This is particularly useful in the face of Equation (3.21) and Equation (3.22).

A linear, time invariant, continuous time system of the form

$$\dot{x} = Ax + Bu \quad (3.23)$$

can be converted to the discrete form (with sample time  $T$ ) by taking the matrix exponential of an augmented matrix.

$$\begin{bmatrix} F & G \\ 0 & I \end{bmatrix} = \exp \begin{bmatrix} AT & BT \\ 0 & 0 \end{bmatrix} \quad (3.24)$$

The ultimate goal is to determine the derivative of the discrete model matrices with

respect to the continuous model parameters. By differentiating Equation (3.24) one easily comes to the following equation.

$$\begin{bmatrix} \frac{dF}{dp} & \frac{dG}{dp} \\ 0 & 0 \end{bmatrix} = \frac{d}{dp} \exp \begin{bmatrix} AT & BT \\ 0 & 0 \end{bmatrix} \quad (3.25)$$

This differentiation is executed by using the Taylor series definition of the exponential function.

$$\exp(M) \equiv e^M = I + M + \frac{M^2}{2!} + \frac{M^3}{3!} + \frac{M^4}{4!} + \dots \quad (3.26)$$

Therefore, in order to determine the derivative of  $e^M$  the derivative of  $M^n$  must first be determined.

$$\begin{aligned} \frac{dM^n}{dp} &= \frac{d}{dp}(M \cdot M \cdot \dots \cdot M) \\ &= \frac{dM}{dp} M^{n-1} + M \frac{dM}{dp} M^{n-2} + \dots + M^{n-1} \frac{dM}{dp} \end{aligned} \quad (3.27)$$

Using Equations (3.26) and (3.27) a recursive algorithm can be defined to calculate the parameter gradients. First, define the following two matrices.

$$\begin{aligned} D_n &= \frac{1}{n!} \frac{dM^n}{dp} = \frac{1}{n!} \frac{d}{dp} [M M^{n-1}] = \frac{1}{n!} \left[ \frac{dM}{dp} M^{n-1} + M \frac{dM^{n-1}}{dp} \right] \\ &= \frac{dM}{dp} \frac{C_{n-1}}{n} + \frac{M}{n} D_{n-1} \\ C_n &= \frac{M^n}{n!} = \frac{M}{n} C_{n-1} \end{aligned} \quad (3.28)$$

The matrix derivatives are then calculated using the dc2d algorithm outlined in Table 3.2.



1. Form the matrices:

$$M = \begin{bmatrix} A & B \\ 0 & 0 \end{bmatrix} T, dM = \begin{bmatrix} dA & dB \\ 0 & 0 \end{bmatrix} T$$

where  $T$  is the sample time.

2. Initialize the recursive values:

$$C = I, D = 0, dexpM = 0, n = 1$$

3. Repeat the recursion:

$$\begin{aligned} D &= \frac{1}{n}(MD + dMC) \\ C &= \frac{1}{n}MC \\ dexpM &= dexpM + D \\ n &= n + 1 \end{aligned}$$

until satisfactory convergence is reached. The derivatives  $\frac{dF}{dp}$  and  $\frac{dG}{dp}$  are then extracted from  $dexpM$  using Equation (3.27).

Table 3.2: The dc2d Algorithm

With an efficient method of calculating the matrix derivative, the PP-EKF can easily be used to identify unknown parameters. Even with this easy and efficient method of calculating the matrix derivative, evaluating it at every epoch may be prohibitively expensive. As an alternative, the gradients defined in Equation (3.21) are calculated only periodically and assumed to remain linear or constant in the interim. The gradient updates are estimated by projecting the linearized gradient forward with the changing parameters. The model derivatives are then approximated by

$$\begin{aligned} F_{k+1} &\approx F_k + F_k^p(p_{k+1} - p_k) \\ G_{k+1} &\approx G_k + G_k^p(p_{k+1} - p_k) \\ H_{k+1} &\approx H_k + H_k^p(p_{k+1} - p_k) \end{aligned} \tag{3.29}$$

Keller's method is a set of approximations to make the PP-EKF algorithm less computationally intensive. It offers nearly identical convergence as the traditional PP-EKF algorithm at a lower cost. Unfortunately it also suffers the same limitation on noise model accuracy. Keller's method must also periodically recalculate all of the parameter gradients.

### 3.5 The LMS/EKF method

The Least Mean Square / Extended Kalman Filter is a blend of the EKF and the LMS algorithms. This method attempts to identify the system parameters without extending the number of states in the filter to include the unknown system parameters. It exists as a traditional Kalman filter, implemented with the most current estimates

of the parameters, running in an inner loop with an LMS filter running as an outer loop to identify the unknown model parameters. This method has the advantage of making a full state estimate available for control with only a modest increase in computational and storage demands.

At each epoch the LMS/EKF algorithm begins with a standard Kalman filter. The parameters are not included in the state and it is assumed that the observation matrix is independent of the parameters. The dynamic model is therefore expressed as

$$\begin{aligned} X_{k+1} &= F(p_k)X_k + G(p_k)u_k \\ z_{k+1} &= HX_k \end{aligned} \tag{3.30}$$

The Kalman filter yields an estimate of the state after the time update,  $X_k^{(-)}$  and after the measurement update,  $X_k^{(+)}$ . These estimates are then used to generate an expected change in the measurement and compared to the measured change. The error is thus

$$\epsilon_k = (z_k - z_{k-1}) - H(X_k^{(-)} - X_{k-1}^{(+)}) = \Delta z_k - H\Delta X_k \tag{3.31}$$

The cost function to be optimized is simply the expected power contained in this error.

$$J = E [\epsilon^T \epsilon] \tag{3.32}$$

As shown in Section 3.2 this cost function can be minimized in a manner similar to Newton's method using an approximated gradient with respect to the interesting

parameters. The LMS parameter update equation is the update equation utilized for the parameters in the LMS/EKF method:

$$p_{k+1} = p_k - \mu \frac{\partial J}{\partial p_k} \quad (3.33)$$

The derivative can be approximated and expanded using the chain rule

$$\frac{\partial J}{\partial p_k} \approx \frac{\partial J}{\partial \epsilon_k} \frac{\partial \epsilon_k}{\partial \Delta(X_k)} \frac{\partial \Delta(X_k)}{\partial p_k} = -2\epsilon_k^T H \frac{\partial(\Delta X_k)}{\partial p_k} \quad (3.34)$$

The evaluation of  $\frac{\partial(\Delta X_k)}{\partial p_k}$  may be approximated by many methods such as a Euler or Trapezoidal integration.

### 3.5.1 Practical Computational Advantages of the LMS/EKF algorithm

The LMS/EKF algorithm can offer significant computational advantages over a traditional PP-EKF. System models are represented in state space format. These models are represented as matrixes and storage of the state transition matrix is an  $O(N^2)$  proposition, where N represents the number of states to be stored. A PP-EKF augments the system with parameter estimates increasing the size of the matrix and consequently, the memory requirements. The more dynamic states in the system, the faster augmentation of these states consumes memory. The LMS/EKF algorithm does not augment the entire system, rather it carries the state estimates in parallel to the parameters. Consequently, the only additional memory required is enough to store the parameters themselves.

In addition to increased storage requirements, the augmentation of states induced

by the PP-EKF algorithm (and avoided by the LMS/EKF algorithm) greatly increases the computational requirements of the estimator. The increase in computation is even more dramatic than the increase in the storage requirements. If the parameter estimates are in the continuous time domain and the estimator is implemented in the discrete domain a continuous to discrete (c2d) conversion must be implemented. This c2d conversion is often realized through a matrix exponential, an  $O(N^3)$  operation. In addition to the c2d operation, several matrix multiplications (also  $O(N^3)$  operations) are required of the state transition matrix at each epoch for the time update. In light of this, it is clear that keeping the number of states in the estimator to a minimum yields significant returns in terms of required computer power.

### 3.5.2 A Simple LMS/EKF Example

To illustrate the LMS/EKF algorithm it will be demonstrated on a simple spring mass system. The input to the system is a commanded velocity on the mass on the left as illustrated in Figure 3.1. The resulting dynamic equations are

$$\begin{aligned}\ddot{x} &= \kappa(y - x) + \beta(\dot{y} - \dot{x}) \\ \dot{y} &= u\end{aligned}\tag{3.35}$$

where

$\kappa = k/M$  and

$\beta = b/M$ .

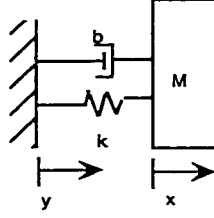


Figure 3.1: Spring mass system used in LMS/EKF example

In matrix form this system becomes

$$\frac{d}{dt} \begin{bmatrix} x \\ \dot{x} \\ y \end{bmatrix} = \begin{bmatrix} 0 & 1 & 0 \\ -\kappa & -\beta & \kappa \\ 0 & 0 & 0 \end{bmatrix} \begin{bmatrix} x \\ \dot{x} \\ y \end{bmatrix} + \begin{bmatrix} 0 \\ \beta \\ 1 \end{bmatrix} u \quad (3.36)$$

The measurement of  $x$  and  $y$  are available resulting in an observation matrix of

$$H = \begin{bmatrix} 1 & 0 & 0 \\ 0 & 0 & 1 \end{bmatrix} \quad (3.37)$$

At each epoch a linear Kalman filter is run based on the system in Equation (3.36) yielding  $X_{k+1}^{(-)}$  and  $X_{k+1}^{(+)}$ . The error is then generated

$$\epsilon_{k+1} = \begin{bmatrix} \epsilon_{k+1}^x \\ \epsilon_{k+1}^y \end{bmatrix} = z_{k+1} - z_k - H(X_{k+1}^{(-)} - X_k^{(+)}) \quad (3.38)$$

The gradients with respect to  $\kappa$  and  $\beta$  can be approximated by a simple trapezoidal

integration:

$$\begin{aligned}
\frac{\partial(\Delta X)}{\partial \kappa} &\approx \frac{\Delta t}{2} \left( \frac{\partial \dot{X}}{\partial \kappa} \Big|_{x_{k+1}^{(+)}} + \frac{\partial \dot{X}}{\partial \kappa} \Big|_{x_k^{(+)}} \right) \\
&= \left( (y_{k+1}^{(+)} - x_{k+1}^{(+)}) + (y_k^{(+)} - x_k^{(+)}) \right) \begin{bmatrix} \frac{\Delta t}{2} \\ \frac{\Delta t^2}{4} \\ 0 \end{bmatrix}
\end{aligned} \tag{3.39}$$

$$\begin{aligned}
\frac{\partial(\Delta X)}{\partial \beta} &\approx \frac{\Delta t}{2} \left( \frac{\partial \dot{X}}{\partial \beta} \Big|_{x_{k+1}^{(+)}} + \frac{\partial \dot{X}}{\partial \beta} \Big|_{x_k^{(+)}} \right) \\
&= \left( 2u_k - \dot{x}_{k+1}^{(+)} - \dot{x}_k^{(+)} \right) \begin{bmatrix} \frac{\Delta t}{2} \\ \frac{\Delta t^2}{4} \\ 0 \end{bmatrix}
\end{aligned}$$

Integrating this and the observation matrix into the update equation results in the update for both parameters

$$\begin{aligned}
\hat{\kappa}_{k+1} &= \hat{\kappa}_k + 2\mu_\kappa \epsilon_k^x \frac{\Delta t}{2} \left( (y_{k+1}^{(+)} - x_{k+1}^{(+)}) + (y_k^{(+)} - x_k^{(+)}) \right) \\
\hat{\beta}_{k+1} &= \hat{\beta}_k + 2\mu_\beta \epsilon_k^x \frac{\Delta t}{2} \left( 2u_k - \dot{x}_{k+1}^{(+)} - \dot{x}_k^{(+)} \right)
\end{aligned} \tag{3.40}$$

It is important to note that  $\epsilon^y$  is not utilized at all in the identification. This is due to the fact that  $\kappa$  and  $\beta$  have no affect on the dynamics of  $y$  in this example. There are no degrees of freedom to adjust that will minimize  $\epsilon^y$ .

A simulation of this algorithm was run and compared to the performance of an EKF. The results are plotted in Figure 3.2 The performance of the LMS/EKF filter was comparable to that of the EKF at a computationally lower cost.

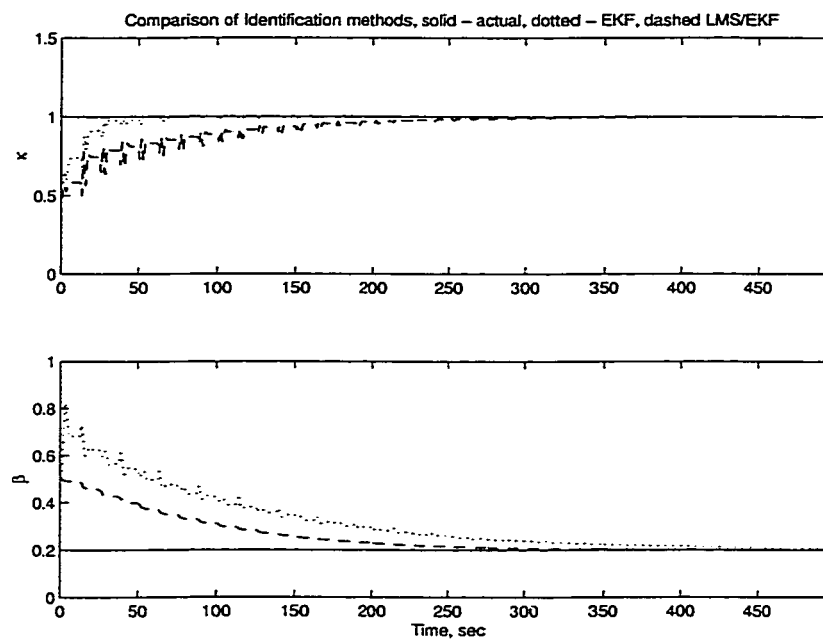


Figure 3.2: Learning Curves for the Spring Mass System Example





## CHAPTER 4

# Vehicle Parameter Identification Methods

In order to provide the most accurate possible control of a wheeled vehicle through steering inputs alone, the dynamics of the vehicle must be accurately known. There have been several excellent approaches at providing fixed models for the dynamics of a farm tractor. [O'C97],[EOBP97], [Owe82] These methods approach the problem of varying parameters as either a calibration problem or a robust control problem. There are obvious disadvantages to using a pre-calibration approach. While this provides excellent identification, it is tedious and impractical in an agricultural application and cannot account for local variations. A robust control requires little user effort but yields sub-optimal control. The ideal system would have exact knowledge of the dynamics at any given moment without requiring extensive user interaction. The methods that are described below attempt to realize this ideal as well as possible. These methods break the various sub-systems of the farm tractor up into relatively independent systems and address them separately and independently.

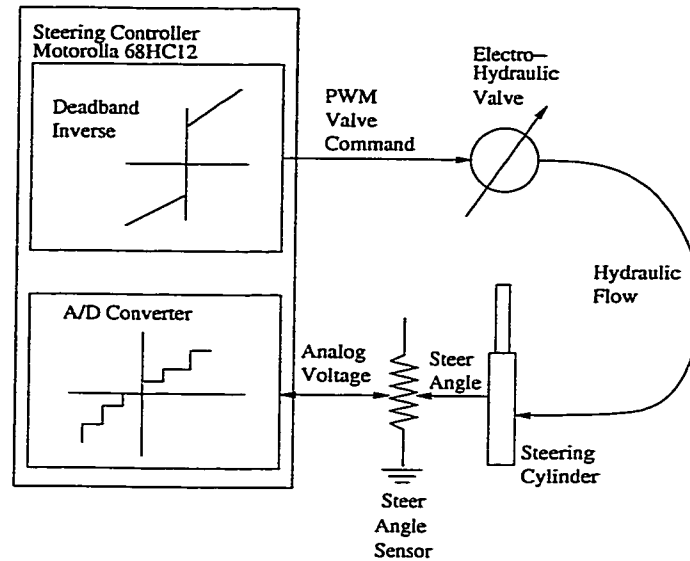


Figure 4.1: Steering Actuator

## 4.1 Steering Actuator Identification

The actuator on the John Deere test vehicles was a rather complex system. As shown in Figure 4.1 it consisted of a pair of hydraulic cylinders mounted between the axle and the steering knuckles. These cylinders adjusted the steering angle and were actuated by a pair of electric solenoids. Pulse width modulated (PWM) currents were driven into one of the two solenoids which opened a hydraulic valve allowing a controlled rate of fluid flow resulting in a slew rate at the wheels. A microcontroller serially connected to the control computer was used to generate the PWM signal. As a result, the overall system input was an integer  $(-255 - +255)$  generated by the control computer and the system response was a roughly proportional slew rate at the front wheels. The hydraulic steering system installed was of relatively low cost. Its low quality performance displayed a significant deadzone in the input /

output characteristics of the actuator system (see Figure 2.1). In addition to the deadzone, there existed relatively complex dynamics associated with the input to output response. These inexpensive units are expected to have significant variation from unit to unit. In a mass production setting, without some kind of parameter identification method, large variations would likely lead to degraded overall system performance.

Deadzone characteristics were identified in real time with the LMS algorithm. This algorithm was first presented in [RJP98]. In general, it breaks the non-linearities up into piecewise linear regions and identifies them separately.

For the purposes of the remainder of this section the basic system model illustrated in Figure 2.2 and Equation (2.1) will be used. The steepest descent method of the algorithm required a definition of an error paraboloid. If this surface were simply the overall error squared, the inclusion of the deadzone would make for a very complex error surface with many local minima. The piecewise linearity of the system make the error surface becomes much more manageable.

Consider any series of inputs that result in an output that resides in the upper portion of the deadzone. Also, assume the model parameters were fixed, as they would be if the model were already in its optimal state. The error surfaces could then be expressed as

$$\varepsilon \equiv y - \hat{y} = y - m(W^T U - b) \quad (4.1)$$

where

$\varepsilon$  is the instantaneous error in the output estimate,

$y$  is the measured response of the system,

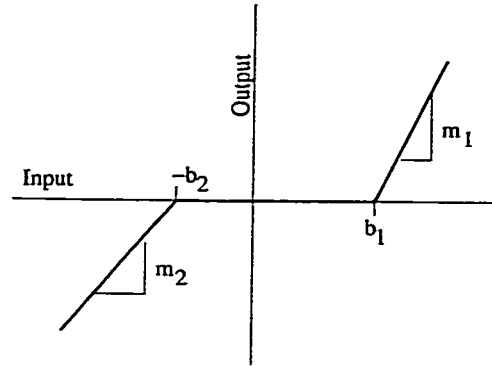


Figure 4.2: Deadzone Parameter Definition

$\hat{y}$  is the predicted response based on the most current model estimate and known input  $U$ ,

$m$  is the deadzone slope as shown in Figure 4.2,

$W$  is a vector of the FIR filter gains representing the dynamics of the system and

$b$  is the deadzone breakpoint.

Two error surfaces are defined to take advantage of the piece-wise linearity of the system. The first model ( $\varepsilon^{(+)}$ ) represents the system when a positive output is achieved and the other surface ( $\varepsilon^{(-)}$ ) matches the system with a negative response. Both systems share the same dynamic FIR filter,  $W$ .

It is the intention to minimize the expected mean squared error. This must be done independently with both error surfaces. To do this first square the upper error surface:

$$\varepsilon^{(+0)^2} = y^2 + m_1^2 W^T U U^T W + (m_1 b_1)^2 + 2 [y m_1 b_1 - (y m_1 - m_1^2 b_1) W^T U] \quad (4.2)$$

Then, take the expected value of  $\varepsilon$ :

$$\zeta = E[\varepsilon^2] = E[y^2] + m_1 W^T E[U U^T] W + (m_1 b_1)^2 - 2m_1 W^T (E[yU] + m_1 b_1 E[U]) \quad (4.3)$$

To simplify notation, introduce the autocorrelation and cross-correlation matrices of  $U$  as

$$\begin{aligned} R &\equiv E[U U^T] \\ P &\equiv E[(y + m_1 b_1) U] \end{aligned} \quad (4.4)$$

Making the appropriate substitutions in Equation (4.3) yields

$$\zeta = E[y^2] + m_1^2 W^T R W + (m_1 b_1)^2 - 2m_1 W^T P \quad (4.5)$$

Equation (4.5) shows that  $\zeta$  is quadratic in all the parameters. A simple differentiation yields the slope with respect to the FIR filter dynamic model

$$\nabla_W \equiv \frac{\partial \zeta}{\partial W} = 2m_1^2 R W - 2m_1 P \quad (4.6)$$

If the excitation signal is real, then  $R$  can be inverted [WS85] and this equation can be easily solved to yield the optimal weights for the FIR model

$$W^* = \frac{1}{m_1} R^{-1} P \quad (4.7)$$

The optimal states for the deadband parameters may also be obtained in the same

manner as for the dynamics. Remembering that

$$W^T U = X \quad (4.8)$$

the gradient with respect to the deadband slope is

$$\nabla_{m_1} = 2(m_1 b_1^2 + m_1 E[X^2] - W^T E[yU] - 2m_1 b_1 E[X]) \quad (4.9)$$

and the gradient with respect to the upper deadzone breakpoint is

$$\nabla_{b_1} = 2m_1(m_1 b_1 - m_1 E[X]) \quad (4.10)$$

Setting both these gradients equal to zero and solving for  $m_1^*$  and  $b_1^*$  yields the optimal deadzone parameters

$$\begin{aligned} m_1^* &= \frac{E[Xy]}{E[X^2] - (E[X])^2} \\ b_1^* &= E[X] \end{aligned} \quad (4.11)$$

This provides the optimal solution for each of the parameters in the upper portion of the deadzone. The derivation for the lower portion of the deadzone follows exactly as above with the appropriate parameter substitutions.

It is useful to notice that the magnitudes of the dynamic weights for the FIR filter and the deadzone parameters are interrelated. This is most easily seen in Equation (2.1). A scalar coefficient can be factored out and arbitrarily redistributed between both sets of parameters. An additional constraint is therefore needed. This constraint comes from a normalization of the FIR filter. This provides a relatively static gain

setting for both the dynamics model and the deadzone model.

The utility of this optimal solution is somewhat limited. One must know a great deal about the input and output characteristics of the plant in order to recover these optimal parameters. The LMS algorithm readily lends itself to this application.

#### 4.1.1 Actuator Parameter Gradient Estimation

The gradients expressed in Equations (4.6), (4.9) and (4.10) can be approximated by utilizing the LMS algorithm. To do this the model must be broken into three regions: positive measured output, negative output and zero output. The latter region provides no output excitation and therefore cannot be utilized for identification purposes. The prior two regions can individually be used to identify the portion of the model corresponding to the appropriate output region.

If the output is known to be in the upper band of the deadzone, i.e. it has resulted in positive measured output, then the gradient with respect to the weights can be approximated as

$$\hat{\nabla}_W = \frac{\partial \varepsilon^2}{\partial \varepsilon} \frac{\partial \varepsilon}{\partial \hat{y}} \frac{\partial \hat{y}}{\partial X} \frac{\partial X}{\partial W} = -2\varepsilon m_1 U \quad (4.12)$$

It is quite easy to show that for the upper deadzone case, the expected value of the gradient estimate is the true gradient

$$E \left[ \hat{\nabla}_W \right] = -2m_1 E [\varepsilon U] = 2m_1^2 R W - 2m_1 P = \nabla_W \quad (4.13)$$

Equation (4.13) shows that the estimate of  $\nabla_W$  is unbiased. As a result the estimate of  $W$  is also unbiased.



Similar methods as above are employed to estimate the gradients with respect to the deadzone parameters. For an output in the upper deadzone region

$$\begin{aligned}
\hat{\nabla}_{m_1} &= \frac{\partial \varepsilon^2}{\partial \varepsilon} \frac{\partial \varepsilon}{\partial \hat{y}} \frac{\partial \hat{y}}{\partial m_1} = -2\varepsilon W^T U \\
E \left[ \hat{\nabla}_{m_1} \right] &= 2 \left( b_1 E[y] + m_1 b_1^2 + m_1 E[X^2] - W^T E[yU] - 2m_1 b_1 E[X] \right) = \nabla_{m_1} \\
\hat{\nabla}_{b_1} &= \frac{\partial \varepsilon^2}{\partial \varepsilon} \frac{\partial \varepsilon}{\partial \hat{y}} \frac{\partial \hat{y}}{\partial b_1} = -2\varepsilon m_1 \\
E \left[ \hat{\nabla}_{b_1} \right] &= 2m_1 (E[y + m_1 b_1] - m_1 E[X]) = \nabla_{b_1}
\end{aligned} \tag{4.14}$$

Using the gradient estimates in Equations (4.12) and (4.14) the parameters may easily be updated each epoch

$$\begin{aligned}
W_{k+1} &= W_k + 2\mu_W \varepsilon_k m_{1,k} U_k \\
m_{1,k+1} &= m_{1,k} + 2\mu_{m_1} \varepsilon_k X_k \\
b_{1,k+1} &= b_{1,k} - 2\mu_{b_1} \varepsilon_k m_{1,k}
\end{aligned} \tag{4.15}$$

For outputs that are known to be in the lower deadband zone, the updates are nearly identical to those in (4.15) with  $m_2$  replacing  $m_1$  and  $b_2$  replacing  $b_1$ .

### 4.1.2 Actuator Model Stability

The convergence rate and stability of each of the parameters is controlled by the character of the inputs and the learning coefficient,  $\mu$ . A large value of  $\mu$  will

yield rapid convergence but may drive the algorithm to instability, or at the least be overly sensitive to noisy data and provide a large amount of random walk about the minimum. On the other hand, a small learning coefficient will provide little random walk and ensure stability but yield very slow learning and poor tracking performance for non-stationary systems.

To determine the bounds for the learning coefficient associated with the dynamic model a change of coordinates similar to the one put forth in Section 3.2.2 is proposed

$$V_k^W = W_k - W_k^* \quad (4.16)$$

The expected value of the next weight vector is

$$E [V_{k+1}^W] = (I - 2\mu_W m^2 R) E [V_k^W] \quad (4.17)$$

For the purpose of this analysis,  $m$  can be either the upper or the lower deadband region dependant on which region the output lies in. It can now be seen that the expected value of the weight vector at any iteration can be calculated from any prior error (provided the output remains entirely within either the upper or lower deadband regions for the duration between sample  $k$  and sample  $k + n$ .)

$$E [V_{k+n}^W] = (I - 2\mu_W m^2 R)^n V_k^W \quad (4.18)$$

From this equation the interrelation between the learning coefficient and the character of the inputs (manifesting themselves within  $R$ ) can be seen. For stability, each

eigenvalue of  $(I - 2\mu_W m^2 R)$  must be less than 1. This puts the constraints

$$0 < \mu_W < \frac{1}{m^2 \lambda_{max}} \quad (4.19)$$

on the learning coefficient.

A similar approach is taken to reveal the stability requirements for the deadband slope.

$$V^m = m - m^* \quad (4.20)$$

$$E[V_{k+n}^m] = (1 - 2\mu_m (b^2 + E[X^2] - 2bE[X]))^n V_k^m \quad (4.21)$$

$$0 < \mu_m < \frac{1}{b^2 + E[X^2] - 2bE[X]} \quad (4.22)$$

For the deadband width,

$$V^b = b - b^* \quad (4.23)$$

$$E[V_{k+n}^b] = (1 - 2\mu_b m^2)^n V_k^b \quad (4.24)$$

$$0 < \mu_b < \frac{1}{m^2} \quad (4.25)$$

A small note of caution for the actual implementation of this algorithm is in order.

As illustrated above, the only time the actual identification takes place is when an output is measured. When no output is measured, one can make no inferences about the intermediate parameter,  $X$ . Because no information about the internal state of the system can be made, identification can only be done during times of output excitation.

## 4.2 Vehicle Steering Dynamics Identification

In a field environment, the main vehicle control is the steering wheel. The operator typically selects a constant speed to maximize the efficiency of the current operation and steers the tractor around the field to complete the day's objectives. It is therefore apparent that a thorough understanding of the vehicle's steering dynamics is necessary for accurate control. A complication to this is the fact that the steering dynamics of the vehicle are very dependent on vehicle configuration and operating conditions.

### 4.2.1 O'Connor Parameter Identification

There are many possible methods to identify the parameters in Equation (2.7). The method presented here is a two step method utilizing a standard Kalman filter to estimate the states of the system, and the LMS algorithm (utilizing the estimated states) to estimate the parameters. In doing this, a large and very non-linear EKF is avoided.

The first part of the algorithm is to generate state estimates using a standard EKF based on the states in Equation (2.7). If the Kalman filter is not using the "optimal" values, there will be a mismatch in the dynamics of the filter and the dynamics of the system. The mismatch will cause a serial correlation in the innovation. The

information provided by this correlation is leveraged to back out a better estimate of the parameters.

In the experimental vehicle, measurements of position, heading and steer angle were available. The observation vector was therefore defined as

$$z = \begin{bmatrix} E \\ N \\ \Psi \\ \delta \end{bmatrix} \quad (4.26)$$

The dynamics of the system manifested themselves as differences between subsequent measurements. The error was therefore defined as

$$\varepsilon_k \equiv \begin{bmatrix} \varepsilon_k^E \\ \varepsilon_k^N \\ \varepsilon_k^\Psi \\ \varepsilon_k^\delta \end{bmatrix} = (z_k - z_{k-1}) - C \left( X_k^{(-)} - X_{k-1}^{(+)} \right) = \Delta z_k - \Delta \hat{z}_k \quad (4.27)$$

where

$Z$  was an unbiased measurement vector,

$C$  was the observation matrix

$$C = \begin{bmatrix} 1 & 0 & 0 & 0 & 0 & 0 & 0 & 0 & 0 \\ 0 & 1 & 0 & 0 & 0 & 0 & 0 & 0 & 0 \\ 0 & 0 & 1 & 0 & 0 & 0 & 1 & 0 & 0 \\ 0 & 0 & 0 & 0 & 1 & 0 & 0 & 1 & 0 \end{bmatrix} \quad (4.28)$$

and  $X_k^{(-)}$  and  $X_k^{(+)}$  are the estimates of the state at time step  $k$  before and after the measurement update. The components of the  $X$  vector are

$$X = \begin{bmatrix} E & N & \Psi & \Omega & \delta & \omega \end{bmatrix}^T \quad (4.29)$$

with the same state definitions as in Equation (2.2).

With these definitions, the performance cost function may be defined as the expected power of the error

$$J \equiv E [\varepsilon^T \varepsilon] \quad (4.30)$$

If the identified parameters accurately represent the system dynamics, the error will contain only system noise and introduce no bias. [Ste94b] When the parameters are misidentified, there will exist a strong correlation between the system input and the error in the prediction of state movement. It is this correlation that is used to adjust the model to best fit the system.

If each component of  $\varepsilon$  were independent, an independent minimization of each component would yield an overall minimization of  $J$ . The components of  $\varepsilon$  are not independent in this case but they are also not strongly coupled together. If the gradients of the errors are calculated as in [Kel93] with nominal values of  $p =$

$\begin{bmatrix} -0.2, 3.5, 1.8, 1.7 \end{bmatrix}^T$  the results are

$$\begin{aligned}
\frac{\partial \varepsilon^{E,N}}{\partial p_2} &= -0.14\Omega - 0.0289\delta - 0.001865\omega - 0.0001667u \\
\frac{\partial \varepsilon^{E,N}}{\partial p_3} &= -0.00349\Omega - 0.00043\delta - 0.000021\omega - 0.00144u \\
\frac{\partial \varepsilon^{E,N}}{\partial p_4} &= 0.0043\delta + 0.00026\omega + 0.000022u \\
\frac{\partial \varepsilon^{E,N}}{\partial p_5} &= -0.000022\omega + 0.000022u \\
\\
\frac{\partial \varepsilon^\Psi}{\partial p_2} &= 0 \\
\frac{\partial \varepsilon^\Psi}{\partial p_3} &= -0.0127\Omega - 0.00172\delta - 0.000085\omega - 0.00615u \\
\frac{\partial \varepsilon^\Psi}{\partial p_4} &= 0.016\delta + 0.0010\omega + 0.000092u \\
\frac{\partial \varepsilon^\Psi}{\partial p_5} &= -0.000091\omega + 0.000092u \\
\\
\frac{\partial \varepsilon^\delta}{\partial p_2} &= 0 \\
\frac{\partial \varepsilon^\delta}{\partial p_3} &= 0 \\
\frac{\partial \varepsilon^\delta}{\partial p_4} &= 0 \\
\frac{\partial \varepsilon^\delta}{\partial p_5} &= 0.016\omega + 0.016u
\end{aligned} \tag{4.31}$$

As shown in Equation (4.31), each parameter in the model has a strong primary affect on either one or two specific errors and a much weaker influence on the others. To aid in the identification the weak cross couplings were assumed to be negligible.

|                      | $p_2$ | $p_3$ | $p_4$ | $p_5$ |
|----------------------|-------|-------|-------|-------|
| $\varepsilon^E$      | X     |       |       |       |
| $\varepsilon^N$      | X     |       |       |       |
| $\varepsilon^\Psi$   |       | X     | X     |       |
| $\varepsilon^\delta$ |       |       |       | X     |

Table 4.1: Primary Parameter Influences on Measurement Errors

Table 4.1 illustrates which errors are primarily influenced by the various parameters.

### Identification of $p_2$

The parameter  $p_2$  can be interpreted as the influence of yaw rate on the lateral velocity. This parameter manifested itself primarily in two states, E and N, requiring two measurements to be used for identification. The error cost equation used for identification of  $p_2$  was

$$J^{E,N} = \varepsilon_k^{E,NT} \varepsilon_k^{E,N} \quad (4.32)$$

where

$$\varepsilon_k^{E,N} = \begin{bmatrix} \varepsilon_k^E \\ \varepsilon_k^N \end{bmatrix} \quad (4.33)$$

Calculating the gradient of  $J^{E,N}$  with respect to  $p_2$  yields

$$\frac{\partial J^{E,N}}{\partial p_2} = \frac{\partial J^{E,N}}{\partial \varepsilon_k^{E,N}} \frac{\partial \varepsilon_k^{E,N}}{\partial \Delta \hat{X}_k} \frac{\partial \Delta \hat{X}_k}{\partial p_2} = -2\varepsilon_k^{E,NT} \frac{\partial \Delta \hat{X}_k}{\partial p_2} \quad (4.34)$$



To a first order trapezoidal approximation

$$\frac{\partial \Delta \hat{X}_k}{\partial p_2} \approx \frac{\Delta t}{2} \left( \hat{\Omega}_k^{(+)} \begin{bmatrix} -\cos \hat{\Psi}_k^{(+)} \\ \sin \hat{\Psi}_k^{(+)} \end{bmatrix} + \hat{\Omega}_{k-1}^{(+)} \begin{bmatrix} -\cos \hat{\Psi}_{k-1}^{(+)} \\ \sin \hat{\Psi}_{k-1}^{(+)} \end{bmatrix} \right) \quad (4.35)$$

From this result, Newton's method can be used for updating  $p_2$

$$p_2 = p_2 + \mu_2 \Delta t \left[ \varepsilon_k^N \left( \hat{\Omega}_k^{(+)} \sin \hat{\Psi}_k^{(+)} + \hat{\Omega}_{k-1}^{(+)} \sin \hat{\Psi}_{k-1}^{(+)} \right) - \varepsilon_k^E \left( \hat{\Omega}_k^{(+)} \cos \hat{\Psi}_k^{(+)} + \hat{\Omega}_{k-1}^{(+)} \cos \hat{\Psi}_{k-1}^{(+)} \right) \right] \quad (4.36)$$

### Identification of $p_3$ and $p_4$

$p_3$  is the inverse of the time constant associated with the lag between the actual yaw rate and the steady state yaw rate while  $p_4$  defines the yaw acceleration achieved from a given forward speed and steer angle. The gradients of  $\varepsilon^\Psi$  with respect to  $p_3$  and  $p_4$  were calculated as follows:

$$\begin{aligned} \frac{\partial (\varepsilon_k^\Psi)^2}{\partial p_3} &= \frac{\partial (\varepsilon_k^\Psi)^2}{\partial \varepsilon_k^\Psi} \frac{\partial \varepsilon_k^\Psi}{\partial \Delta \hat{\Psi}_k} \frac{\partial \Delta \hat{\Psi}_k}{\partial p_3} = -2\varepsilon_k^\Psi \frac{\partial \Delta \hat{\Psi}_k}{\partial p_3} \\ \frac{\partial (\varepsilon_k^\Psi)^2}{\partial p_4} &= \frac{\partial (\varepsilon_k^\Psi)^2}{\partial \varepsilon_k^\Psi} \frac{\partial \varepsilon_k^\Psi}{\partial \Delta \hat{\Psi}_k} \frac{\partial \Delta \hat{\Psi}_k}{\partial p_4} = -2\varepsilon_k^\Psi \frac{\partial \Delta \hat{\Psi}_k}{\partial p_4} \end{aligned} \quad (4.37)$$

Again using trapezoidal integration

$$\begin{aligned} \frac{\partial \Delta \hat{\Psi}_k}{\partial p_3} &\approx -\frac{\Delta t^2}{4} \left( \hat{\Omega}_k^{(+)} + \hat{\Omega}_{k-1}^{(+)} \right) \\ \frac{\partial \Delta \hat{\Psi}_k}{\partial p_4} &\approx \frac{\Delta t^2}{4} V_x \left( \hat{\delta}_k^{(+)} + \hat{\delta}_{k-1}^{(+)} \right) \end{aligned} \quad (4.38)$$

Resulting in update equations of

$$\begin{aligned} p_3 &= p_3 - \mu_{3,4} \varepsilon_k^\Psi \frac{\Delta t^2}{2} \left( \hat{\Omega}_k^{(+)} + \hat{\Omega}_{k-1}^{(+)} \right) \\ p_4 &= p_4 + \mu_{3,4} \varepsilon_k^\Psi \frac{\Delta t^2}{2} V_x \left( \hat{\delta}_k^{(+)} + \hat{\delta}_{k-1}^{(+)} \right) \end{aligned} \quad (4.39)$$

### Identification of $p_5$

The parameter  $p_5$  represents the lag between the actual steer angle slew rate and the steady state rate. This parameter manifests itself mainly in the steering angle error,  $\varepsilon^\delta$ . The gradient is

$$\frac{\partial \varepsilon_k^{\delta^2}}{\partial p_5} = \frac{\partial \varepsilon_k^{\delta^2}}{\partial \varepsilon_k^\delta} \frac{\partial \varepsilon_k^\delta}{\partial \Delta \hat{\delta}_k} \frac{\partial \Delta \hat{\delta}_k}{\partial p_5} = -2\varepsilon_k^\delta \frac{\partial \Delta \hat{\delta}_k}{\partial p_5} \quad (4.40)$$

The trapezoidal integration is slightly different in this step due to the addition of the zero order hold on the input. The input,  $u$ , is held constant throughout the epoch and therefore needs no averaging.

$$\frac{\partial \Delta \hat{\delta}_k}{\partial p_5} \approx -\frac{\Delta t^2}{4} \left( \hat{\omega}_k^{(+)} + \hat{\omega}_{k-1}^{(+)} - 2u_{k-1} \right) \quad (4.41)$$

Leaving the final update equation as

$$p_5 = p_5 - \mu_5 \varepsilon_k^\delta \frac{\Delta t^2}{2} \left( \hat{\omega}_k^{(+)} + \hat{\omega}_{k-1}^{(+)} - 2u_{k-1} \right) \quad (4.42)$$

### 4.2.2 Stability Of Parameters

The characterization of the requirements for stability on the identified parameters is an important part of the identification process. The stability of each of these parameters is determined by the learning coefficient,  $\mu$ , and the nature of the inputs. Because the nature of the inputs is constrained by the guidance requirements, the main engineering design consideration is the learning coefficient.

#### Stability of $p_2$

Begin by defining the change of coordinates for this parameter

$$V^{p_2} = p_2 - p_2^* \quad (4.43)$$

and examine the update equation

$$\begin{aligned} V_{k+1}^{p_2} = p_{2,k+1} - p_2^* = V_k^{p_2} + 2\mu_2 \Delta t \varepsilon_k^N \left( \Omega_k^{(+)} \sin \Psi_k^{(+)} + \Omega_{k-1}^{(+)} \sin \Psi_{k-1}^{(+)} \right) \\ - 2\mu_2 \Delta t \varepsilon_k^E \left( \Omega_k^{(+)} \cos \Psi_k^{(+)} + \Omega_{k-1}^{(+)} \cos \Psi_{k-1}^{(+)} \right) \end{aligned} \quad (4.44)$$

Using the trapezoidal approximation and assuming small time steps,  $\varepsilon^E$  and  $\varepsilon^N$  can be approximated by

$$\begin{aligned} \varepsilon_k^E = \Delta E_k - \Delta \hat{E}_k \approx \frac{\Delta t}{2} \left( \Omega_k^{(+)} \sin \Psi_k^{(+)} + \Omega_{k-1}^{(+)} \sin \Psi_{k-1}^{(+)} \right) V_k^{p_2} + noise \\ \varepsilon_k^N = \Delta N_k - \Delta \hat{N}_k \approx -\frac{\Delta t}{2} \left( \Omega_k^{(+)} \cos \Psi_k^{(+)} + \Omega_{k-1}^{(+)} \cos \Psi_{k-1}^{(+)} \right) V_k^{p_2} + noise \end{aligned} \quad (4.45)$$

combining these equations and taking the expected value of the next parameter error yields

$$E[V_{k+1}^{p_2}] = (1 - \mu_2 \Delta t^2 R_2) V_k^{p_2} \quad (4.46)$$

where

$$R_2 = E \left[ \left( \Omega_k^{(+)} \cos \Psi_k^{(+)} + \Omega_{k-1}^{(+)} \cos \Psi_{k-1}^{(+)} \right)^2 + \left( \Omega_k^{(+)} \sin \Psi_k^{(+)} + \Omega_{k-1}^{(+)} \sin \Psi_{k-1}^{(+)} \right)^2 \right]$$

As before, this places the following constrain on  $\mu_2$

$$0 \leq \mu_2 \frac{\Delta t^2}{2} \leq \frac{1}{R_2} \quad (4.47)$$

### Stability of $p_3$ and $p_4$

The change of coordinates used in this section will be

$$V^{3,4} = \begin{bmatrix} p_3 \\ p_4 \end{bmatrix} - \begin{bmatrix} p_3^* \\ p_4^* \end{bmatrix} \quad (4.48)$$

Utilizing the update equations from above, the parameter error updates as

$$V_{k+1}^{p_3, p_4} = V_k^{3,4} + \mu_{3,4} \frac{\Delta t^2}{2} \begin{bmatrix} \Psi_k^{(+)} + \Psi_{k-1}^{(+)} \\ \delta_k^{(+)} + \delta_{k-1}^{(+)} \end{bmatrix} \varepsilon_k^\Psi \quad (4.49)$$

The error can be approximated as

$$\varepsilon_k^\Psi = \Delta \Psi_k - \Delta \hat{\Psi}_k \approx \frac{\Delta t^2}{4} \begin{bmatrix} (\Omega_k^{(+)} + \Omega_{k-1}^{(+)} & (\delta_k^{(+)} + \delta_{k-1}^{(+)} \end{bmatrix}^T V_k^{p_3, p_4} + noise \quad (4.50)$$

and the expected value of the next parameter error can be expressed as

$$E[V_{k+1}^{p_3, p_4}] = \left( I - \mu_{3,4} \frac{\Delta t^4}{8} R_{3,4} \right) V_k^{p_3, p_4} \quad (4.51)$$

where

$$R_{3,4} = E \begin{bmatrix} \left( \Omega_k^{(+)} + \Omega_{k-1}^{(+)} \right)^2 & \left( \Omega_k^{(+)} + \Omega_{k-1}^{(+)} \right) \left( \delta_k^{(+)} + \delta_{k-1}^{(+)} \right) \\ \left( \Omega_k^{(+)} + \Omega_{k-1}^{(+)} \right) \left( \delta_k^{(+)} + \delta_{k-1}^{(+)} \right) & \left( \delta_k^{(+)} + \delta_{k-1}^{(+)} \right)^2 \end{bmatrix}$$

therefore, the stability limits for  $\mu_{3,4}$  are

$$0 \leq \mu_{3,4} \frac{\Delta t^4}{16} \leq \frac{1}{\lambda_{max}} \quad (4.52)$$

where  $\lambda_{max}$  is the largest eigenvalue of  $R_{3,4}$ . The matrix  $R_{3,4}$  is solely a function of the rates of change in the states. When there is little change in the states, the eigenvalues of  $R_{3,4}$  become very small. This may lead one to believe the best time to identify  $p_3$  and  $p_4$  would be when the vehicle is nearly stationary. As will be shown in Section 4.6 this would be a bad idea. At low speeds, the sensor noise overpowers the identification process so that little effective identification can be achieved.

### Stability of $p_5$

The change for  $p_5$  is

$$V^{p_5} = p_5 - p_5^* \quad (4.53)$$

Utilizing the update equation, the parameter error updates as

$$V_{k+1}^{p_5} = V_k^{p_5} - \mu_5 \frac{\Delta t^2}{2} \varepsilon_k^\delta \left( \omega_k^{(+)} + \omega_{k-1}^{(+)} - 2u_{k-1} \right) \quad (4.54)$$

The steering angle estimate error may be approximated as

$$\varepsilon_k^\delta = \Delta\delta_k - \Delta\hat{\delta}_k \approx \frac{\Delta t^2}{4} \left( \omega_k^{(+)} + \omega_{k-1}^{(+)} - 2u_{k-1} \right) V_k^{p_5} + noise \quad (4.55)$$

and the expected value of the next estimate can be expressed as

$$E[V_{k+1}^{p_5}] = \left( 1 - \mu_5 \frac{\Delta t^4}{8} R_5 \right) V_k^{p_5} \quad (4.56)$$

where

$$R_5 = E \left[ \left( \omega_k^{(+)} + \omega_{k-1}^{(+)} - 2u_{k-1} \right)^2 \right]$$

indicating that the stability limits for  $\mu_5$  are

$$0 \leq \mu_5 \frac{\Delta t^4}{16} \leq \frac{1}{R_5} \quad (4.57)$$

As with the steering deadband identification, one must constantly excite the dynamics in order to identify them reliably. Unfortunately, many tractors spend much of their time driving in straight lines. When the vehicle is driving in a straight line the learning coefficients should be made relatively small (or turned off) in order to keep the identified parameters from wandering.

A Caveat: When this algorithm is used for adaptive control of the vehicle there arises a danger of divergent behavior when the estimate of  $p_5$  is larger than the actual value. A larger estimate causes a bang-bang type of behavior in the control input. This greatly increases the value of  $R_5$  causing a subsequent decrease in the stability limits in Equation (4.57). A better approach to identifying  $p_5$  is to constrain the value of  $R_5$  by applying the signum function to the inputs and to utilize the update

equation

$$p_5 = p_5 - \mu_5 \varepsilon_k^\delta \frac{\Delta t^2}{2} \text{sgn} \left( \hat{\omega}_k^{(+)} + \hat{\omega}_{k-1}^{(+)} - 2u_{k-1} \right) \quad (4.58)$$

This change results in a new expression for  $R_5$

$$R_5 = E \left[ \text{sgn} \left( \omega_k^{(+)} + \omega_{k-1}^{(+)} - 2u_{k-1} \right)^2 \right] = 1 \quad (4.59)$$

This minor change produces a more consistent stability range for  $\mu_5$  and can increase the robustness of the identification of  $p_5$  dramatically.

### 4.3 Vehicle Longitudinal Dynamics Identification

To control the position of a tractor reliably in formation with another, both the steering dynamics and the longitudinal dynamics must be understood. The difficulty associated with a farm tractor is that the amount of tire slip varies a great deal during operation. Fortunately, the longitudinal dynamics of a farm tractor may be quite simply and reasonably accurately modeled utilizing Equation (2.6).

#### 4.3.1 Longitudinal Parameter Identification

When Equation (2.6) is discretized for a time step of  $\Delta t$  seconds, the time update equation is

$$V_{x,k+1} = \phi V_{x,k} + \kappa_g (1 - \phi) \omega_{command} \quad (4.60)$$

where  $\phi = e^{-\frac{\Delta t}{\tau_g}}$

A good measure of performance is the difference between the measured value of  $V_{x,k}$  and the predicted value. The approach is to use the same methods as presented in Sections 4.1 and 4.2. Actually calculating the error is slightly more difficult in this case as there is no direct measurement available. The error used is the difference in state estimates after and before the measurement update

$$\varepsilon_k \equiv \frac{1}{\Delta t} \sqrt{\Delta E_k^2 + \Delta N_k^2} - V_{x,k}^{(-)} \quad (4.61)$$

This error is different than the error in 4.2.1 since there is no direct measurement of velocity unlike the other states in that section. There is, however, a very accurate measurement of position which can be easily differenced for an estimate of velocity.

The gradient of the error with respect to  $\kappa_g$  can be calculated quite easily by assuming that  $\frac{\partial V_x^{(+)}}{\partial \kappa_g}$  is small and using the chain rule.

$$\frac{\partial \varepsilon^2}{\partial \kappa_g} = \frac{\partial \varepsilon^2}{\partial \varepsilon} \frac{\partial \varepsilon}{\partial V_x^{(-)}} \frac{\partial V_x^{(-)}}{\partial \kappa_g} = -2\varepsilon_k \left(1 - e^{-\frac{\Delta t}{\tau}}\right) \omega_{command} \quad (4.62)$$

This produces in the update equation:

$$\kappa_g = \kappa_g - 2\mu_\kappa \varepsilon_k \left(1 - e^{-\frac{\Delta t}{\tau}}\right) \omega_{command} \quad (4.63)$$

It is very difficult to determine a learning equation with respect to  $\tau$  that has reasonable form to analyze stability. As an alternative, the stability with respect to  $\phi$  is relatively straightforward to analyze. Also, it is quite easy to see that stability in  $\phi$  assures stability in  $\tau$  as it is a simple function of  $\tau$ . For these reasons, the parameter



$\phi$  is directly identified and  $\tau$  is inferred from it. The gradient of the error with respect to  $\phi$  is

$$\frac{\partial \varepsilon^2}{\partial \phi} = \frac{\partial \varepsilon^2}{\partial \varepsilon} \frac{\partial \varepsilon}{\partial V_{x,k}^{(-)}} \frac{\partial V_{x,k}^{(-)}}{\partial \phi} = 2\varepsilon_k \left( \kappa_g \omega_{command} - V_{x,k-1}^{(+)} \right) \quad (4.64)$$

Resulting in the update equation

$$\phi = \phi - 2\mu_\phi \varepsilon_k \left( V_{x,k-1}^{(+)} - \kappa_g \omega_{command} \right) \quad (4.65)$$

### 4.3.2 Longitudinal Parameter stability

As in the previous sections, the clearest way to express the stability of the identification of the longitudinal parameters is to use a change in coordinates to be centered on the optimal estimate of  $\kappa$ . For the effective gear ratio, the translated state will be

$$V^{\kappa_g} = \kappa_g - \kappa_g^* \quad (4.66)$$

and the update equation will be

$$V_{k+1}^{\kappa_g} = V_k^{\kappa_g} - 2\mu_\kappa \varepsilon_k (1 - \phi) \omega_{command} \quad (4.67)$$

The error can be approximated as

$$\varepsilon_k \approx (1 - \phi) \omega_{command} V_k^{\kappa_g} \quad (4.68)$$

which yields an expected value for the next parameter error of

$$E[V_{k+1}^{\kappa_g}] = (1 - 2\mu_\kappa (1 - \phi)^2 R_\kappa) V_k^{\kappa_g} \quad (4.69)$$

with  $R_\kappa = E[\omega_{command}^2]$ . From this, the stability limits for  $\mu_\kappa$  can be easily determined

$$0 \leq \mu_\kappa \leq \frac{1}{(1 - \phi)^2 R_\kappa} \quad (4.70)$$

The analysis for the stability of  $\phi$  is similar to the other parameters. First, define a coordinate transformation:

$$V^{\phi_g} = \phi_g^* - \phi_g; \quad (4.71)$$

the update equation will then be

$$V_{k+1}^{\phi_g} = V_k^{\phi_g} - 2\mu_\phi \varepsilon_k \left( V_{x,k}^{(+)} - \kappa_g \omega_{command} \right) \quad (4.72)$$

with an approximation for the error as

$$\varepsilon_k \approx V_k \left( V_{x,k}^{(+)} - \kappa_g \omega_{command} \right) \quad (4.73)$$

substituting Equation (4.73) into (4.72) and taking the expected value yields

$$E[V_{k+1}^{\phi_g}] = (1 - 2\mu_\phi R_\phi) V_k^{\phi_g} \quad (4.74)$$

with  $R_\phi = E \left[ \left( V_{x,k}^{(+)} - \kappa_g \omega_{command} \right)^2 \right]$  from this, the stability is

$$0 \leq \mu_\psi \leq \frac{1}{R_\phi} \quad (4.75)$$

Because  $\kappa_g$  is effectively a gain factor from engine RPM to ground speed, the ground speed need not constantly change in order to identify this parameter. The time lag parameter  $\tau_g$  (identified through  $\phi_g$ ), on the other hand, must be exercised through varying ground speed to be correctly identified.

## 4.4 Vehicle Parameter Identifiability

Just as observability is important in state estimators, identifiability is important in identification algorithms. Grewal and Glover [GG76] and Reid [Rei77] illustrate a method of quantifying the identifiability of a parameter using the derivatives of the Markov parameters of the system. The Markov matrix is formed as:

$$M = \begin{bmatrix} CB \\ CAB \\ CA^2B \\ \vdots \\ CA^{2n-1}B \end{bmatrix} \quad (4.76)$$

For purposes of this discussion, the identifiability will be defined as the derivative of the norm of the singular value decomposition (SVD) of  $M$  with respect to the

parameter. The more identifiable a parameter is, the less sensitive the parameter estimate is to noise and disturbances.

As will be shown in Section 5.2, several of the experimental vehicle parameters proved relatively difficult to identify. This proves to be only a minor inconvenience if one takes into account the sensitivity of the system to accurate estimates. The sensitivity is defined as the derivative of the norm of the SVD of the Controllability matrix with respect to the parameter. The Controllability matrix is defined as:

$$C = \begin{bmatrix} B \\ AB \\ A^2B \\ \vdots \\ A^{n-1}B \end{bmatrix} \quad (4.77)$$

The difficulty of identification (defined as the inverse of identifiability) is plotted versus the system sensitivity is shown in Figure 4.3. The parameter values used to generate this graph were reasonable values reflecting the dynamics of the experimental vehicle.

In this graph, the further to the right the parameter is, the more important it is to accurately identify the parameter. The higher the parameter is the more difficult it is to accurately identify. In the experimental vehicle the more difficult parameters to identify are also the least important to identify accurately.

$P_5$ , the lag in the steering response, proves to be the factor most important to be identified accurately. The overall system is very sensitive to variations in this

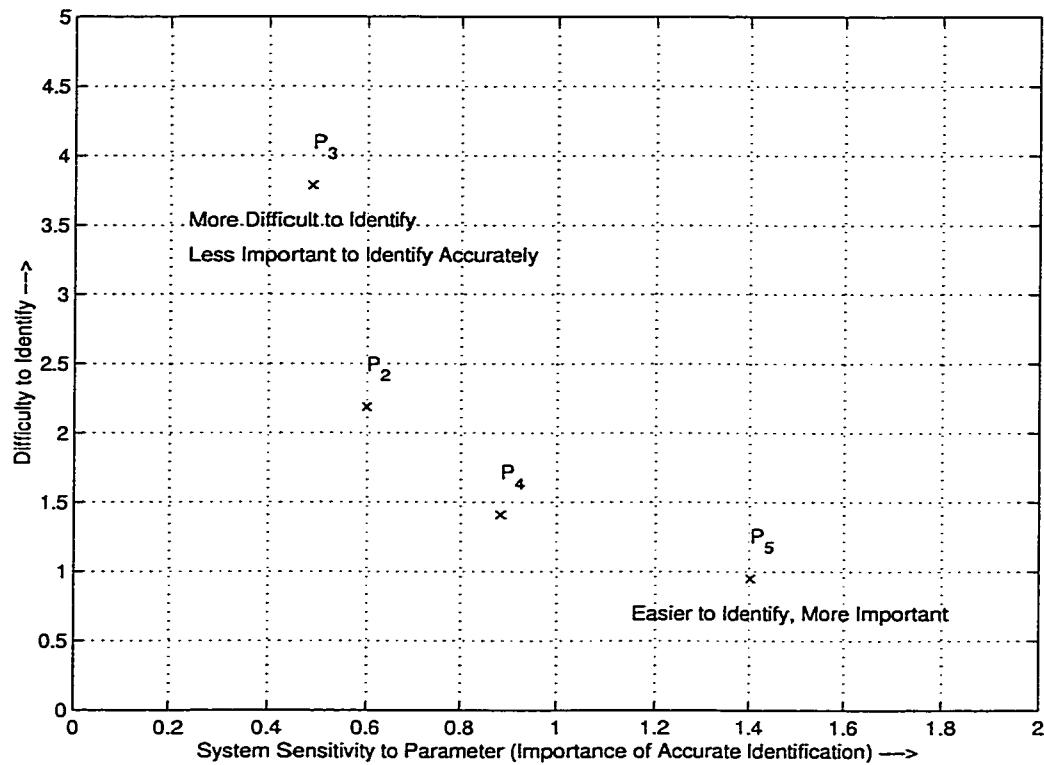


Figure 4.3: Parameter Identification Cost Trade off with  $p_2 = -0.2$ ,  $p_3 = 3.5$ ,  $p_4 = 1.8$  and  $p_5 = 1.7$

parameter. This is to be expected. The lateral dynamics of a farm tractor consist of basically a series of integrations between the input slew rate and the output position. Any change in this parameter is going to be integrated several times.  $P_5$  is also very identifiable. This is due to its close proximity to the input and one of the sensors. The steering angle and slew rate can be very accurately estimated and consequently,  $p_5$  can be accurately identified. As will be shown in Section 5.2 the estimate of  $p_5$  can quickly converge to a very smooth estimate

$P_3$ , the damping in the yaw response, is significantly more difficult to identify. This is due to the inability to estimate accurately the yaw rate of the vehicle. This system is very insensitive to yawing accelerations. It takes a large change in steer angle and consequently a very large slew rate to induce a substantial acceleration in the heading of the vehicle. It is very difficult to incur much energy in the  $\Omega$  state. In addition to the low power in the primary state, there is no direct measurement of the yaw rate. The estimate of the yaw rate comes from differentiating the position data twice, the heading measurement once and integrating the steer angle. The result is a very poor signal to noise ratio in the yaw rate. The identifiability of  $p_3$  can be substantially improved by adding a yaw rate measurement (see Figure 4.4.)

## 4.5 Parameter Identification Computation

In farm tractor steering parameter identification the LMS/EKF algorithm offers substantial computational saving over the traditional PP-EKF. Table 4.2 illustrates the computational requirements at each time step for each method. The LMS/EKF algorithm requires significantly fewer operations. This is due to two primary features. First, the PP-EKF algorithm requires the gradients of the discrete time models with

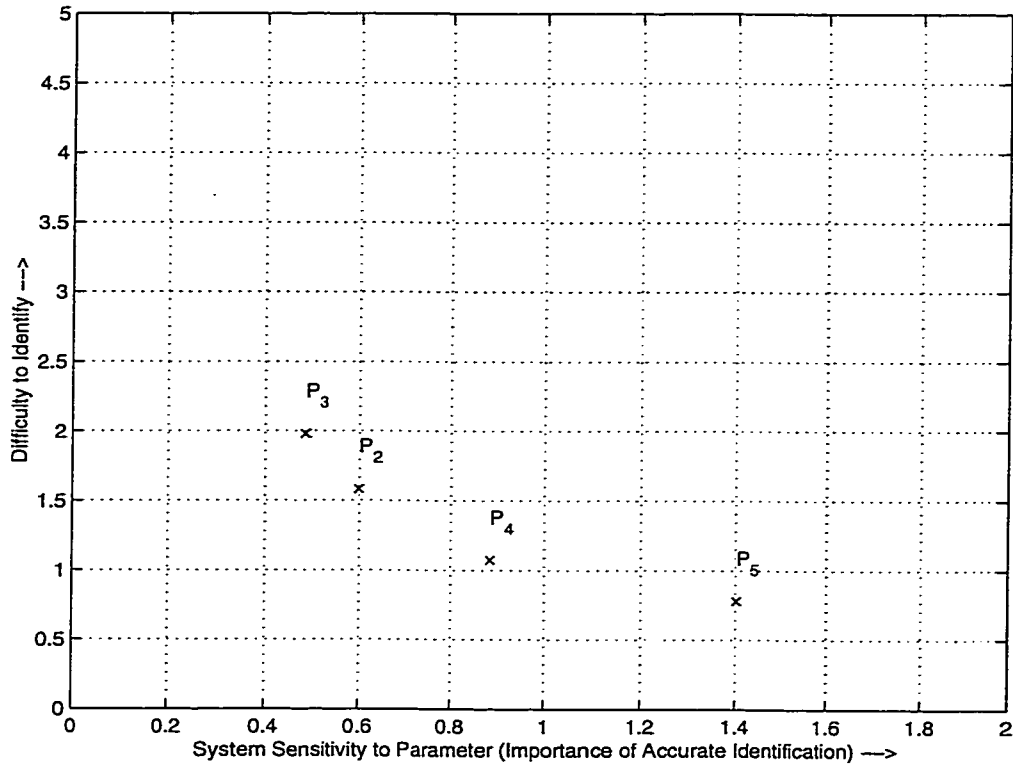


Figure 4.4: Parameter Identification Cost Trade off with Yaw Rate Measurement

|                    | PP-EKF  | LMS/EKF | Improvement |
|--------------------|---------|---------|-------------|
| Filter Setup       | 210,271 | 9,551   | 95.5 %      |
| Time Update        | 5,766   | 1,743   | 69.8 %      |
| Measurement Update | 6,844   | 2,865   | 58.1 %      |
| Total              | 222,881 | 14,159  | 93.6 %      |

Table 4.2: Floating Point Operations Count for PP-EKF and LMS/EKF Algorithms

respect to the continuous time parameters be calculated every epoch. The LMS/EKF algorithm approximates this calculation during the parameter update step. Secondly, the PP-EKF algorithm extends the states to include the parameters. Matrix multiplication is an  $O(N^3)$  operation. Every parameter that is added to the state vector substantially increases the computational requirements. The LMS/EKF algorithm foregoes this extension to the states by identifying the parameters in parallel with the states rather than concurrently.

## 4.6 Parameter Identification With Realistic Paths

The ability to identify accurately the dynamic parameters is strongly dependent on the ability to excite important states enough to provide a strong signal to noise ratio. A large signal to noise ratio usually results in a good parameter estimate. It is usually not possible to decrease sensor noise. Typically, in order to improve the signal to noise ratio, the dynamics of the system must be energized. This energizing of the states is often achieved through adding a small amount of random noise or dither into the input. The effect of this dither is to increase the energy in the system at the cost of reduced controller accuracy.

During simulation it is possible to achieve exact knowledge of all states resulting in an infinite signal to noise ratio. In a realistic setting this is much more difficult. There are, however, certain trajectories that increase the energy in the various states and, conversely, other trajectories with little energy associated with these states. Identification of when these conditions occur will indicate optimal times to identify parameters without adding undesirable dither.

Equations (4.36), (4.39) and (4.42) show which states need to be energized for



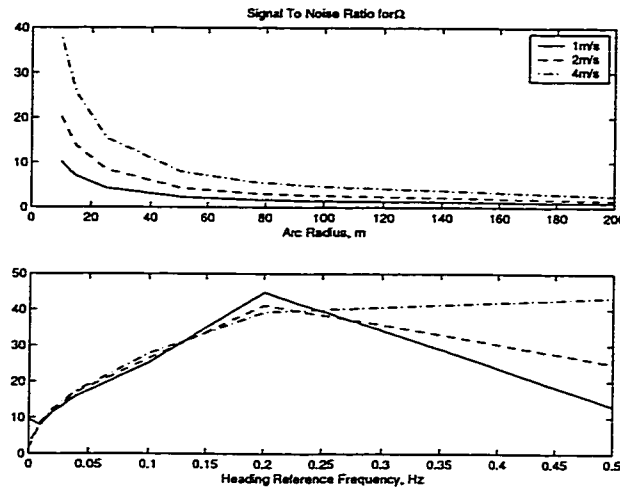


Figure 4.5: Signal to noise ratio for tractor yaw rate,  $\Omega$

strong identification.  $P_2$  and  $p_3$  require a large signal to noise ratio in  $\Omega$  (yaw rate),  $p_4$  requires a large signal to noise ratio in  $\delta$  (steer angle) and  $p_5$  requires a large signal to noise ratio in  $\omega + u$  (slew rate and control input.)

A series of simulations to characterize the signal to noise ratios for various trajectories were run. These simulations included lateral control along arcs ranging from 10 meters in radius to infinite radius (straight lines) and heading control to a square wave input oscillating between  $\pm 20$  degrees at frequencies ranging from 0 Hertz to  $\frac{1}{2}$  Hertz. The resulting signal to noise ratios between the state estimates and the error in those estimates is shown in Figures 4.5, 4.6 and 4.7.

As expected, the signal to noise ratio for  $\Omega$ , the yaw rate is proportional to the forward speed of the tractor and inversely proportional to the radius of the turn. There is also a resonant frequency that varies with speed between approximately  $\frac{1}{2}$  Hz and  $\frac{1}{5}$  Hz.

The signal to noise ratio for the steer angle,  $\delta$ , is insensitive to speed but also

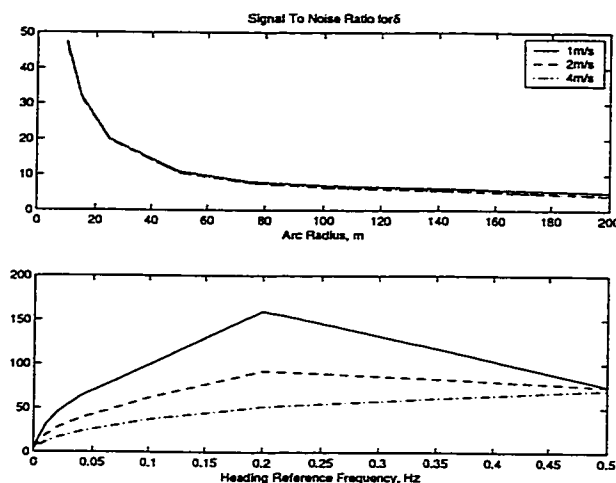


Figure 4.6: Signal to noise ratio for tractor steer angle,  $\delta$

dependent on the reciprocal of the turning radius. The frequency behavior of the signal to noise ratio in  $\delta$  is very similar to that of the yaw rate. It also displays a resonant frequency on the order of  $\frac{1}{5}$  of a Hertz in this parameter configuration. It is clear that a turning radius of zero meters would provide the best signal to noise ratio. Obviously, a real wheeled vehicle could never achieve a turning radius of zero. The best signal to noise ratio is therefore achieved when the steered wheels are hard against their stops. Unfortunately, at tight angles the linearization of  $\dot{\Omega}$  in Equation 2.7 with respect to  $\delta$  becomes less ideal. ( $\dot{\Omega}$  is actually a function of  $\tan\delta$ .) Neglecting the non-linearity at extreme turn angles will cause a bias in the estimate. This can be easily dealt with by using a non-linear estimator.

The signal to noise ratio for the slew rate,  $\omega$ , plus input signal proves to be very sensitive to velocity. This is most likely due to the increased effect of field disturbances on the heading and position. It is only slightly dependent on arc radius.

These Figures indicate that the best signal to noise ratios and consequently the

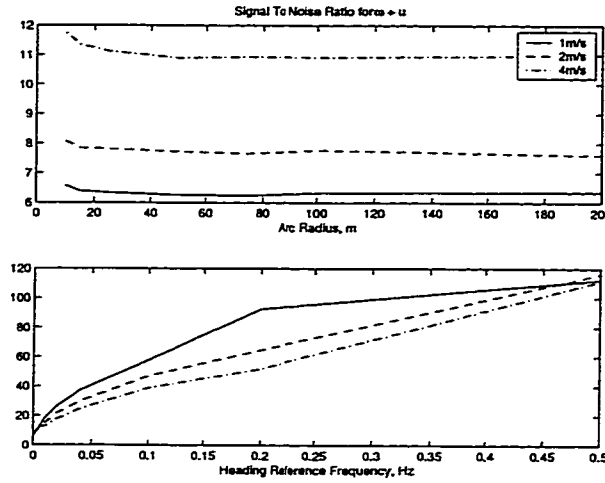


Figure 4.7: Signal to noise ratio for tractor slew rate,  $\omega$

best parameter identification conditions are achieved while the vehicle is actually turning. The tighter the turn the better. Unfortunately a farm tractor typically spends a great deal of time driving down very straight rows. This is not a problem for identification of  $p_5$  which relies on the signal to noise ratio of  $\omega + u$  which is insensitive to the straightness of the trajectory. As will be shown in Section 5.2 in Figure 5.14,  $p_5$  can be reliably identified during straight line operation as well as during turns.

As becomes apparent in this section and will also be shown in Section 5.2,  $p_2$ ,  $p_3$  and  $p_5$  require turning to be accurately identified. This difficulty is most reasonably addressed by realizing that despite the fact that farm tractors typically spend the majority of the time driving straight rows, these rows are of finite length and the tractor must eventually turn around. Usually, the vehicle is required to turn around at the end of the rows within one or two times the implement width. As a result, the ideal time to identify parameters  $p_2 - p_4$  is during these tight, end-of-the-row U-turns

or during curved paths. It is during these U-turns and curve paths that there is enough excitation and diversity in the states that a reasonable signal to noise ratio is reached and, consequently, reasonable identification can be expected.



## CHAPTER 5

# Simulation and Field Tests

### 5.1 Simulation

#### 5.1.1 Actuator Identification

A simulation of the actuator identification algorithm was run. This simulation was run on a system with a simple first order lag for dynamics, a reasonable deadband and no sensor noise. The truth system is represented in Figure 5.1. As an initial guess the dynamic model was assumed to be a simple pass-through system with the output exactly matching the input. A simple, open loop random input was provided for system excitation and the resulting learning curves are presented in Figures 5.2 and 5.3. Figure 5.3 shows the convergence of the Hamming distance which is the norm of the difference between the estimated weights and the optimal weights (obtained from a dimpulse call to MATLAB.)

The simulation presented is fairly typical of the expected performance of this particular algorithm and system. The identification of the deadband parameters relies heavily on an estimate of  $X$ , the output of the dynamics. Therefore, the deadband

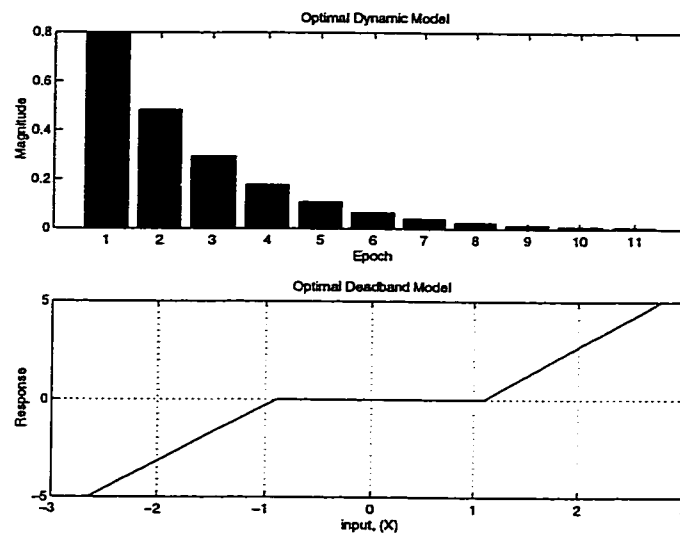


Figure 5.1: Truth system for Actuator Identification Simulation

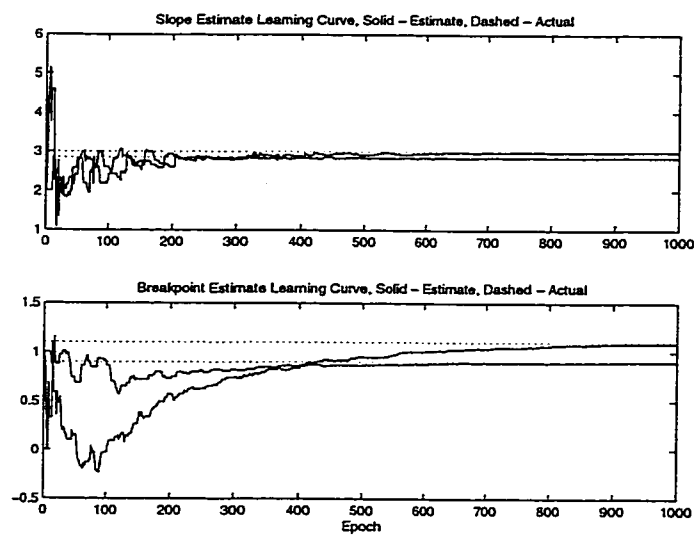


Figure 5.2: Deadband Learning curves for Actuator Identification Simulation

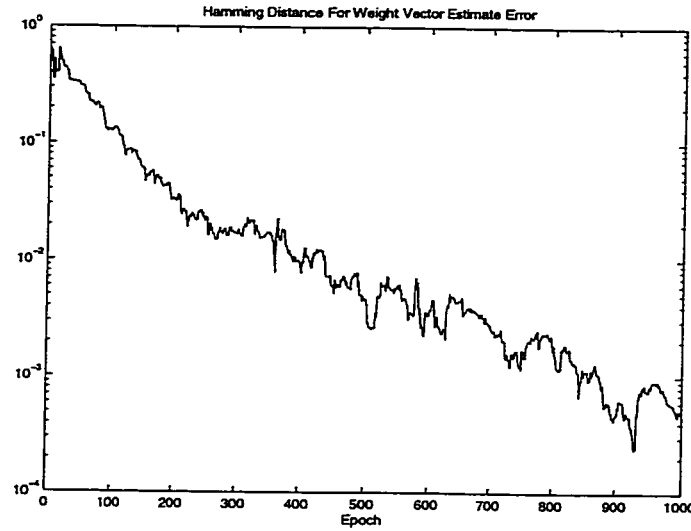


Figure 5.3: Dynamics Estimate Convergence for Actuator Identification Simulation

1

parameters do some initial searching until the dynamic model settles down and begins to reflect the dynamics accurately.

This identification system can also become sensitive to false estimates of the deadband. To increase the robustness of the algorithm one may constrain the deadband parameters. Two suggestions on how to do this is to enforce positive slopes ( $m_{1,2} > 0$ ) as well as non-overlapping breakpoints. To demonstrate this idea a simulation run is presented in Figures 5.4 and 5.5. In this run the dynamics were initialized to have a pass through gain of -1 resulting in an output of the same magnitude but opposite sign as the input. As the figures illustrate, the algorithm did very poorly for the first several hundred iterations. During this time, the dynamics vector existed in a region with a very small gradient and exhibited a random walk type behavior until it correctly identified the approximate sign of the true output. The hard constraints



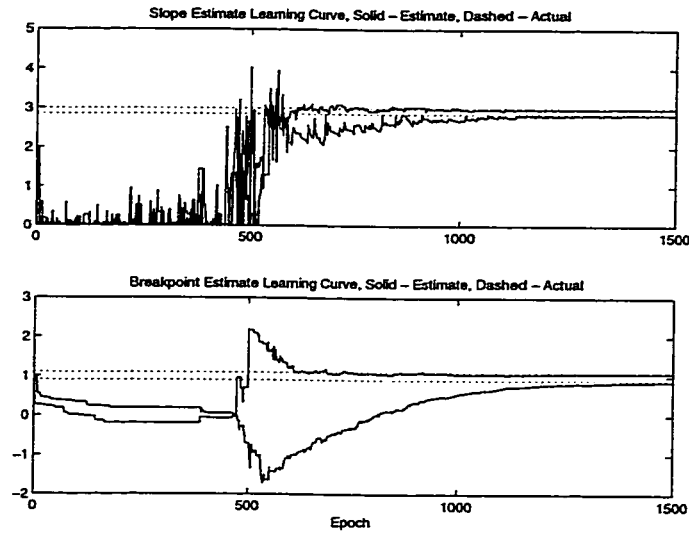


Figure 5.4: Deadband Learning curves for Actuator Identification Simulation with Poor Initial Guess

of the deadband parameters were regularly encountered until this point. As soon as the appropriate sign of the dynamics was obtained, the system moved into a mode of geometric convergence and correctly identified all parameters. When the deadband system constraints were removed, the system diverged on every simulation executed.

### 5.1.2 Tractor Identification

In an effort to gain a better understanding of the behavior of the parameter identification algorithms several simulations were run. The first evaluation was a comparison between the traditional EKF and the LMS/EKF algorithm outlined in Chapter 4. This simulation was run under MATLAB. For simplicity, the system input was simply generated by a LQR controller tracking a square wave reference on

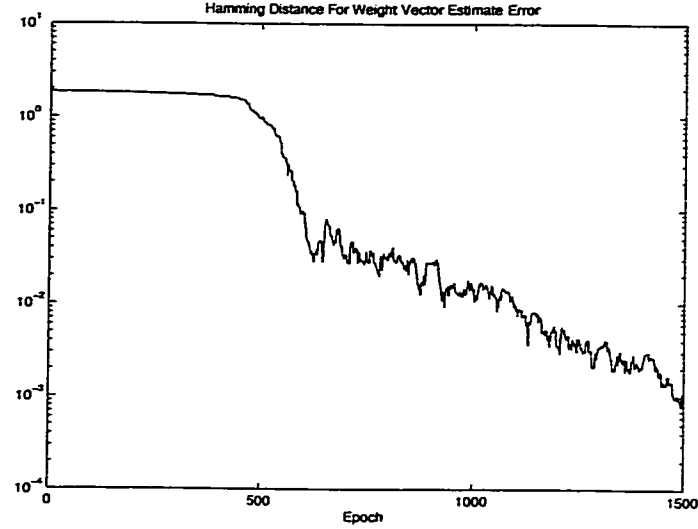


Figure 5.5: Dynamics Estimate Convergence for Actuator Identification Simulation with Poor Initial Guess

the heading. Figures 5.6, 5.7, 5.8 and 5.9 illustrate the convergence of the estimated parameters for both methods with and without sensor noise.

Both methods have little problem identifying the unknown parameters under noise free conditions. Both converge to an unbiased estimate of all four parameters. The estimates produced by the LMS/EKF algorithm have slightly more noise when the estimate is far from the true value than that of the EKF for comparable convergence rates. Also, due to the more limited tuning parameters, the LMS/EKF algorithm may exhibit a more slowly decaying mode than does the EKF. This is hardly surprising given that the LMS/EKF algorithm yields a coarser estimate of the gradient than does the EKF. When the parameters have converged, the noise rejection between the two methods is nearly indistinguishable. The advantage of the LMS/EKF algorithm comes into view when one realizes the extra cost of calculating the EKF gradient as

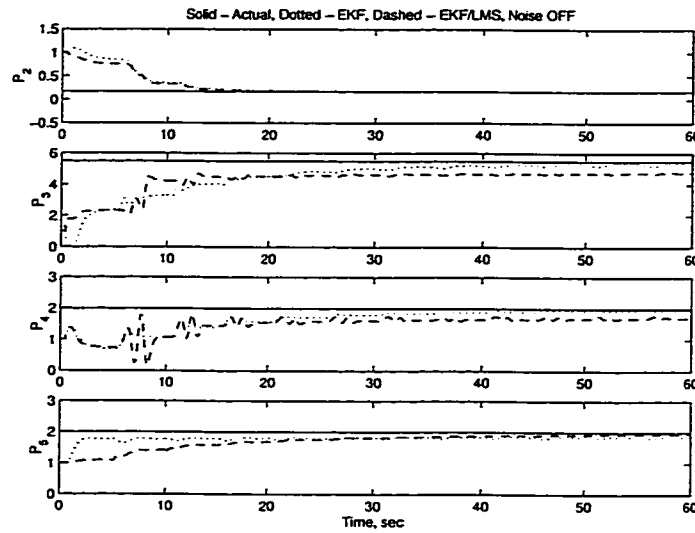


Figure 5.6: Short Term Comparison of EKF and LMS/EKF parameter identification performance on simulated tractor under noise free conditions

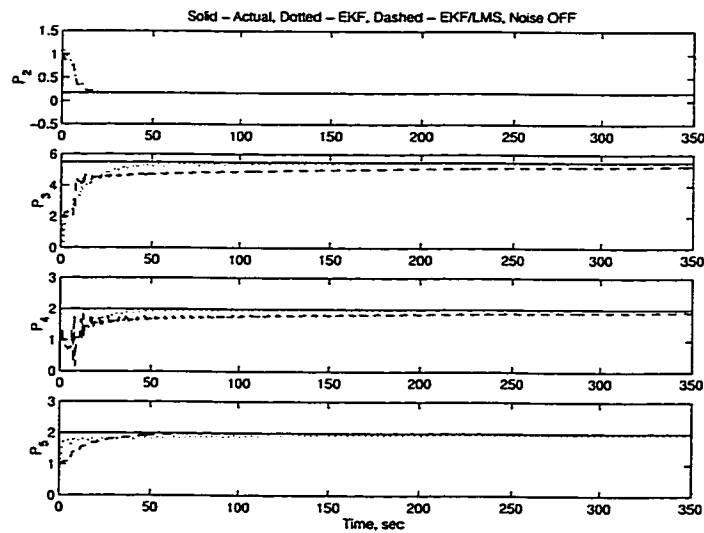


Figure 5.7: Long Term Comparison of EKF and LMS/EKF parameter identification performance on simulated tractor under noise free conditions

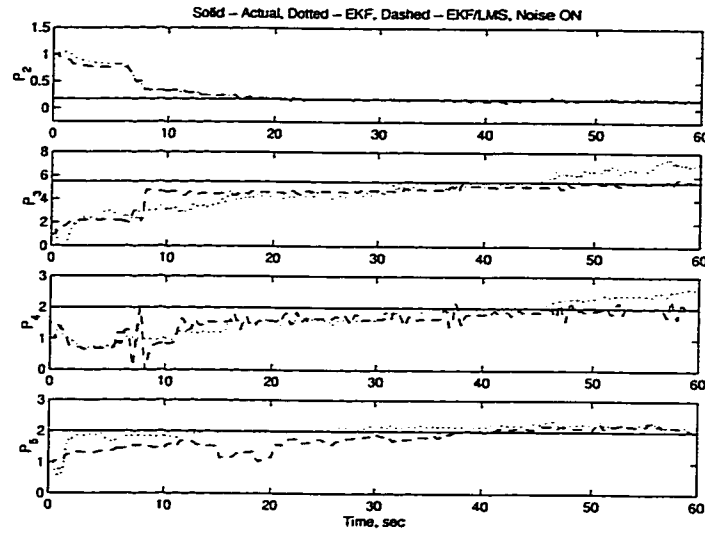


Figure 5.8: Short Term Comparison of EKF and LMS/EKF parameter identification performance on simulated tractor with sensor noise

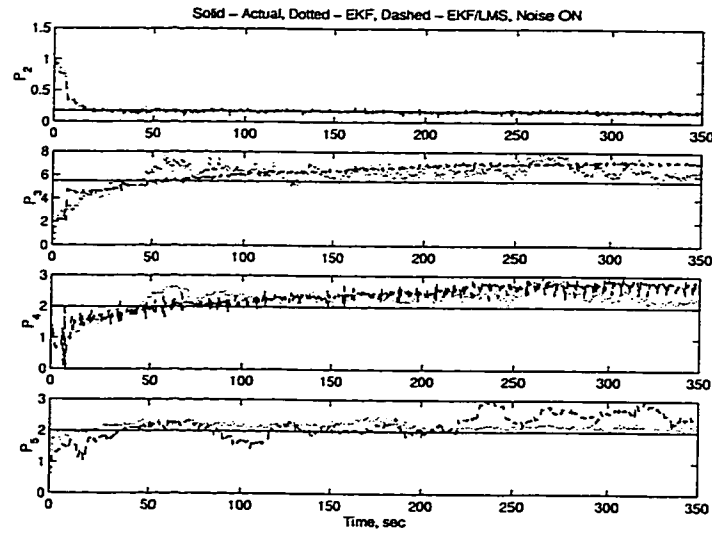


Figure 5.9: Long Term Comparison of EKF and LMS/EKF parameter identification performance on simulated tractor with sensor noise

compared to the LMS/EKF algorithm.

When the simulation is run with process and sensor noise, both algorithms exhibit biased estimates of the parameters. This bias is due to a strong correlation between the noise and the control input when running in closed loop mode. This bias is decreased when the signal to noise ratio is increased.

## 5.2 Experimental Results

The LMS/EKF algorithm was implemented on the experimental tractor. The vehicle was configured with a six row, hitched cultivator. This implement was very heavy and considerably altered the vehicles' handling characteristics<sup>1</sup>. The tractor was driven repeatedly over the 6 pass curved paths shown in Figure 5.11 and the identified parameters were allowed to converge. During the data collection pass for the adaptive controller, the parameters were still free to adjust. Despite the freedom to adjust, the parameters in the data collection pass were well converged as evidenced by the fact that only negligible variations in the parameters were observed during the data collection.

The performance of the adaptive system was then compared to the performance of a fixed controller using the parameters identified by O'Connor [O'C97] over the same trajectory. The performance of both systems over each pass is compared in Table 5.1. A histogram of the overall distribution of lateral errors is presented in Figure 5.12 throughout the entire trajectory. There is a mean bias that is identical in both the fixed and adaptive controllers' performances. This is believed to stem

---

<sup>1</sup>The handling of the tractor changed so much that the author nearly drove the tractor into an irrigation ditch on transport to the test field because the steering had become so ineffective!



Figure 5.10: Experimental Vehicle with 6 Row Cultivator Attached

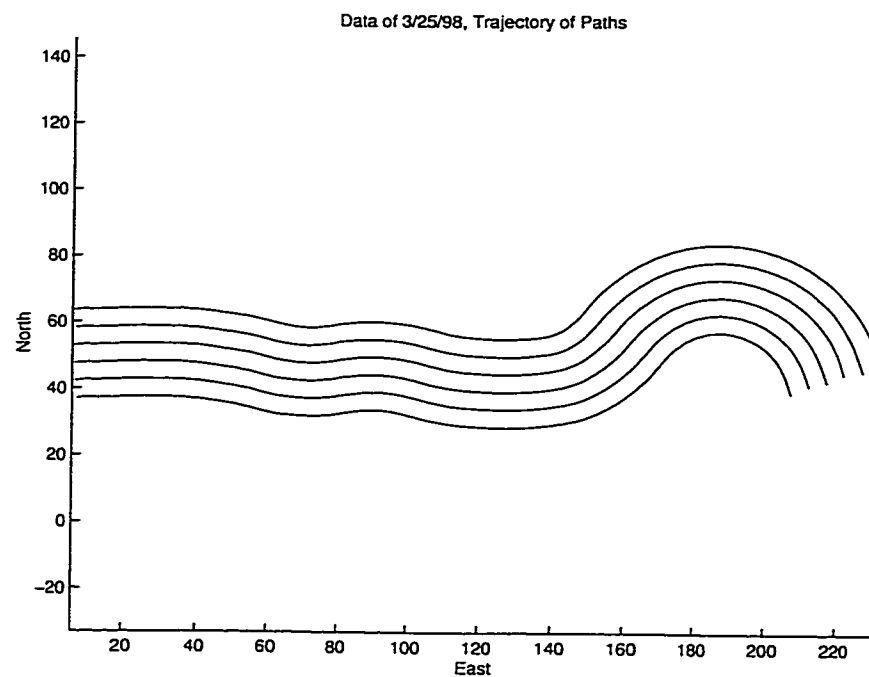


Figure 5.11: Curved Path System Identification Trajectory

| Row Number | Fixed Controller |                | Adaptive Controller |                |
|------------|------------------|----------------|---------------------|----------------|
|            | Mean (cm)        | Std. Dev. (cm) | Mean (cm)           | Std. Dev. (cm) |
| 1          | 2.40             | 5.08           | 3.17                | 3.46           |
| 2          | 2.16             | 3.81           | 1.59                | 2.78           |
| 3          | 3.00             | 4.38           | 3.88                | 3.46           |
| 4          | 2.83             | 3.91           | 1.38                | 2.74           |
| 5          | 2.15             | 4.63           | 3.88                | 3.11           |
| 6          | 2.35             | 4.26           | 1.39                | 3.00           |
| Average    | 2.48             | 4.35           | 2.55                | 3.10           |

Table 5.1: Lateral Error Comparison On Curved Trajectory

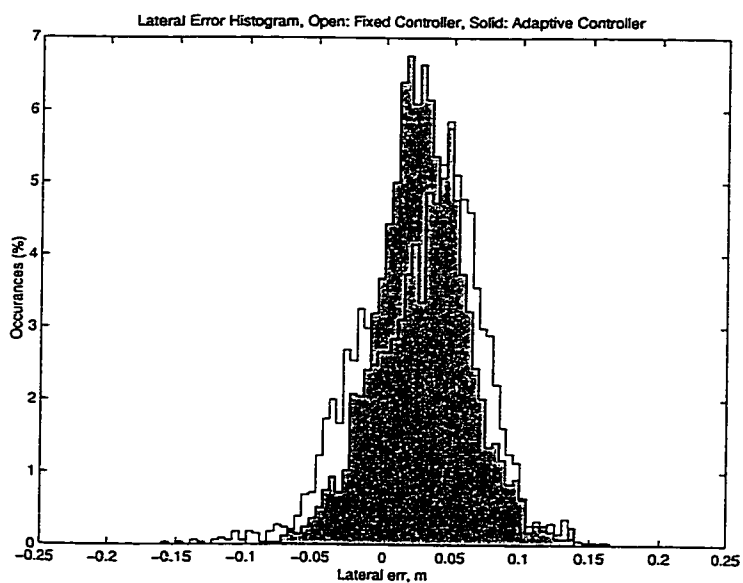


Figure 5.12: Curved Path System Identification Performance

from the fixed horizon regulation method that was identical on both systems. There is also a directionally dependent variation exhibited by the adaptive estimator. This is attributed to a small bias in either the heading or the steer angle measurement which was compensated for in the fixed controller but not the adaptive.

The lateral error distribution shown in Figure 5.12 for the adaptive system is both narrower and more regular than that of the fixed system indicating less searching by the regulator due to poorly modeled dynamics. Both Table 5.1 and Figure 5.12 show a 25% improvement in the lateral error distribution. It is also important to note the larger number of outliers in the non-adaptive control data. It is likely it is these outliers that will cause a problem with crop loss or higher probabilities of collisions.

In addition to the above mentioned experiments, a series of parameter convergence experiments were run. In these experiments, the vehicle was configured with single wheels and no implement. The parameters and learning coefficients were set to various initial conditions and the vehicle was run over a figure 8 trajectory as shown in Figure 5.13.

Parameters  $p_2$  and  $p_5$  showed excellent convergence while  $p_3$  and  $p_4$  exhibited less desirable convergence. The root cause of this was believed to be the trajectory chosen for this experiment. The long, straight sections injected little energy into the yawing rate and steer angle which are required by  $p_3$  and  $p_4$ . The turning effectiveness  $p_4$  could only be identified at the end of the rows during the u-turns. Despite this, Figure 5.14 illustrates a slow trend towards a definite region for the estimate of  $p_4$ .

The yaw damping estimate,  $p_3$  was much less well behaved. There appeared no overall trend nor any preferred value for this parameter estimate. This was due to the fact that this parameter was approximately twice as difficult to identify (as discussed



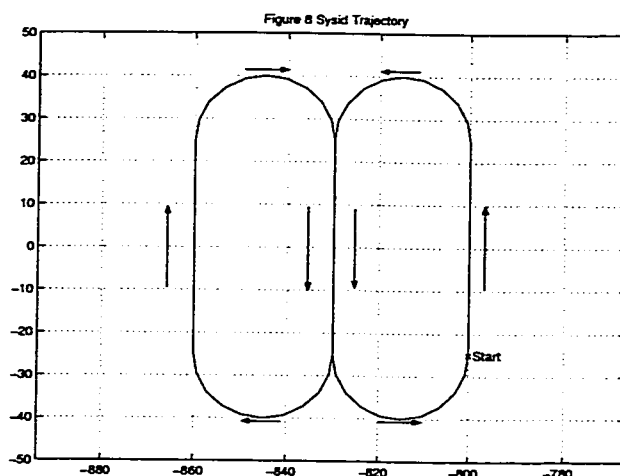


Figure 5.13: Figure 8 Sysid Trajectory used in Parameter Estimation

previously in Section 4.4) coupled with the lack of the ability to introduce significant yaw rates resulting in very little energy in this mode.

Another clue to understanding the difficulty in identifying  $p_3$  and  $p_4$  is in Equation (2.7). There are two states that can be thought of as inputs to the angular acceleration, the yaw rate,  $\Omega_z$  and steering angle,  $\delta$ . These two states have an extremely strong correlation at low frequencies. This strong correlation makes it difficult to resolve each input's contribution to the total angular acceleration and therefore to evaluate the appropriate correction to the two parameters.

This problem of resolving the parameters contribution to the angular error is further confounded by the trajectory chosen for this identification run and the physical constraints on the machine itself. Good identification is achieved with a strong signal to noise ratio. This requires large changes in steer angle between epochs in order to induce large angular accelerations. For a perfectly tracked trajectory with constant

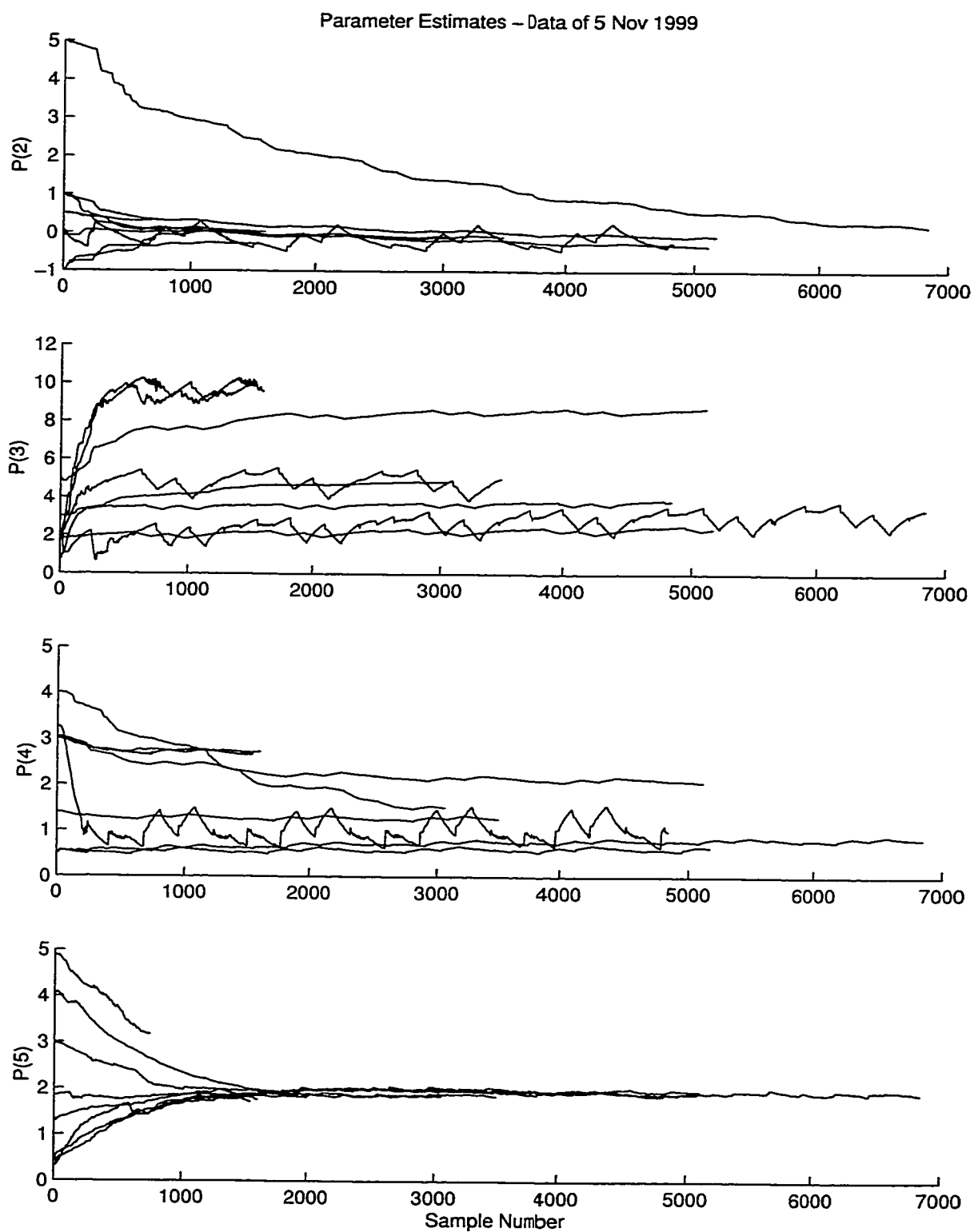


Figure 5.14: Learning Curves from Data of 5 Nov 1999

speed and constant radius, from (2.7):

$$\frac{p_3}{p_4} = \frac{V_x}{\Omega_z} \tan \delta \quad (5.1)$$

It is apparent from Equation (5.1) that, without angular accelerations, only the ratio of  $p_3$  and  $p_4$  can be identified. Achieving large angular accelerations requires large changes in steer angles. Large changes in steer angles require very large slew rates, rates not necessarily achievable by the hydraulic system in a practical tractor. This would also require very curvy, jerky trajectories which are not of particular usefulness in a real world setting. The trajectory chosen for this identification consisted of very smooth arcs and straight lines. The vehicle spent the vast majority of the time commanding very small slew rates.

The only large slew rates occurred on the transitions between the lines and arcs. During these transitions, some identification was achieved. Once the initial transient slew had been completed and the vehicle was well established on a constant radius or a straight line, the signal to noise ratio for parameters  $p_3$  and  $p_4$  would drop along with the slew rates resulting in the parameter estimates to wander.

One possible solution to the angular excitation dilemma is implied in Figure 4.3. The system is least sensitive to variations in parameter  $p_3$ . This parameter could possibly be estimated and held fixed. This would help resolve the contribution of errors in  $p_4$  to the angular acceleration estimate.

## **Part II**

# **Formation Driving**



# CHAPTER 6

## Introduction

Formation driving is simply the concept of two or more vehicles holding a position relative to each other. This is an integral part of co-operative vehicle control in which multiple vehicles are working together to accomplish a common task. An example of this would be a combine harvesting grain and an autonomous tractor pulling into formation to allow the combine to unload grain while continuing to harvest. A second example would be a lead vehicle pulling a plow and a second vehicle following closely behind seeding the freshly plowed furrows.

### 6.1 Classes of Similar Problems

There has been much work on the autonomous control of aircraft and spacecraft for the purpose of formation holding. [OPH98], [ZC95], [GB96] These references address the problem of maintaining the relative position of moving vehicles using GPS.

Differential GPS is particularly well suited for formation / station keeping applications. Typically in these applications the absolute position of the group is not as important as the relative position of the participants with respect to each other or

some other datum.

One such application is the formation flying of aircraft. Close formation flying is necessary during mid-air refueling. Military aircraft also often fly in formation during long cross-country movements. Conventional autopilots are not sufficient to accomplish these applications safely and it is a very demanding task. Pilots often relate stories of finding themselves “drenched in sweat” following a night refueling. An auto pilot that could hold formation would greatly assist in this task.

Accurate relative position regulation of vehicles could greatly assist in the implementation of large baseline antennas. The beam pattern of array antennas is a direct function of the baseline distances between array elements. The longer the baseline, the higher the directivity of the antenna. Physically attached antennas have practical limits. The ability to mount array elements on separate vehicles and accurately control their relative positions could add considerable flexibility to antenna designers.

Squadrons of aircraft could benefit from accurate relative position regulation. The efficiency of an aircraft wing is a function of the aspect ratio, the ratio of wingspan to the average chord. A long, skinny wing is more aerodynamically efficient than a short stubby wing. Unfortunately, it is very difficult to provide the strength required to support a long wing and still maintain a light wing. A group of aircraft flying wingtip to wingtip could increase the effective aspect ratio of the group wing planform as a whole. Each aircraft would increase the wing efficiency of the others without increasing the structural integrity required for any of them.

|                         |   |
|-------------------------|---|
| 1939                    | Early Concepts-GM Futurama at World's Fair (NY)       |
| 1950s & 60s             | Electronic Highway Experiments by GM and RCA          |
| 1964                    | GM Futurama II at World's Fair (NY)                   |
| 1960s & 70s             | Experiments by Ohio State University                  |
| 1970s                   | Personal Rapid Transit and Automated Guideway Transit |
| 1986                    | PATH program founded by Caltrans and UCB              |
| Reproduced from [Tom94] |   |

Table 6.1: Automated Highway System History

## 6.2 Previous Work in Formation Driving

There has been much work in the area of automotive formation driving in an area referred to as “The Automated Highway”. The goal in this work is to take the human operator, and the slow reflexes associated with them, out of the driving loop. With a computer driving, it is thought that much tighter spacing (as little as several meters) can be safely maintained. The typical expectation in these applications is that there exists something embedded in the roadway, such as magnets, to provide lateral guidance. The resulting research typically focuses on the longitudinal control of the vehicles and the interaction between vehicles. [Ben91], [Var93], [HMNS91]

The Automated Highway System (AHS) concept is over sixty years old. Its history is summarized in Table 6.1 [Tom94]. In 1986 the California Partners for Advanced Transit and Highways program was founded by Caltrans and the University of California at Berkeley. These researchers envision an automated highway system with platoons of vehicles speeding down the highway with just a few meters of spacing.

Longitudinal control is achieved through a complex controller that attempts to model the entire vehicle drive train. This model accounts for variables such as engine torque curve and brake non-linearities, changes in road grade and wind gust drag.



The controller used is a smoothed form of sliding mode control [HTV94]. This complex model is required to achieve the controller bandwidth required for such tight formations.

When driving in platoons, often each vehicle only senses the distance, speed and acceleration of the vehicle directly in front of it. The longitudinal controllers of each of the vehicles following the platoon leader must exhibit string stability [AH97]. If a velocity disturbance enters one of the leading vehicles the following vehicles must not allow this disturbance to amplify from one vehicle to another.

This controller was tested in using a four car platoon on the carpool lanes of I-15 in San Diego. The first car in the platoon accelerated and decelerated manually while each of the following vehicles maintained automatic speed control. The accuracy of these controllers has been shown to be about 20 centimeters.

Lateral control in the PATH program is achieved with magnetic markers buried in the road. These magnets are sensed by a pair of magnetic field sensors, one on each of the front and rear bumpers. The magnetic field measurement yields both a position and heading measurement relative to the lane. This system was chosen because of its ease of maintenance and robustness to varying road conditions. Additionally, the polarity of these markers can be utilized to encode information such as a preview of road curvature.

Each platoon of vehicles is assumed to be in a single lane. In the PATH program there is no lateral control dependent on adjacent vehicles to the sides. It is assumed that the vehicles alongside will maintain good lane position and not wander into the wrong lane.

Recently, there has been some initial work on formation driving for military and

agricultural vehicles by ITT industries. [FCA99] This system expands the role of the GPS base station to a master tracking and control station. This base station tracks the positions of each vehicle and commands each slaved vehicle with an appropriate state. This centralized architecture has some significant advantages. The foremost is the ability to globally optimize the trajectories of all vehicles rather than each vehicle attempting to predict the actions of the others and optimizing it's own actions accordingly. (Similar to the mini-max problem from game theory.) This technique concentrates the computation required to a central point, greatly increasing performance requirements for the master station.

## 6.3 Problem Statement

It is a small stretch of imagination from one vehicle working autonomously in a field to multiple vehicles working together in concert to accomplish a common task. One such example would be the harvesting operation (figure 6.1.) Several combines may be driving in formation, each one swath over from the others. This would allow each combine to skip one or more swathes, reducing u-turn requirements and requiring less headland, while the other vehicles fill in the gaps. Meanwhile, another set of vehicles pulling grain carts would wait just out of the way of the combines. When the combine bins are full, the grain cart vehicle would pull up alongside the combine, allowing it to unload on the move, and a loaded grain cart would return to a central collection point to unload. This cycle would repeat for each vehicle until the field is fully harvested.

Harvesting of cotton may also benefit from have multiple vehicle cooperation. Often, agricultural vehicles are not capable of turning around within the width of the



Figure 6.1: A Combine Unloading Grain Into a Grain Cart Pulled by a Tractor in South Texas

vehicle. This leads to either shifting from forward to reverse once or more times or skipping several rows on the first pass and coming back later to fill in the gaps. A lead vehicle may desire to skip several rows to allow faster turn around at the end of each row and have a following vehicle harvest the skipped rows (figures 6.2 and 6.3.) It would be even more desirable if only one operator was necessary to oversee the automatic operation of these vehicles.

There are several problems that need to be addressed before these futuristic applications can be realized. The first problem is how to determine where each vehicle needs to be going to at any given time. This problem is fairly easily solved when all the vehicles are autonomous. One must simply pre-map the trajectories for each vehicle and ensure the field requirements are met and there are no conflicts. This process becomes considerably more difficult when there is a lead vehicle controlled by a human operator. Humans are unpredictable. It is an exercise in futility to attempt

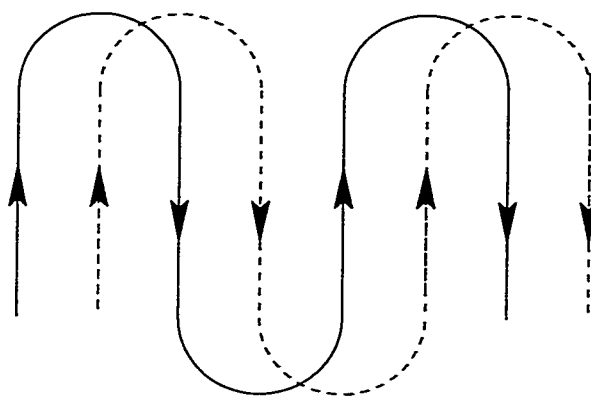


Figure 6.2: Cooperative Row-Skipping Trajectories

,

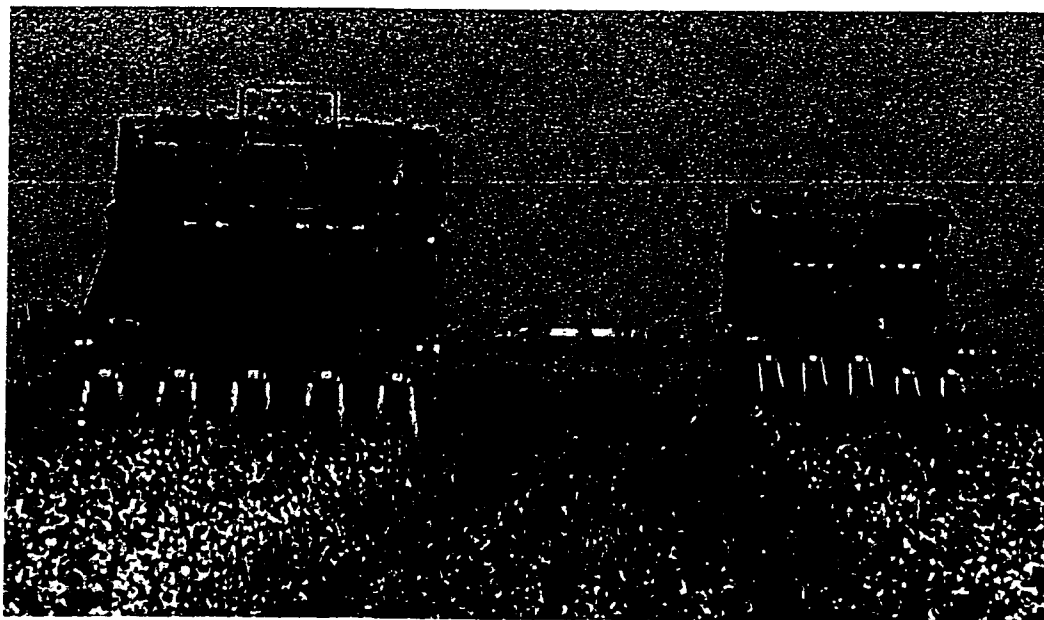


Figure 6.3: A Pair of Cotton Pickers Cooperating to Harvest Cotton in California's Central Valley

,

to predict, with any degree of certainty, the actions of a human operator. The following vehicles must therefore be capable of following the lead (master) vehicle with little or no a-priori knowledge of the trajectory to be followed.

This latest requirement in turn requires another important feature: conflict resolution. The “optimal” trajectory may minimize the time or distance required to acquire a station but it may also direct the vehicle directly through another. Obviously a collision would be undesirable. A sacrifice of system speed and efficiency may be necessary to ensure system safety. This requirement is very similar to the conflict resolution requirements for aircraft in free flight. One strategy to detect and resolve conflicts is to provide a protected “no-fly zone” around the vehicle [TPS98]. This is simply a region around a vehicle in which other vehicles are forbidden to enter. The complexity increases when two vehicles work in very close proximity to each other such as in the combine and grain buggy example above. A simple no-fly zone would exist as a circle or a box around each vehicle large enough to ensure that no matter what the relative orientations of the two vehicles there would be no conflict. When the two vehicles are working closely together they may have to violate any such zone in order to accomplish the prescribed task. It is therefore necessary not only to take the relative positions of the two vehicles into account but also the relative orientations to allow safe, close proximity work.

## CHAPTER 7

# Formation Driving Algorithms

When neglecting the danger of vehicle collisions, formation driving is a relatively simple task with the vehicle described in Part I. The problem of keeping station becomes one of data communications and generating a desired position.

### 7.1 Dynamic Models

The dynamics of each individual vehicle do not change when one goes from single mode control to formation control. The type and amount of information the slave vehicles must estimate, however, does change. The slave vehicle must also estimate the master vehicle's state to a limited degree. The primary information regarding the master vehicle that the slave must estimate is relative position, heading and speed. The heading and speed can accurately be estimated from position data alone. For this reason the only sensor requirement for the master vehicle is a GPS position receiver.

### 7.1.1 Estimator Model

When working in tight formation, typically the master vehicle attempts to drive in a straight line at constant speed. This influences the design of the estimator by allowing the slave to guess the rate of change for the master heading and speed to be zero with only a small disturbance covariance. The slave estimator used in this research has the states

$$\begin{aligned}
 \dot{E}_s &= V_{xs} \sin \Psi_s - p_2 \Omega_s \cos \Psi_s \\
 \dot{N}_s &= V_{xs} \cos \Psi_s + p_2 \Omega_s \sin \Psi_s \\
 \dot{\Psi}_s &= \Omega_s \\
 \dot{\Omega}_s &= -p_3 \Omega_s + p_4 V_{xs} \tan \delta_s \\
 \dot{\delta}_s &= \omega_s \\
 \dot{\omega}_s &= p_5 (u - \omega_s) \\
 \dot{V}_{xs} &= \frac{1}{\tau_g} (\kappa_g \omega_{command} - V_{xs}) \\
 \dot{E}_m &= V_{xm} \sin \Psi_m \\
 \dot{N}_m &= V_{xm} \cos \Psi_m \\
 \dot{\Psi}_m &= 0 \\
 \dot{V}_{xm} &= 0
 \end{aligned} \tag{7.1}$$

where

$(\cdot)_s$  refers to a slave state,

$(\cdot)_m$  refers to a master state,

$E$  and  $N$  refer to a vehicles East and North position,

$\Psi$  refers to a vehicle heading,

$\Omega$  refers to a vehicle yaw rate and

$\delta$  and  $\omega$  refer to a steer angle and slew rate.

The master heading and velocity states are included in the slave's estimator to allow for master vehicle maneuvering. The slave vehicle estimates these states as simple random walk states. This induces a lag in the state estimate but relieves the requirement of including additional measurements on the master vehicle.

### 7.1.2 Regulator Model

With these states, a regulator to maintain slave position can be designed. It is the relative position of the slave vehicle that is of interest. The coordinate transformation from an East / North reference station centered frame to a Right / Forward master vehicle centered frame is

$$\begin{bmatrix} Y_r \\ X_r \\ \Psi_r \end{bmatrix} = \begin{bmatrix} \cos \Psi_m & -\sin \Psi_m & 0 \\ \sin \Psi_m & \cos \Psi_m & 0 \\ 0 & 0 & 1 \end{bmatrix} \begin{bmatrix} E_s - E_m \\ N_s - N_m \\ \Psi_s - \Psi_m \end{bmatrix} \quad (7.2)$$

With the assumption of constant speed and straight line paths being driven by the master vehicle, the equations of motion for the slave vehicle in the master vehicle



coordinate frame are

$$\begin{aligned}
 \dot{Y}_r &= V_{xs} \sin \Psi_r - p_2 \Omega_s \cos \Psi_r \\
 \dot{X}_r &= V_{xs} \cos \Psi_r - V_{xm} + p_2 \Omega_s \sin \Psi_r \\
 \dot{\Psi}_r &= \Omega_s - \Omega_m \approx \Omega_s \\
 \dot{\Omega}_s &= -p_3 \Omega_s + p_4 V_{xs} \tan \delta_s \\
 \dot{\delta}_s &= \omega_s \\
 \dot{\omega}_s &= p_5 (u - \omega_s) \\
 \dot{V}_{xs} &= \frac{1}{\tau_g} (\kappa_g \omega_{command} - V_{xs})
 \end{aligned} \tag{7.3}$$

The preceding equations are identical to Equations (2.7) (save for the offset  $V_{xm}$  in  $\dot{X}_r$ ). As a result, a controller identical to a controller developed for the East / North coordinate frame can be immediately implemented.

### 7.1.3 Sensor Network and Communications

It was the goal of this research to produce a system which safely executes formation driving without adding unnecessary sensors. For this reason, only position measurements were made on the master vehicle, no attitude or wheel angle measurements were made. The addition of attitude and wheel angle measurements would increase the accuracy of the master vehicle estimate and alleviate much of the lag in the estimates. Though untested, the accuracy with these additional sensors could be expected to be comparable to a stand alone vehicle with identical sensors, approximately 2 - 3 cm in position and 0.1 degrees in heading.

The communications network consisted of a three way radio link configured as in

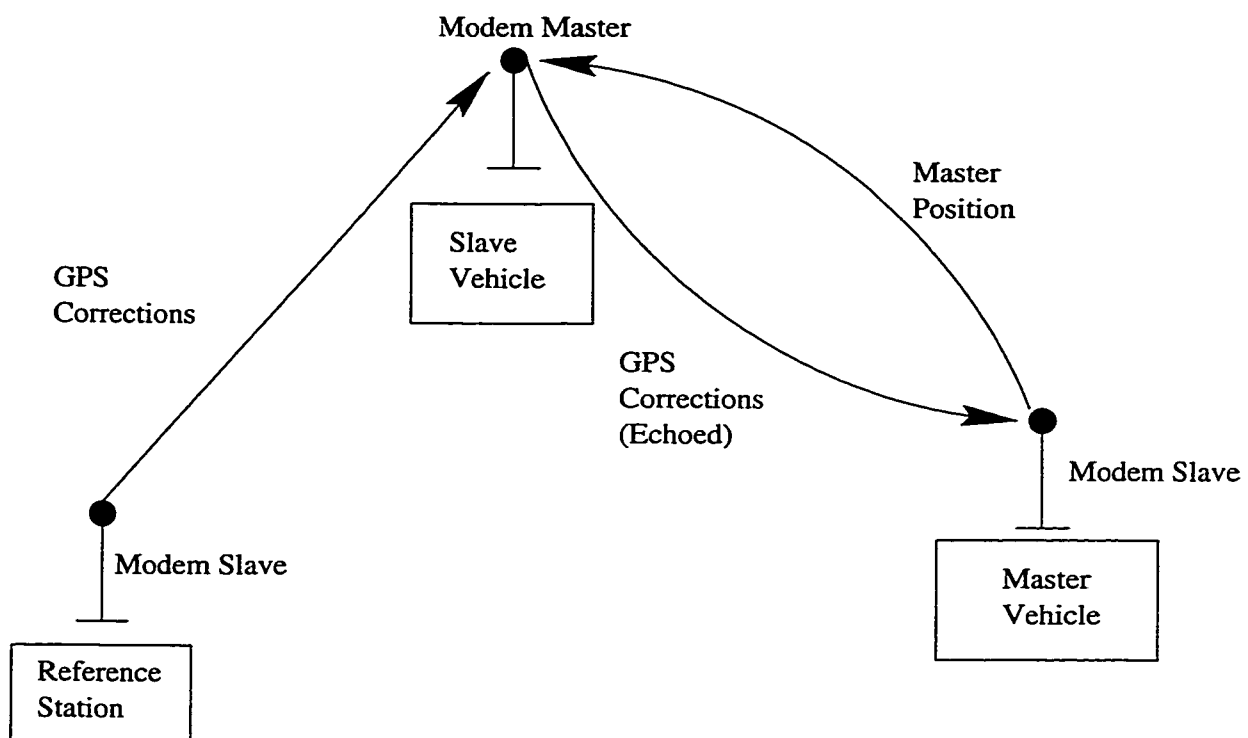


Figure 7.1: Radio Modem Communication Configuration

Figure 7.1. The radio modem hardware was capable of a master-slave configuration allowing one central modem master to communicate with several periphery modem slaves at once. Unfortunately, modem slaves could not communicate directly with each other. The modem master was mounted in the slave vehicle. When the slave vehicle received a differential correction from the reference station, the data packet was routed to the master vehicle as well as the slave vehicle positioning software. When the master vehicle received the differential correction it routed this information to the positioning software. When position solutions were available for the master vehicle, they would be transmitted in their raw state over the same radio network back to the slave vehicle. When master vehicle positions were received by the slave vehicle, they would be routed to the control software.

## 7.2 Formation Lateral Position Regulation

### 7.2.1 The Carrot on the Stick

The simplest method for formation position regulation is to point the nose of the vehicle at the desired position and drive towards it. This position is defined by an offset from the master vehicle, in master vehicle co-ordinates, that defines the desired position of the slave in master vehicle coordinates. This offset is expressed as a right offset and a forward offset. The mapping of this offset from master vehicle coordinates to east / north coordinates is accomplished by the following transformation

$$\begin{bmatrix} E_d \\ N_d \end{bmatrix} = \begin{bmatrix} E_{master} \\ N_{master} \end{bmatrix} + \begin{bmatrix} \cos \Psi_{master} & \sin \Psi_{master} \\ -\sin \Psi_{master} & \cos \Psi_{master} \end{bmatrix} \begin{bmatrix} \Delta_{right} \\ \Delta_{forward} + \Delta_{lead} \end{bmatrix} \quad (7.4)$$

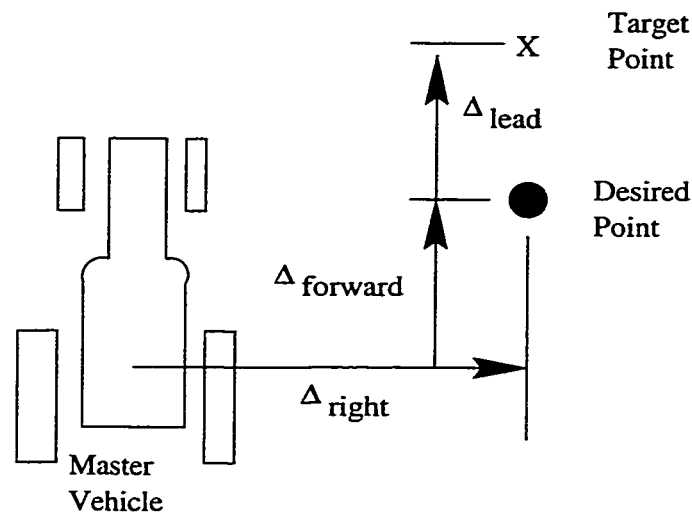


Figure 7.2: Carrot on the Stick Geometry

This absolute desired position is then transformed by Equation 7.3 into the relative co-ordinate frame to calculate state error. A problem arose when the slave vehicle was longitudinally very close to the desired position. When this occurred the slave vehicle had to move the nose of the vehicle through a large arc to track a small amount of lateral deviation. To alleviate this situation a  $\Delta_{lead}$  was added, as shown in Figure 7.2, which, for desired heading calculations, effectively moved the position to track several meters forward and allowed a smoother trajectory. This lead was added only to the desired position tracked by the heading controller. The lateral sensitivity is inversely proportional to the lead added. The longitudinal controller was still regulating about the desired point. Ultimately, the controller is still tracking the desired point, just the calculation of the desired heading is slightly modified.

In this mode, the main control criteria was the heading error measured with respect to a vector from the slave vehicle to the desired position. The regulator used

for lateral control was based on the linearized heading dynamic model

$$\begin{bmatrix} \dot{\Psi}_s \\ \dot{\Omega}_s \\ \dot{\delta}_s \\ \dot{\omega}_s \end{bmatrix} = \begin{bmatrix} 0 & 1 & 0 & 0 \\ 0 & -p_3 & p_4 V_{xs} & 0 \\ 0 & 0 & 0 & 1 \\ 0 & 0 & 0 & -p_5 \end{bmatrix} \begin{bmatrix} \Psi_s \\ \Omega_s \\ \delta_s \\ \omega_s \end{bmatrix} + \begin{bmatrix} 0 \\ 0 \\ 0 \\ p_5 \end{bmatrix} u \quad (7.5)$$

The feed-forward reference state that was generated to regulate the heading was

$$\begin{bmatrix} \Psi_{ref} \\ \Omega_{ref} \\ \delta_{ref} \\ \omega_{ref} \end{bmatrix} = \begin{bmatrix} \tan^{-1} \frac{E_d - E_s}{N_d - N_s} \\ 0 \\ 0 \\ 0 \end{bmatrix} \quad (7.6)$$

During position acquisition, this method has an interesting behavior. The slave vehicle points its nose towards the appropriate point as the master vehicle is moving forward. This causes the slave vehicle typically to fall behind the master vehicle and gently acquire the correct heading as it falls into line behind the master. This translates into a large region in which the station point can be safely acquired without danger of collision.

### 7.2.2 The Virtual Tether and Line, “Tractor on a Stick”

The goal in this approach was for the slave to maintain a fixed position with respect to the master in master vehicle coordinates. Simply put, an operator would see the slave in the same position relative to his vehicle at all times. This position is calculated utilizing Equation (7.4) without the  $\Delta_{lead}$ . When the slave was far away

from the desired station point, the Carrot on the Stick technique was used. When the slave vehicle was sufficiently close in the lateral direction, a line was generated passing through the desired point and in the same heading as the master vehicle. The slave vehicle then maintained control about this line which was updated as the master vehicle moved along. The regulator utilized for this control was based on the lateral controller originally developed by O'Connor [O'C97] and based on the lateral position dynamic model. The lateral position dynamic model used was

$$\begin{bmatrix} \dot{Y}_r \\ \dot{\Psi}_r \\ \dot{\Omega}_s \\ \dot{\delta}_s \\ \dot{\omega}_s \end{bmatrix} = \begin{bmatrix} 0 & V_{xs} & -p_2 & 0 & 0 \\ 0 & 0 & 1 & 0 & 0 \\ 0 & 0 & -p_3 & p_4 V_{xs} & 0 \\ 0 & 0 & 0 & 0 & 1 \\ 0 & 0 & 0 & 0 & -p_5 \end{bmatrix} \begin{bmatrix} Y_r \\ \Psi_r \\ \Omega_s \\ \delta_s \\ \omega_s \end{bmatrix} + \begin{bmatrix} 0 \\ 0 \\ 0 \\ 0 \\ p_5 \end{bmatrix} u \quad (7.7)$$

The reference state used for regulation was

$$\begin{bmatrix} Y_r \\ \Psi_r \\ \Omega_r \\ \delta_r \\ \omega_r \end{bmatrix} = \begin{bmatrix} \Delta_{right} \\ 0 \\ 0 \\ 0 \\ 0 \end{bmatrix} \quad (7.8)$$

### 7.2.3 The Cookie Crumb Trail

The most complex technique is the Cookie Crumb Trail. This technique is used when the relative position of the two vehicles is not as important as the relative

ground track of the two vehicles. In this approach the trajectory of the master vehicle is emulated as closely as possible (perhaps with an east/north translation included). In this method the master vehicle positions are used to generate a pair of splines of east and north positions versus pseudo-arclength. The pseudo-arclength is defined as the sum of the Euclidean distances to a particular coordinate pair

$$\begin{aligned} s_k &= s_{k-1} + \sqrt{(n_k - n_{k-1})^2 + (e_k - e_{k-1})^2} \\ s_o &= 0 \end{aligned} \tag{7.9}$$

The trajectory coordinates are then parameterized by a cubic spline

$$\begin{aligned} n(s) &= A_{n,k} + B_{n,k}(s - s_k) + C_{n,k}(s - s_k)^2 + D_{n,k}(s - s_k)^3 \\ e(s) &= A_{e,k} + B_{e,k}(s - s_k) + C_{e,k}(s - s_k)^2 + D_{e,k}(s - s_k)^3 \end{aligned} \tag{7.10}$$

As the master vehicle moves along its trajectory more points are added to the spline. The slave vehicle then follows the curve in the same manner it would on a pre-defined curve. [Bel99]

#### 7.2.4 Lateral Formation Control Along Arcs

The algorithms presented in Sections 7.2.1 and 7.2.2 assume a straight line trajectory for the master vehicle. When an arc is traced out by the master vehicle, the proper reference state must be fed forward into the controller in order to accurately track the desired slave trajectory. The methods for calculating these reference states for an arc are presented in [Bel99]. The calculation of these reference states, shown in Equation (7.11), is assisted by Figure 7.3.

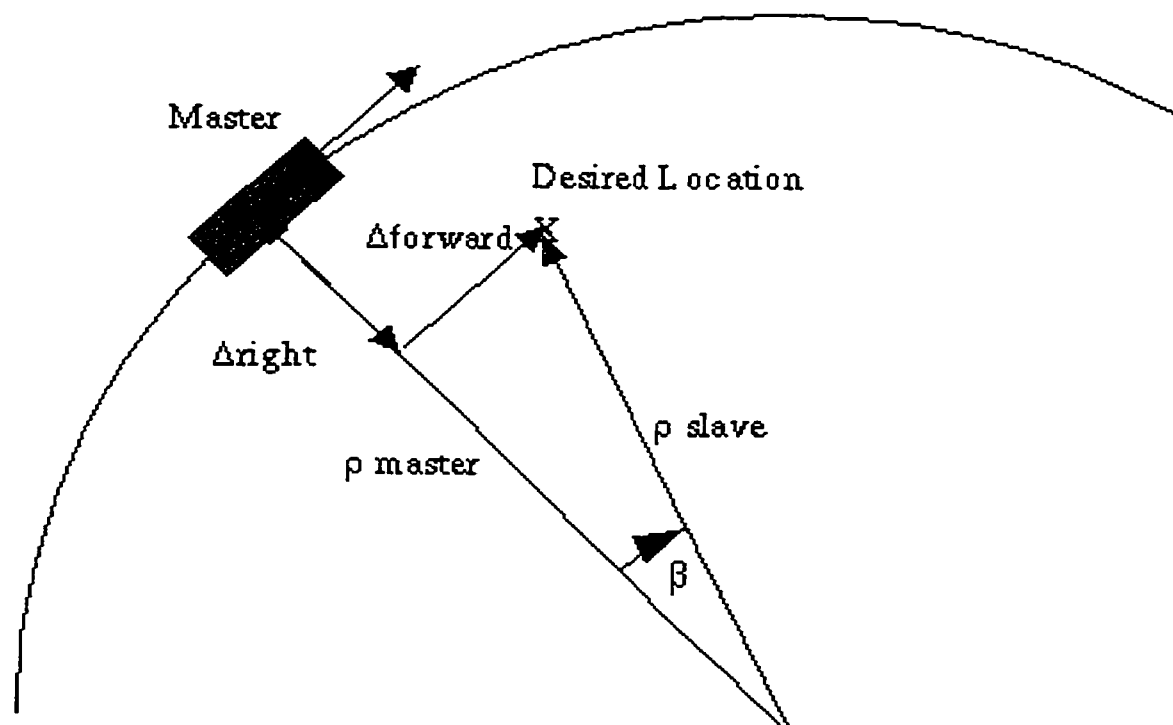


Figure 7.3: Geometry for Arc Formation Driving Reference State Generation



$$\begin{aligned}
\rho_{s,ref} &= \sqrt{(\rho_m - \Delta_{right})^2 + \Delta_{forward}^2} \\
\Psi_{s,ref} &= \Psi_m + \beta = \Psi_m + \tan^{-1} \frac{\Delta_{forward}}{\rho_m - \Delta_{right}} \\
\Omega_{s,ref} &= \dot{\Psi}_m \\
\delta_{s,ref} &= \tan^{-1} \frac{p_3}{p_4 \rho_s} = \tan^{-1} \frac{p_3}{p_4 \sqrt{(\rho_m - \Delta_{right})^2 + \Delta_{forward}^2}} \\
\omega_{s,ref} &= 0
\end{aligned} \tag{7.11}$$

The difficulty in using this type of reference state is that it relies on full master vehicle state access. The only measurement available to the slave vehicle during experimentation was position. All other states must be estimated. This forced the heading measurement to be essentially a differentiation of the position and the yaw rate to be a double differentiation of the position. Using a Kalman estimator this resulted in a very noisy estimate of these states. An alternative would be to use zero reference states on the  $\Omega$  through  $\omega$  states and add an integral to the lateral or heading error. The reference state from Equation (7.6) becomes

$$\begin{aligned}
\begin{bmatrix} \Psi_{ref} \\ \Omega_{ref} \\ \delta_{ref} \\ \omega_{ref} \end{bmatrix} &= \begin{bmatrix} \tan^{-1} \frac{E_d - E_s}{N_d - N_s} + \Psi_i \\ 0 \\ 0 \\ 0 \end{bmatrix} \\
\dot{\Psi}_i &= \frac{1}{\tau_\Psi} (\Psi_s - \Psi_{ref})
\end{aligned} \tag{7.12}$$

and the reference state from Equation (7.8) becomes

$$\begin{bmatrix} Y_r + Y_i \\ \Psi_r \\ \Omega_r \\ \delta_r \\ \omega_r \end{bmatrix} = \begin{bmatrix} \Delta_{right} \\ 0 \\ 0 \\ 0 \\ 0 \end{bmatrix} \quad (7.13)$$

$$\dot{Y}_i = \frac{1}{\tau_Y} (\Delta_{right} - Y_s)$$

This integral control had the affect of fooling the regulator into thinking the desired lateral position or heading was at a different position than actually desired. The addition of yaw rate sensors to both vehicles would alleviate this problem and reduce the need for this type of integral control. Master vehicle yaw rate information would provide much more accurate master vehicle heading information allowing a better projection of the reference position.

### 7.3 Formation Longitudinal Position Regulation

The basic behavior of the vehicle in the longitudinal direction was that of a first order lag between the input velocity and the actual velocity. This allowed for a very simple regulator to be designed. Recall that

$$\begin{aligned} \dot{\omega}_e &= \frac{1}{\tau} (\omega_{command} - \omega_e) \\ V_{xs} &= \kappa \omega_e \\ \dot{l} &= V_{xm} - V_{xs} \end{aligned} \quad (7.14)$$

where

$V_{xm}$  and  $V_{xs}$  were the master and slave vehicles,

$\kappa$  was the effective slave gear ratio,

$\omega_e$  was the slave vehicle engine speed,

$\tau$  was the lag in the engine response and

$l$  was the longitudinal error in the slave vehicle position.

The desired longitudinal response was a simple, second order decaying system. The dynamic equation for this system was

$$\ddot{l} + 2\omega_n\zeta\dot{l} + \omega_n^2 l = 0 \quad (7.15)$$

where  $\omega_n$  and  $\zeta$  were the natural frequency and damping coefficient of the regulator's response.

Combining Equations (7.14) and (7.15) yields the required commanded engine speed for a given time

$$\omega_{command} = \frac{1}{\kappa} (V_{xs} - 2\omega_n\zeta\tau(V_{xm} - V_{xs}) - \omega_n^2\tau l) \quad (7.16)$$

This algorithm works very well when the gear ratio is exactly known. The difficulty in tractor control is that this ratio is anything but constant. Factors such as tire size and tire slip conspire to change the effective gear ratio from the mechanical ratio. When the incorrect value for  $\kappa$  is utilized, the following steady state error in the

longitudinal position occurs:

$$\begin{aligned}
 \dot{l} &= 0 \Leftrightarrow V_{xs} = V_{xm} \\
 \dot{\omega}_e &= 0 \Leftrightarrow \omega_{command} = \omega_e \\
 V_{xs} &= \tilde{\kappa} \omega_e \\
 \Rightarrow l_{ss} &= \frac{\kappa - \tilde{\kappa}}{\omega_n^2 \tau} \omega_{e,ss}
 \end{aligned} \tag{7.17}$$

Equation (7.17) shows that the steady state longitudinal error is directly proportional to the error in the estimate of the gear ratio. To combat this steady state error, an integral controller command was added to the command from Equation (7.16) resulting in a final control input of

$$\begin{aligned}
 \omega_{command} &= \frac{1}{\kappa} (V_{xs} - 2\omega_n \zeta \tau (V_{xm} - V_{xs}) - \omega_n^2 \tau l) + \omega_i \\
 \dot{\omega}_i &= -\frac{1}{\tau_\omega} l
 \end{aligned} \tag{7.18}$$

To constrain integrator “wind up” during periods of acquisition, saturation limits were set on the integral state during the experimental verification of the controller.

## 7.4 Formation Driving Trajectory Types

It has been the custom of the autonomous tractor research group at Stanford to break trajectory types into several basic trajectory primitives. [Bel99], [O’C97] To date these primitives have included points, lines, arc, spirals and arbitrary curves. Formation driving requires new primitives for successful execution. These trajectory components include:

- **Acquire Point:** A point, typically further behind the master vehicle than is ultimately desired, to which the slave vehicle moves to allow a smoother final acquisition of the desired point. This point is considered successfully acquired when the slave vehicle state converges sufficiently close to the desired state (as opposed to the formation point which is acquired only when the operator signals.)
- **Formation Point:** A point or state relative to the master vehicle about which the slave vehicle is to regulate its position. Several methods for defining these positions are outlined in Section 7.2. The criteria for successful completion of these points occur only when a human operator in the master vehicle signals (via. the radio modem) accordingly.
- **Hold Point:** A point at which the slave vehicle attains a position and heading, halts and waits to be summoned. This point also requires a signal from the master vehicle to signal successful completion.

A typical trajectory set is illustrated in Figure 7.4. In this sequence, the combine is considered the master vehicle and the tractor pulling the grain buggy is the slave. The grain truck is parked in a known location. The sequence begins as the tractor heads for the acquisition point (1) and then smoothly pulls into formation (2.) The combine then begins transferring grain to the buggy. When the buggy is full the tractor breaks formation (3) and heads to a point (4) that will allow enough room to stabilize heading and pull up next to the road tractor-trailer and stop at a hold point(5.) The tractor then unloads the grain buggy onto the tractor-trailer and when complete, heads to another holding point (6) to await the next unloading cycle.

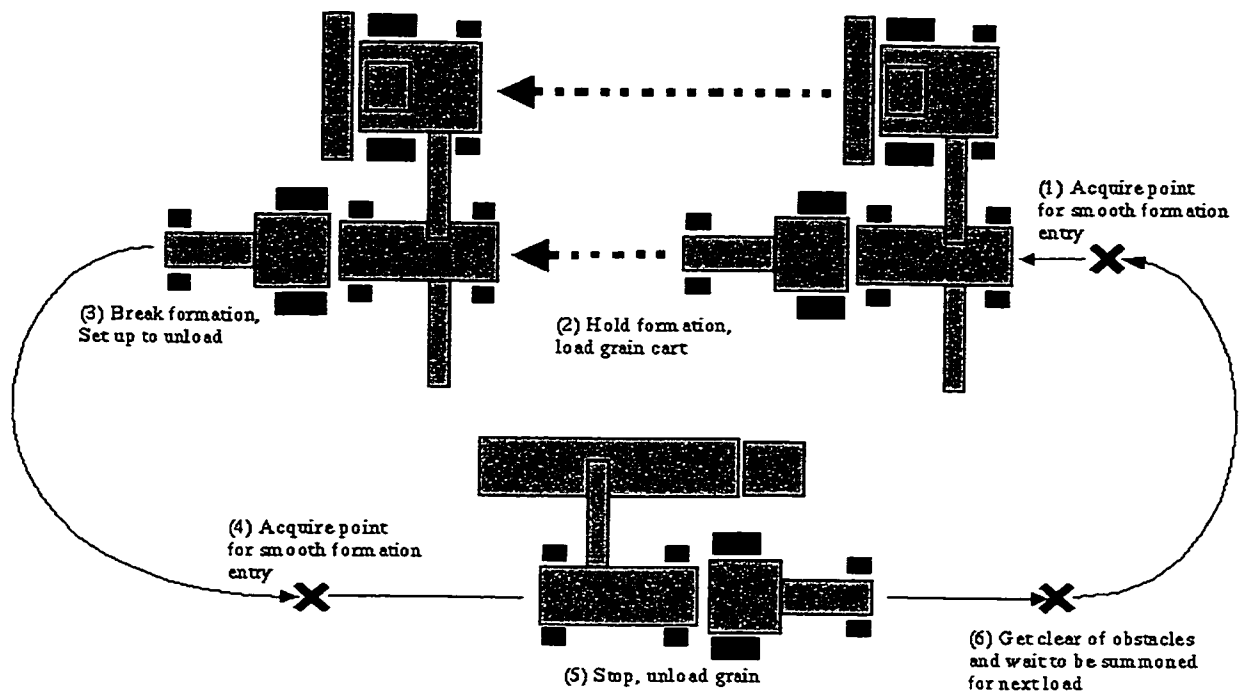


Figure 7.4: A Typical Trajectory Set to Transfer Grain from a Combine to a Grain Truck Using Formation Algorithms



## CHAPTER 8

# Collision Avoidance

One cannot address the issue of multiple autonomous vehicle working in proximity to each other without asking the question “How do we keep them from hitting each other?” This is the same question that those working on the free flight concept for air traffic management must ask themselves. In this scheme, each aircraft goes about it’s business in the most efficient way for that vehicle alone until a possible conflict is identified, hopefully well ahead of time. Obviously, not even a computer can very practically keep track and predict the actions of every airplane in the sky. Instead, each aircraft has two zones around it. The first, larger zone, is the alert zone. When another aircraft enters this zone, each aircraft must monitor the other aircraft for possible conflicts. The second, smaller zone is the Protected, or No Fly zone. Under no circumstances is another aircraft to be allowed to pierce this protective bubble.

### 8.1 Fuzzy Logic

Fuzzy logic is the recognition that world is not black and white. In the world we live in, very rarely do we encounter bivalence in “truth.” Rather, the truths



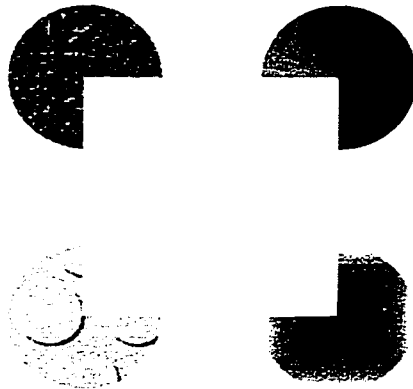


Figure 8.1: Fuzzy Kanizsa Square

and falsehoods we encounter are to a matter of degree. For instance, in classical mathematics or in a computer's CPU  $x = y$  is either 0 (100% false) or 1 (100% true.) There is no ambiguity. In fuzzy logic, the truth of something may take on a value in the continuous spectrum between 0 (completely false) and 1 (completely true.) Indeed, seemingly competing states, such as  $A$  and not  $A$ , can both be true to some degree at the same time. A set of examples from the current discussion would be the danger of two vehicles colliding and the occurrence of that collision. The collision itself is a bivalent state, either the vehicles have made contact or they have not. The danger of collision is more of a fuzzy concept. The danger ranges from low when the vehicles are very far apart to very high when there is no action left that either vehicle can take to prevent a collision.

Human cognition works very differently than the real world to computer interface. Consider the Kanizsa square [Kan76] in Figure 8.1. We, as humans quickly recognize a square framed by four circles. The computer this dissertation is being prepared on interprets Figure 8.1 as a series of bits. Even though there are no defined boundaries

or even complete shapes, these shapes are mostly there. We, as humans, are happy to accept that these shapes are what they are despite the fact that in a strict sense, none of these shapes exist. In a crisp logic world, there are no circles and no square. The vague shapes in Figure 8.1, not having well defined boundaries, do not meet the criteria for either circles or squares. The borders of the circles do not extend all the way around in a continuous arc and the square does not even have borders. In contrast to this we, as humans living in the fuzzy world, are able to extrapolate what we know we should see without any well defined rules or training.

This difference in philosophy has been called the “Aristotle vs. The Buddha” by Kosko [Kos93] or the prophet of  $A$  OR not  $A$  meets  $A$  AND not  $A$ . In the Aristotelian view,  $A$  is mutually exclusive with not  $A$ . Either  $A$  is true or it is not. In the Buddhist view, everything is true or false to varying degrees. Figure 8.2 illustrates this. In fuzzy logic, for certain values, both  $A$  and not  $A$  can be active to a certain degree at the same time where in crisp logic, they cannot.

### 8.1.1 Fuzzy Membership Functions

The functions that map values to fuzzy truths are referred to as Membership Functions or Fuzzy Sets.[Zad65] Some common membership functions are presented in Figure 8.3. These are by no means the only functions possible. Any function is admissible as a membership function provided it meets the following criteria:

- The function describes a vague concept. (Excellent or Rancid)
- The function admits the possibility of partial membership (The service was good to the degree .7)

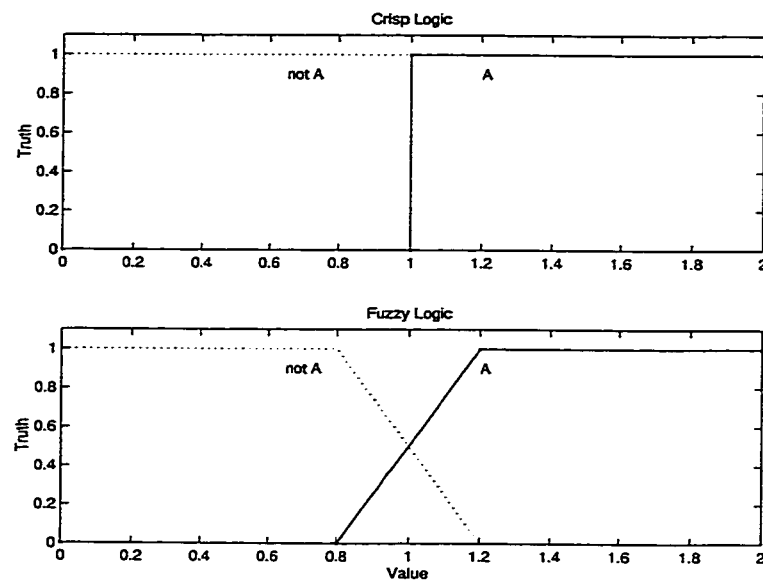


Figure 8.2: Fuzzy Truth Example

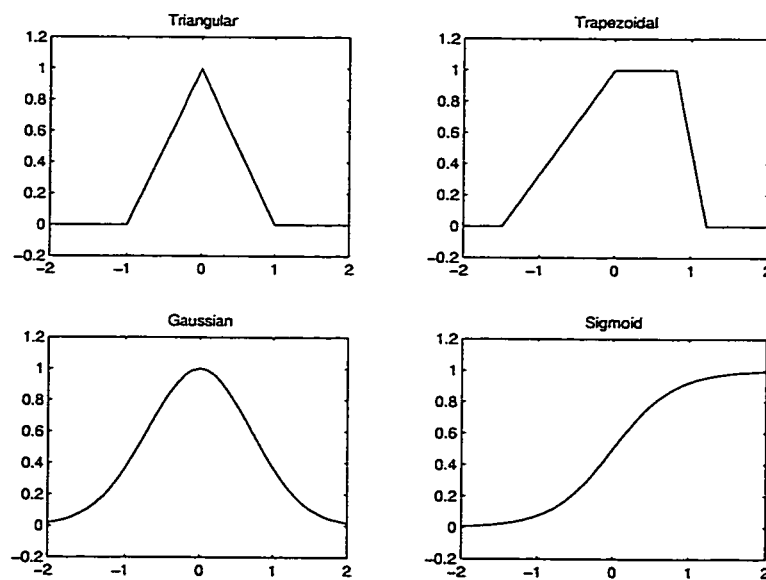


Figure 8.3: Fuzzy Membership Function Examples

- The degree an object belongs to the described set varies from 0 to 1.

### 8.1.2 Fuzzy Rules

An excellent application for fuzzy logic is to translate vague, human world concepts into a mathematically precise, computer ready rule system. An example would be a tipping algorithm. [JG97]

```
If SERVICE is POOR      or FOOD is RANCID      then TIP is CHEAP
If SERVICE is GOOD                               then TIP is AVERAGE
If SERVICE is EXCELLENT or FOOD is DELICIOUS then TIP is GENEROUS
```

Excellent service and Delicious food can both have varying degrees. A set of fuzzy rules like this one is often referred to as a “Fuzzy Inference System.” Because in fuzzy logic everything is true to a degree all rules are “fired” and evaluated at every instance. Each rule contributes to the result depending on how true the antecedent is. The more true the requirements are, the more heavily weighted that rule’s output is. This process is briefly outlined in Table 8.1.

## 8.2 The No Fly Zone

The case for multiple farm tractors working together shares many similarities with free flight. Although the potential for loss of life and property is much reduced in the agricultural setting, the results of an accident would certainly be extremely undesirable. The agricultural case can be thought of as a simplified case of free flight. There are (most likely) fewer vehicles in the area of interest alleviating the need for a protected zone. Unlike aircraft in free flight, however, often agricultural vehicles are

- Step 1 Fuzzify Inputs: The first step is to evaluate how true each input is. This step is essentially mapping the inputs to a value between 0 and 1.
- Step 2 Apply Fuzzy Operator: This step is the application of the evaluation of the antecedent.
- Step 3 Apply Implication Method: In this step, each rule is evaluated and an output command along with some definition of how much weight to give that command is generated.
- Step 4 Defuzzify: The final step is to take all the outputs generated and take some kind of weighted average of the output's command dependent on the weights associated with each of those commands.

Table 8.1: The Fuzzy Inference System

required to drive in close formation. This necessitates the need for a protected zone that is a function of not only the spatial separation, but also the angular separation of the vehicles. A vehicle may (and often must) approach much closer to another with matching headings than it can safely do so with a heading at a right angle to the other.

### 8.3 The Fuzzy Box Controller

A logical approach to defining the no fly zone is simply to define a box around the master vehicle. This box should be large enough to ensure no collisions yet small enough to allow for tight formations. This type of box simply attempts to keep the slave vehicle out of the forbidden region. Figure 8.4 defines the dimensional notation to be used.

The approach taken in this controller is to use a LQR regulator the majority of

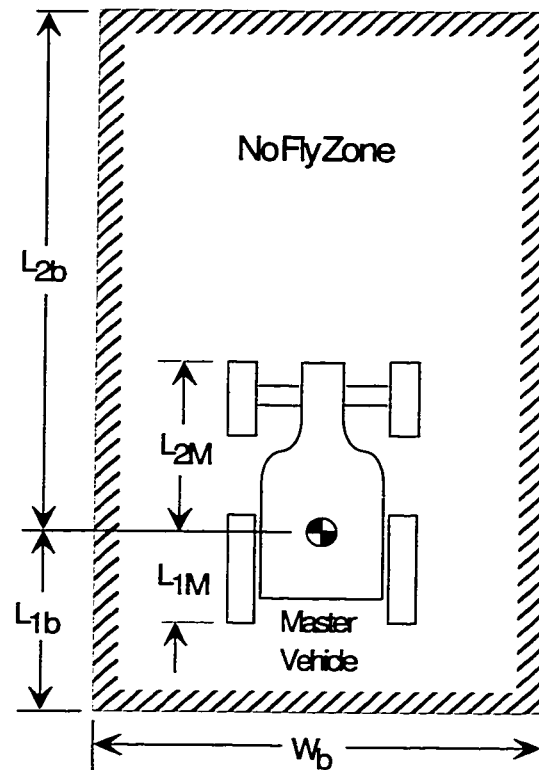


Figure 8.4: Fixed Box No Fly Zone Dimensions

the time and only use the fuzzy controller for conflict resolution. A separate fuzzy system determines which control law should be used. When no conflict is detected, the LQR regulator receives complete control authority. As a conflict becomes more and more imminent, the fuzzy regulator receives more control authority until a conflict is completely true and the fuzzy regulator has complete authority.

### Fuzzy Sets and Rules

There were several sets to describe and predict an imminent collision. These included

- *TOO CLOSE LONGITUDINAL* Based solely on the relative longitudinal position of the slave vehicle.
- *TOO CLOSE LATERAL* Based on the relative lateral position of the slave vehicle.
- *CLOSE LATERAL* Similar to *TOO CLOSE LATERAL* but further out from the master vehicle.
- *ON RIGHT/LEFT and POINTING RIGHT/LEFT* these sets define which side of the master the slave is on and in what relative directions they point.

These sets were used to generate a *COLLISION IMMINENT* set which was

$$\text{COLLISION IMMINENT} = \text{TOO CLOSE LONGITUDINAL and } [\text{TOO CLOSE LATERAL or } (\text{CLOSE LATERAL and } ((\text{ON RIGHT and POINTING LEFT}) \text{ or } (\text{ON LEFT and POINTING RIGHT}))) ]$$

Simply put, this rule is just “a collision is imminent if the slave is already in the no-fly zone or if it’s near it and pointing towards it.”

Relative velocities are not accounted for in this particular rule set. It was assumed that the convergence of the two vehicles would not be so aggressive that the distance traveled between time intervals would be a significant fraction of the total separation distance. To account for large relative velocities, the boundaries can be expanded to envelop the extra distance closed under nominal braking ( $\Delta X = \frac{3\Delta V_0^2}{2a}$ .)

Once an imminent collision was detected, the fuzzy controller would then take over and dictate a heading and a relative speed for the slave. This controller was designed

| relative heading | Commanded Slave Heading |                 |
|------------------|-------------------------|-----------------|
|                  | Relative Slave Position |                 |
|                  | <i>ON LEFT</i>          | <i>ON RIGHT</i> |
| <i>LEFT</i>      | $-\frac{\pi}{2}$        | 0               |
| <i>CENTER</i>    | $-\frac{\pi}{2}$        | $\frac{\pi}{2}$ |
| <i>RIGHT</i>     | 0                       | $\frac{\pi}{2}$ |

| relative heading | Commanded Slave Speed |                 |
|------------------|-----------------------|-----------------|
|                  | <i>ON LEFT</i>        | <i>ON RIGHT</i> |
| <i>LEFT</i>      | 1                     | 0               |
| <i>CENTER</i>    | $-\frac{1}{2}$        | $\frac{1}{2}$   |
| <i>RIGHT</i>     | -1                    | 1               |

Table 8.2: Fuzzy Controller Conflict Resolution Commands for Desired Point on Right side of Master

to move the slave vehicle out of danger as quickly as possible. The commands for each situation are tabulated in Table 8.2. This table describes the case when the desired slave position was on the right hand side of the master vehicle. The relative headings are referenced with the master vehicle heading defined as zero. When the desired slave position was on the left hand side, the entries in Table 8.2 were simply mirrored.

The weight of the linear (LQR) and the fuzzy controllers' votes was dependent on the fuzzy evaluation of the collision imminent function. With a zero evaluation, the linear position regulator took over completely. With a unity evaluation the fuzzy anticollision controller had complete authority. With an evaluation somewhere between zero and one the two controllers shared authority proportionally.



## 8.4 The Dynamic Fuzzy Box Controller

The dynamic box is very similar to the standard box controller with the dimensions of the box as functions of the relative heading between the master and the slave. This is done to account for the possibility of the slave approaching closer to the master when the headings match than when they are at right angles. Each of the four box dimensions ( $L_{1,b} - L_{4,b}$ ) shown in Figure 8.6 is parameterized as a simple function of the relative heading

$$X = A + B \cos \Psi_{rel} + C \sin \Psi_{rel} + D \cos 2\Psi_{rel} \quad (8.1)$$

where  $X$  is one of the four box parameters,  $L_{1--4,b}$

The coefficients, outlined in Table 8.3, are selected to fit constraints put on the closest approach allowed at each of the four main compass points (in relative heading.) In Table 8.3, the parameters

$$\begin{aligned} \alpha &= \frac{1}{4} (L_{1,s} + L_{2,s} + W_s) \\ \beta &= \frac{1}{2} (L_{1,s} - L_{2,s}) \\ \gamma &= \frac{1}{4} (L_{1,s} + L_{2,s} - W_s) \end{aligned} \quad (8.2)$$

are used for notational simplicity due to their obvious repetition. These coefficients yield a no fly zone as illustrated in Figure 8.7. This figure was generated using arbitrary parameters of  $L_1 = 1\text{m}$ ,  $L_2 = 1\text{m}$  and  $W = 1\text{m}$  for both vehicles.

This rather complex exclusion zone makes a constrained optimization very difficult. A simulation to find the optimal trajectory from an initial condition that would pass through the no-fly zone in an unconstrained case was run using MATLAB's optimization tool box on a Sun Ultra workstation. This simulation was run for two days

|   | $L_{1,b}$          | $L_{2,b}$          | $L_{3,b}$                 | $L_{4,b}$                 |
|---|--------------------|--------------------|---------------------------|---------------------------|
| A | $L_{1,m} + \alpha$ | $L_{2,m} + \alpha$ | $\frac{1}{2}W_m + \alpha$ | $\frac{1}{2}W_m + \alpha$ |
| B | $-\beta$           | $\beta$            | 0                         | 0                         |
| C | 0                  | 0                  | $\beta$                   | $-\beta$                  |
| D | $\gamma$           | $\gamma$           | $-\gamma$                 | $-\gamma$                 |

Table 8.3: Dynamic Box Dimension Coefficients

and over 300,000 candidate trajectories were evaluated. No solution was found that minimized the cost function while meeting the constraints. This simple experiment gives strong support to the idea that alternative methods of trajectory generation must be sought. These solutions may come in the form of more elegant optimization algorithms or alternative optimization criteria.

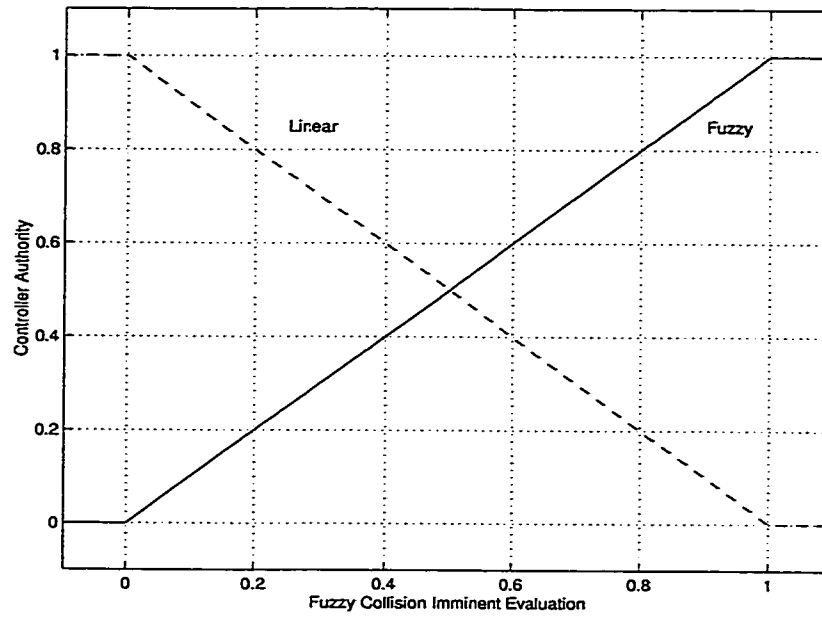


Figure 8.5: Fuzzy and Linear Controller Authority versus Collision Imminence

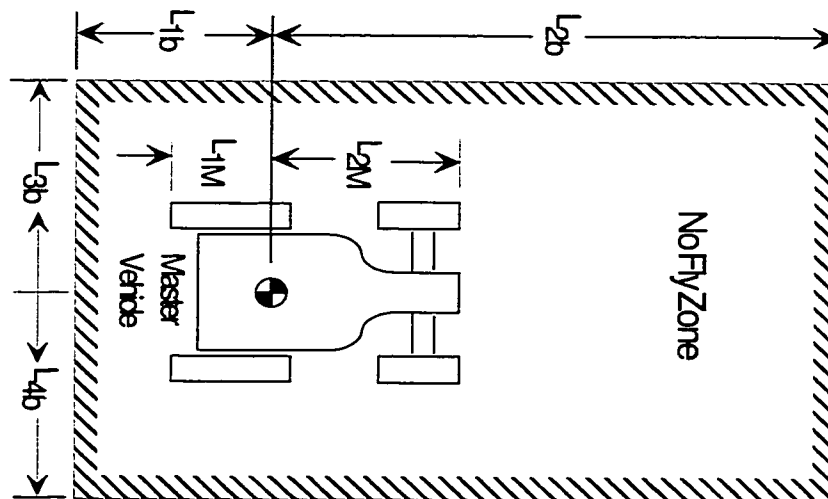


Figure 8.6: Dynamic Box No Fly Zone Dimensions

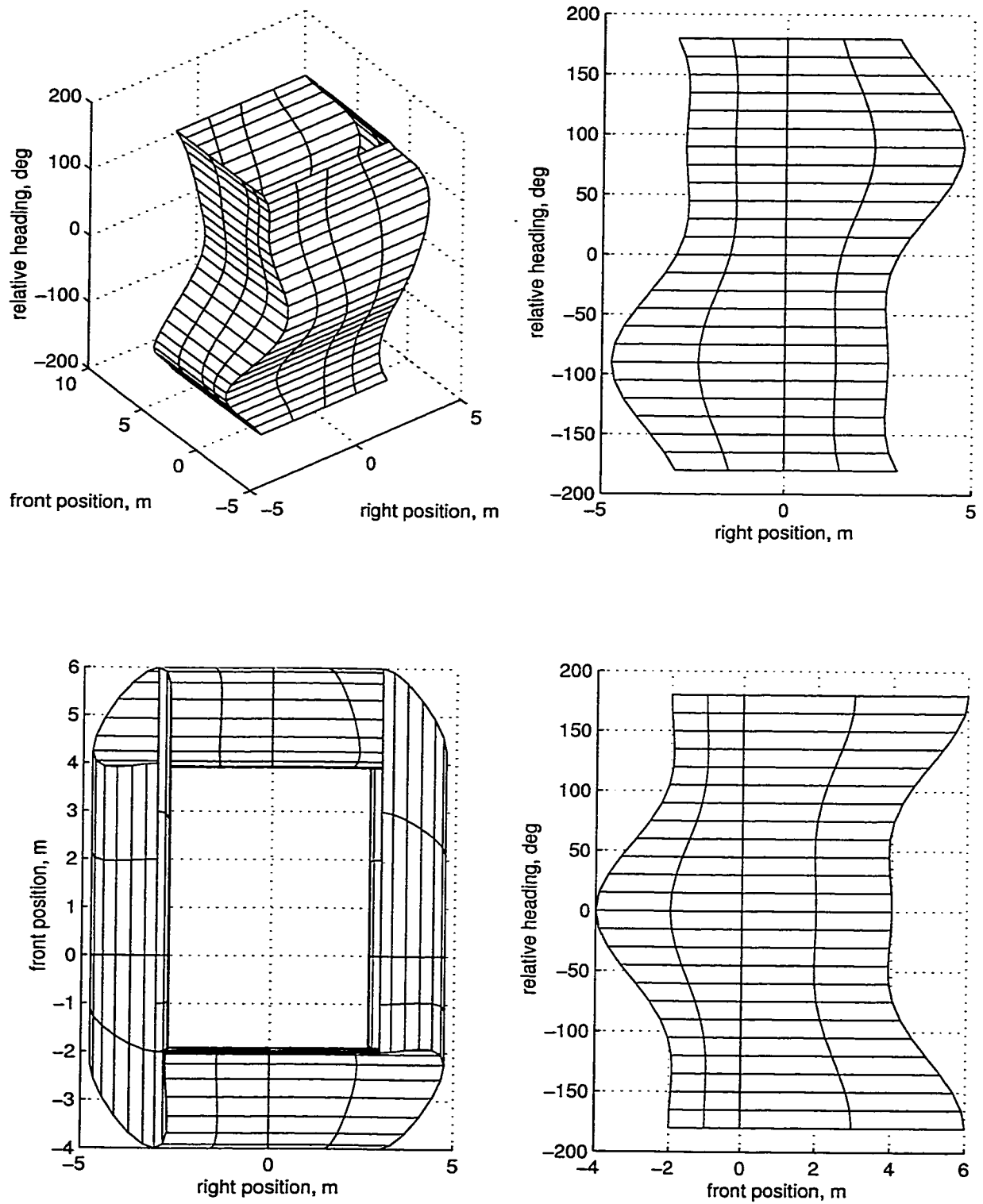


Figure 8.7: Dynamic Box Dimensions



## CHAPTER 9

# Formation Driving Experimental Results

A series of experiments were conducted to verify the validity of the formation driving algorithms. These experiments consisted of the slave vehicle used in the adaptive control experiments following a master vehicle.

The master vehicle was operated manually and only measured GPS position. No velocity, attitude or wheel angle measurements were made. This was done in an attempt to verify the concept that tight formation could be held using master vehicle position only.

The slave vehicle had the capability of both automatic steering and fully automatic speed control, including automatic transmission engagement and gear selection as well as automatic throttle. A more detailed description of the vehicle configurations is available in appendix A. During the experimental runs, GPS position, GPS attitude and steering wheel angle measurements of the slave vehicle were made available to the controller.

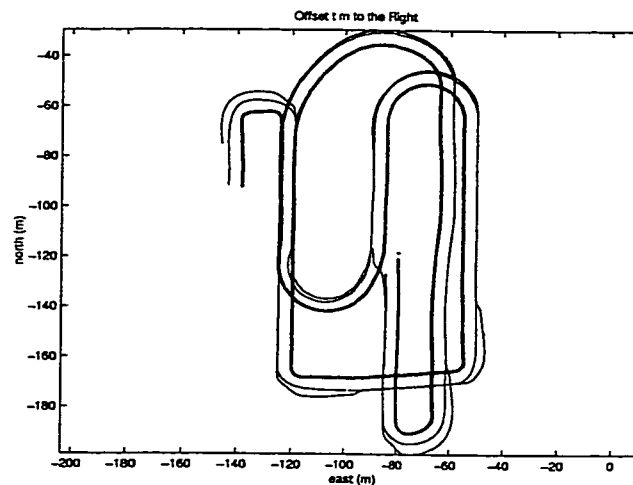


Figure 9.1: Trajectories driven with slave vehicle maintaining position 5 meters to the right of the master vehicle

## 9.1 Position Regulation Performance

A series of trajectories were driven somewhat at random by a human operator in the master vehicle. For the first trajectory, shown in Figure 9.1, the resulting formation position errors are shown in Figure 9.2. When outside of the linear control region, the slave vehicle used “carrot on a stick” control, aiming the nose of the tractor directly at a point slightly in front of the desired final relative position. Longitudinal control was regulated directly about the desired point. When sufficient convergence to the desired point was achieved, control was switched over to tight control mode using the “tractor on a stick” method and lateral and longitudinal control were maintained about a line centered on the desired location. While in tight control mode, both lateral and longitudinal accuracy were maintained to approximately 10 cm.

When the master vehicle executes relatively sharp turns the slave vehicle cannot

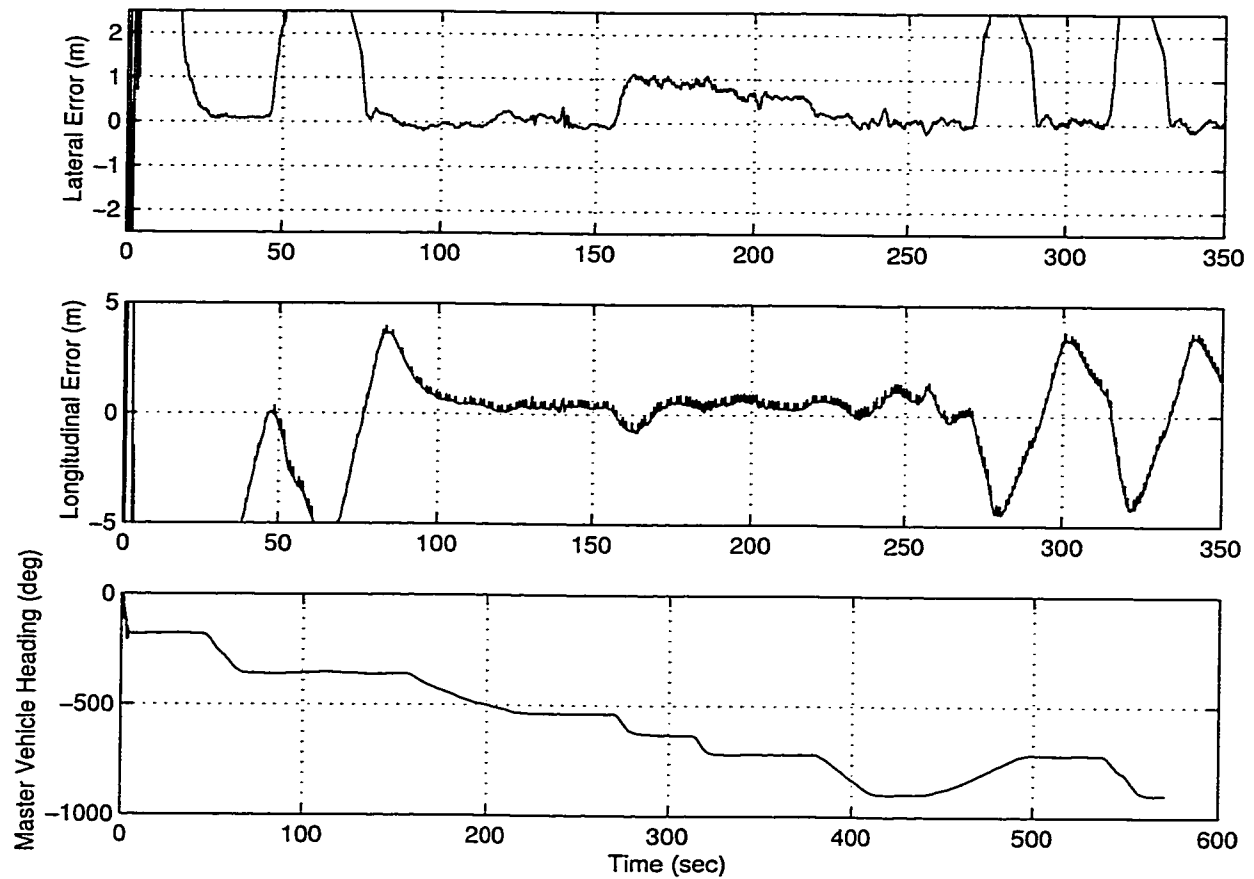


Figure 9.2: Formation position errors for desired position of five meters to the right of the master vehicle



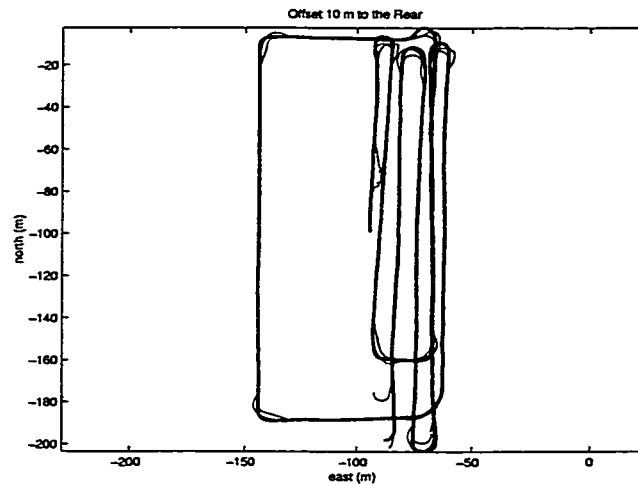


Figure 9.3: Trajectories driven with slave vehicle maintaining position ten meters to the rear of the master vehicle

maintain position lock. This is because the turning master vehicle translates the desired location too quickly, much as a sprayer arm swings around when a sprayer is turned. Without prior knowledge of the trajectory of the master vehicle it is unreasonable to expect the slave vehicle to maintain a tight lock on position throughout a severe turn.

A second set of data illustrates the performance with the slave vehicle following ten meters to the rear of the master vehicle. The trajectory driven is shown in Figure 9.3 and the position errors are shown in Figure 9.4. The same control algorithm was used as with the previous case. Not surprisingly, the performance of the system did not change significantly. Again approximately 10cm accuracy was maintained in both the lateral and longitudinal directions when in tight control mode.

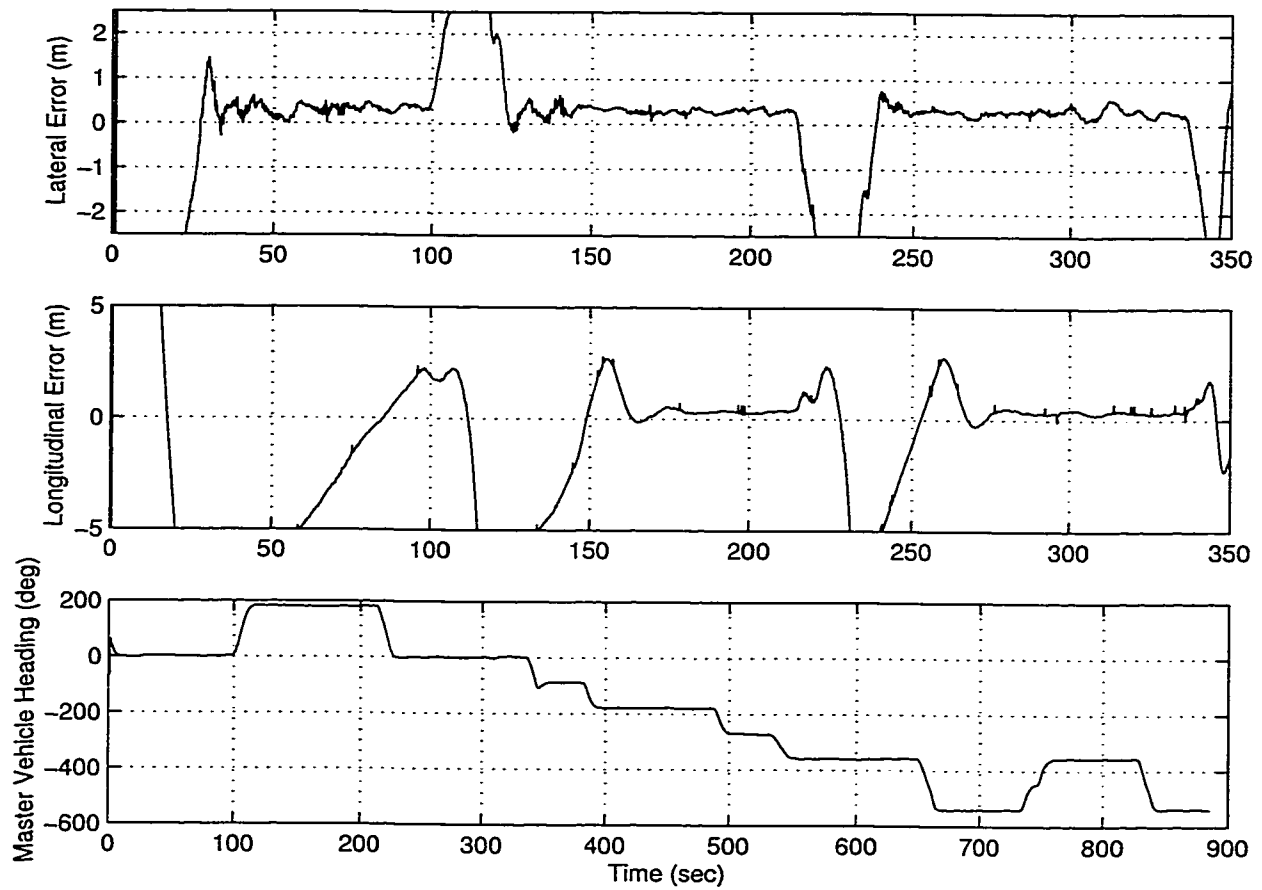


Figure 9.4: Formation position errors for desired position of ten meters to the rear of the master vehicle

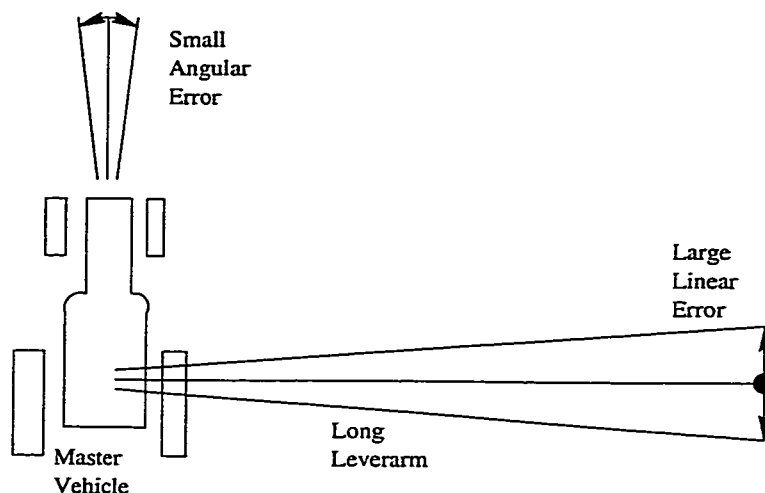


Figure 9.5: How Small Heading Errors Translate Into Large Linear Errors with Large Leverarms

Bell discusses a lever-arm concern in position estimation when there exists a non-trivial angular uncertainty. [Bel99] The uncertainty of the location of a point projected from a known point grows linearly with the length of the projection when the angle of the projection is uncertain. There exists a parallel problem in formation driving where the exact heading angle of the master vehicle can only be estimated. As the distance between master vehicle and desired relative slave position grows so does the error and consequently the uncertainty of the absolute slave position as measured in the navigation frame. A lever-arm of 3.5 meters and heading uncertainty of 0.5 degrees is sufficient to induce as much uncertainty in the position as the CDG-PS position uncertainty. A five meter lever-arm requires a master vehicle heading measurement of better than 0.3 degrees to offer similar performance. The accuracy in heading during experimentation was obtained using only master position information. Heading accuracy of about 5 degrees was achieved for the master vehicle. This

is undoubtedly a major contribution to the accuracy of the overall system.

It is also interesting to note that 11 cm accuracy was predicted by O'Connor in his thesis [O'C97] for a single vehicle with CDGPS position only. A significant improvement to this was made with the addition of a low cost (\$50) steering angle sensor. With the steer angle sensor, expected performance improved to just over 4 cm in lateral accuracy. The addition of an accurate measure of attitude also made a significant improvement to overall system accuracy with or without the steering angle sensor. Accordingly, it is not unreasonable to assume very similar advantages accrue with the addition of these sensors to the master vehicle. This would allow for a more accurate master vehicle state estimate and consequently a more accurate reference position to provide for the slave vehicle.

## 9.2 Collision Avoidance Simulations

Several hundred simulations of the fuzzy anticollision algorithm were run. These were run under MATLAB and began with the slave vehicle at a random location and with a random heading relative to the master vehicle. The slave vehicle was not allowed to begin directly on top of or in front of the master because these initial conditions were deemed unreasonable and unlikely. The simulation was then started and the trajectory of the slave vehicle in relative coordinates was tracked. Some of these trajectories are shown in Figure 9.6. In this figure, the meshed region represents the exclusion zone and the solid lines represent individual trajectories of the slave vehicle in master vehicle relative coordinates.

Several general behaviors of the overall system controllers were noticed. Due to controllability issues at zero slave vehicle velocity, the slave was constrained to positive

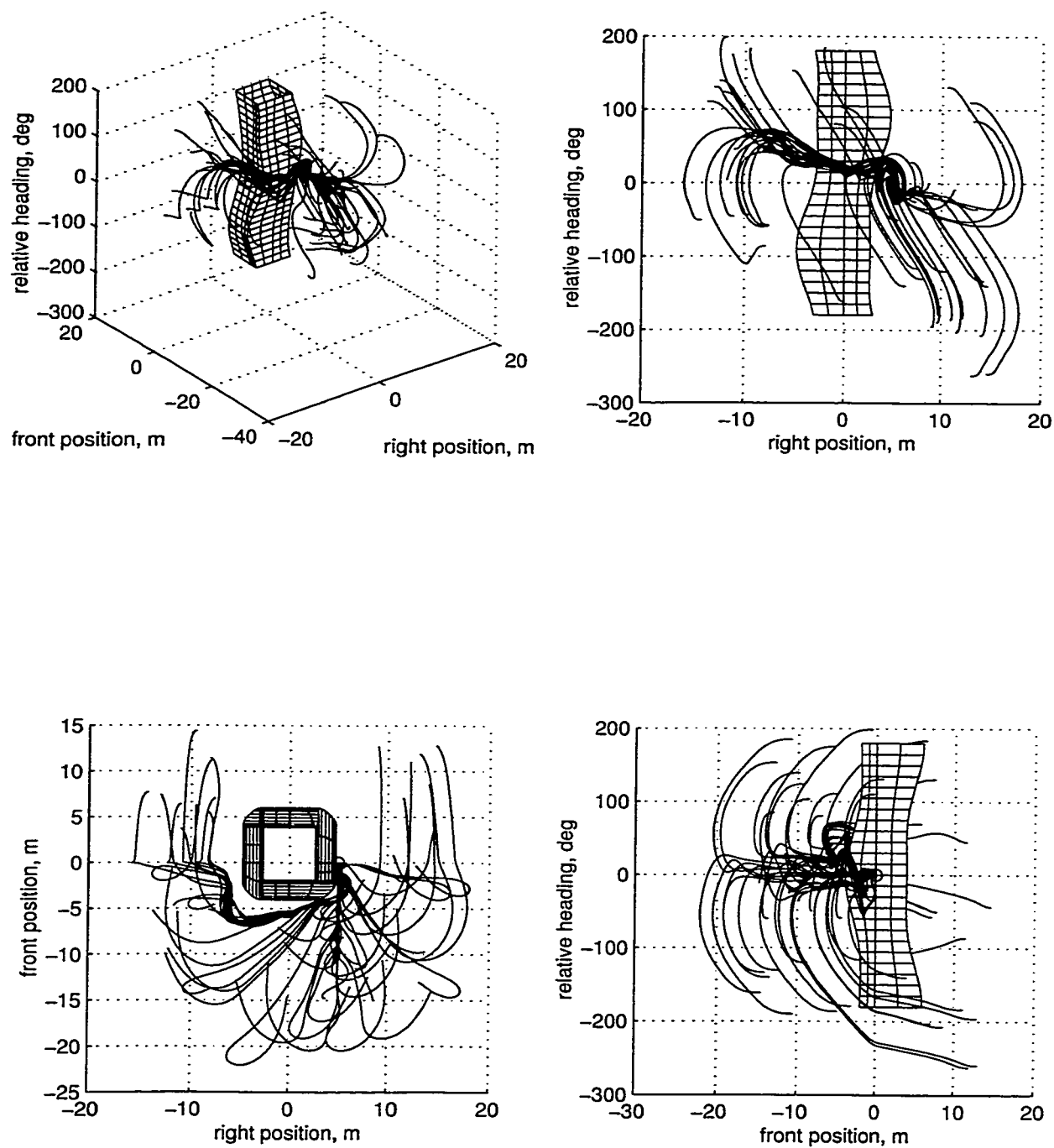


Figure 9.6: Anticollision simulation trajectories

velocities. It was allowed to slow to very low speeds. When the slave was in front of the master vehicle it simply slowed down greatly and waited for the master vehicle to catch up and pass it. It then would acquire and lock on to the desired point quite quickly.

A second behavior noticed was when the slave vehicle was on the opposite side of the master from the desired location and close behind. There existed a conflict between the linear controller trying to get to the desired location and the fuzzy controller attempting to prevent a collision. Each controller was commanding a different direction and each with nearly identical authority. The tractor would slowly drift aft of the master vehicle and towards the command point until reaching the centerline of the master vehicle. At the centerline, both controllers would once again agree on a direction to turn and the slave would quickly move to the side of the master vehicle and acquire the desired point.

The most interesting and important behavior to note is that no vehicle collisions were observed. Over one thousand simulations were run each from a random initial state and no collisions were detected. Furthermore, in each of these simulations the slave vehicle successfully acquired the desired location.



# CHAPTER 10

## Conclusions

### 10.1 Conclusions

This thesis contains the working model for extending the accuracy and capability of automatically guided vehicles. To accomplish this, several important contributions were made to the field.

- An algorithm that will identify and compensate for both deadzone and dynamics in an actuator was developed. This algorithm was applied to an experimental vehicle and shown to satisfactorily compensate for system deadzone.
- A parameter identification algorithm that does not require the extension to the number of states to a Kalman filter was developed. This algorithm was presented in both a generalized form and a specific algorithm to identify the O'Connor parameters in a farm tractor. In the farm tractor case this algorithm maintained a stable parameter estimate where a comparable Extended Kalman Filter became unstable and diverged. The developed algorithm also required 94% fewer computational operations than did the EKF.



- Experimentally verified the stability of the LMS/EKF algorithm on a farm tractor.
- Experimentally showed the benefits of using an adaptive control scheme over a fixed controller. As the operating conditions vary the vehicle dynamics change and the control system must identify and compensate for these variations. This improved the accuracy of the experimental tractor from 4.35 cm to 3.1 cm. The performance increase may be negligible for certain operations such as tillage but may become quite valuable when every centimeter counts such as in a drip tape irrigation setting and cultivating. This improvement represents an approximate improvement of 100:1 in the probability of a cultivator incursion. (See Figure 1.3.)
- Quantified the difficulty and importance of accurate identification of each of the O'Connor parameters on an experimental system. It was illustrated that the steering actuator lag and steering effectiveness are roughly twice as important to identify well than yaw damping or leverarm variation. Consequently, the identification efforts should be focused on the prior two parameters.
- Developed algorithms to allow formation and cooperative control of two or more farm vehicles. The ground path that was required for the slave vehicle was a function of the desired operation to be executed. Consequently, several reference position techniques were developed to cope with the various requirements.
- Developed new formation trajectory components. Prior to this research, work was focused on defining trajectory components for individual vehicles. The

prior components could be combined into very complex and general trajectories. New complimentary formation driving trajectory components were added. With these components added, a slave vehicle may act independently or in co-operation with one or more vehicles.

- Experimentally demonstrated effective speed and longitudinal position control on a farm tractor for formation work. The accuracy of this control was approximately 12 cm while transmitting only master vehicle position to the slave vehicle.
- Experimentally demonstrated effective lateral position control on a farm tractor under formation control. The accuracy of this control was also approximately 12 cm while transmitting only master vehicle position to the slave vehicle.

Two important conclusions can be drawn from this work. First, effective adaptive control of farm vehicles is not only important but practical. Adaptive control can be implemented with no additional sensors over those necessary for reasonably accurate automatic control in the first place.

The second important conclusion is that formation driving of vehicles can be practical. Furthermore, formation control can be achieved with no a-priori trajectory information. This allows one human operator to control multiple vehicles effectively to increase efficiency.

## 10.2 Future Work

Any worthwhile research usually raises more questions than it answers. As the fundamental questions begin to be answered, questions about the details spring up. Similarly, as new capabilities are developed, new applications become apparent. Thankfully, this work was no exception.

This research has been very exciting to work with as it has immediate and highly visible contributions to make to the agricultural community. There has been a great deal of interest in autofarming in general and we have only begun to scratch the surface of capabilities. Some areas that hold promise are listed below.

- *High Speed Control* The model used in this and previous work has been developed and specialized to a specific system and operating regime. Typically the work revolved around rubber tired vehicles driving relatively slowly. Ongoing research has illustrated that the simplifications made for low speed driving do not necessarily hold at higher speeds. Further understanding of wheel and soil interactions must be attained and modeled to allow practical high speed autofarming.
- *Implement Control* To a farmer, the location of the tractor itself is typically of secondary interest to the location of the implement in the ground. There is significant difficulty in accurately and robustly measuring implement position. The sensor must be accurate enough to justify implement control over simple vehicle control yet robust and rugged enough to survive the harsh environments expected.

- *Path Planning* In its current manifestations autofarming systems can only accomplish either straight line control with operator u-turns or they require highly trained people to program their trajectories. There is much work to do in with path planning before a farmer can simply load in a map of the field into the computer and have the tractor automatically generate the optimal trajectory to accomplish a set task.
- *Adaptive Control* Though this dissertation has dealt substantially with the issues involved with adaptive control, there is still much to be done. Only one method of adaptive control has been presented, it may prove beneficial to compare or utilize other adaptive control schemes. Additionally, the factors influencing vehicle performance such as vehicle configuration and soil conditions have been passively identified. It may prove highly beneficial to quantify these affects and feed forward that information into the estimator to allow better initial parameter estimates.
- *Real Time Disturbance Identification* There are certain operating conditions that could significantly benefit from real time disturbance identification. One such condition is when the vehicle is running at a shallow angle relative to previously set furrows. As the vehicle is driving the front wheels fall to the bottom of the furrows. As the tractor moves forward this tends to pull the nose of the tractor in the same direction as the furrows and consequently off course. The controller senses this happening and tries to compensate by gradually increasing the steering up the side of the furrow. Eventually a great enough steer angle is achieved that the front wheels climb over the ridge between furrows and overshoots the desired trajectory because the front wheels now have too much steer

angle. This cycle repeats itself over each furrow. It is thought that this type of disturbance has a narrow frequency content and that a feed forward steer angle command at the right amplitude, frequency and phase could greatly increase the disturbance rejection performance of the system.

- *Other Vehicle Types* More than rubber tired, front wheel steered vehicles exist on the farm. Articulated and tracked vehicles could also greatly benefit from autofarming.
- *Anticollision Algorithms* When there are many vehicles working closely there exists a real possibility of collision. The algorithm presented in this dissertation is only one of many possibilities. There are no guarantees that the presented algorithm can prevent all collisions.
- *Different “No Fly Zone” shapes* There existed a problem with the rectangular no fly zones where the slave vehicle got “stuck” in an undesired location where the LQR controller and fuzzy controllers exactly canceled each other out. Other shapes for the no fly zone, such as an elliptical zone, may alleviate this problem.
- *Multiple slave vehicles* In this work only one slave vehicle was used in formation work. Many farm operations require the choreography of multiple vehicles and multiple types of vehicles to accomplish a common task. These vehicles must compliment each other and any automatic control must take this into account.
- *Extension to Other Areas* Farms may not be the only place where this technology could contribute. Construction sites may greatly benefit from the extremely high accuracy and flexibility offered by automatic steering. The smart highways

of the future may also benefit from implementing lateral as well as longitudinal formation control to improve safety margins.

## 10.3 Closing

Automatic control of farm vehicles utilizing CDGPS has already been shown to be possible. With surprising speed, these techniques are being adopted into the industry and shown to be practical, affordable and beneficial. Autofarming will improve the efficiency of the farm and reduce overall operating costs. Adaptive control of these tractors will further improve the accuracy and reliability of these systems. It will allow for more flexibility while maintaining high standards for precision. Similarly, formation driving will allow multiple vehicles to co-operatively accomplish a common task in a more efficient manor.



# APPENDIX A

## Vehicle Configuration

This research used two full sized John Deere tractors. The first was a model 7800 and the second was a model 8400. Both of these tractors shared substantially the same sensor and control configuration with the only exception being the fully automatic throttle and transmission control on the 8400.

### A.1 John Deere Model 7800

The first test vehicle employed was a John Deere model 7800 tractor. The test vehicle is shown in figure A.1 and had the following characteristics:

- 145 hp turbo charged in-line 6 cylinder diesel engine
- 19 forward speeds with gearing to 22 MPH
- Four wheel drive
- Lockable rear differential
- Adjustable ballast





Figure A.1: John Deere Model 7800 Test Tractor

- 14,300 pound unballasted gross weight
- Length of 173 inches, axle width of 110 inches and height of 116 inches

## A.2 John Deere Model 8400

A second test vehicle, a John Deere 8400 was obtained to allow formation driving. This vehicle is shown in figure A.2. This vehicle has a fully computer controlled transmission and throttle allowing a very simple interface to the transmission. The test vehicle also had the following characteristics:

- 225 hp turbo charged in-line 6 cylinder diesel engine
- 16 forward speeds with gearing to 22 MPH

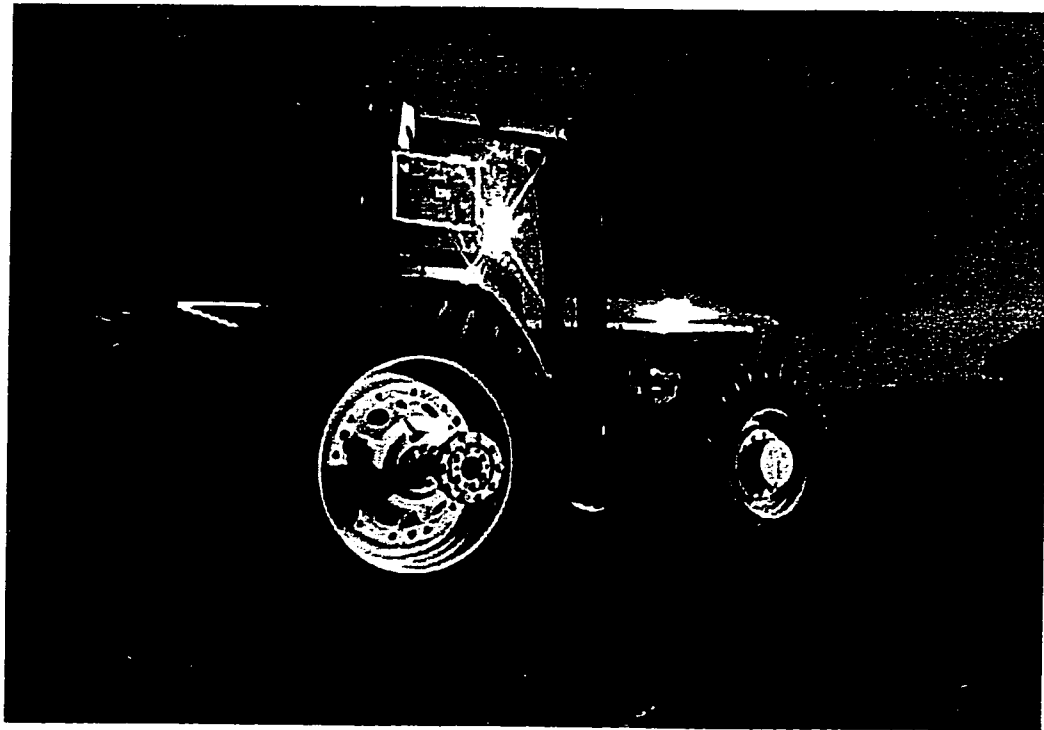


Figure A.2: John Deere Model 8400 Test Tractor

- Four wheel drive
- Lockable rear differential
- Adjustable ballast
- 18,700 pound unballasted gross weight
- PowerShift transmission
- Length of 207 inches, axle width of 118 inches and height of 120 inches

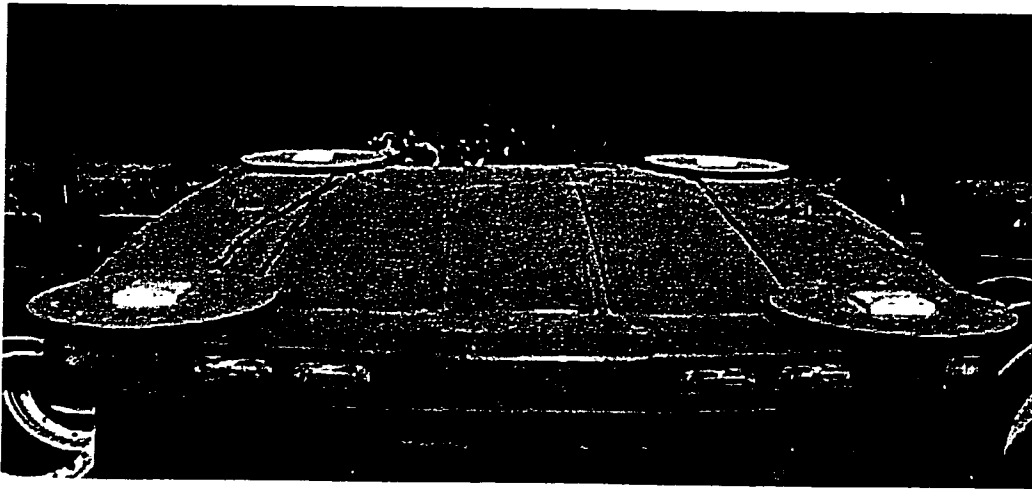


Figure A.3: John Deere Model 8400 Test Tractor Antenna Configuration

### A.3 Sensor and Actuator Hardware

The foundation of the sensor system was the carrier phase differential GPS (CDGPS) hardware provided by the IntegriNautics Corporation. This hardware consisted of a ground based reference station and a mobile positioning unit. The overall system accuracy measured from the reference station to the mobile antenna was approximately 1 to 1.5 cm ( $1\sigma$ ) horizontally and 2 to 3 cm vertically. The reference station transmitted GPS corrections to the tractor through radio modems at 38,400 baud.

Attitude measurements were provided by Trimble Navigations TANS Vector. The antennas were mounted on the four corners of the cab roof (see figure A.3). The front right antenna signal was split and routed to the positioning and attitude systems. The Vector provided 10Hz measurements of roll, pitch and yaw to within approximately 0.1 degrees.

Steering angle measurements were made with a linear potentiometer mounted



Figure A.4: John Deere Model 8400 Test Tractor Steer Angle Sensor



Figure A.5: John Deere Model 8400 Test Tractor Guidance Computer

between the steering knuckle and the axle (figure A.4.) This sensor was excited and sensed by a Motorola 86HC12 which communicated serially to the guidance computer.

The guidance computer consisted of the computer shown in figure A.5. This computer was operating under the Lynx real-time operating system and mounted inside the tractor's cab.

Throttle commands were generated by emulating a foot throttle with a D/A board hooked into the foot throttle wiring harness. Shift and gear selections were made by interfacing with the tractors armrest controller and CCD bus.

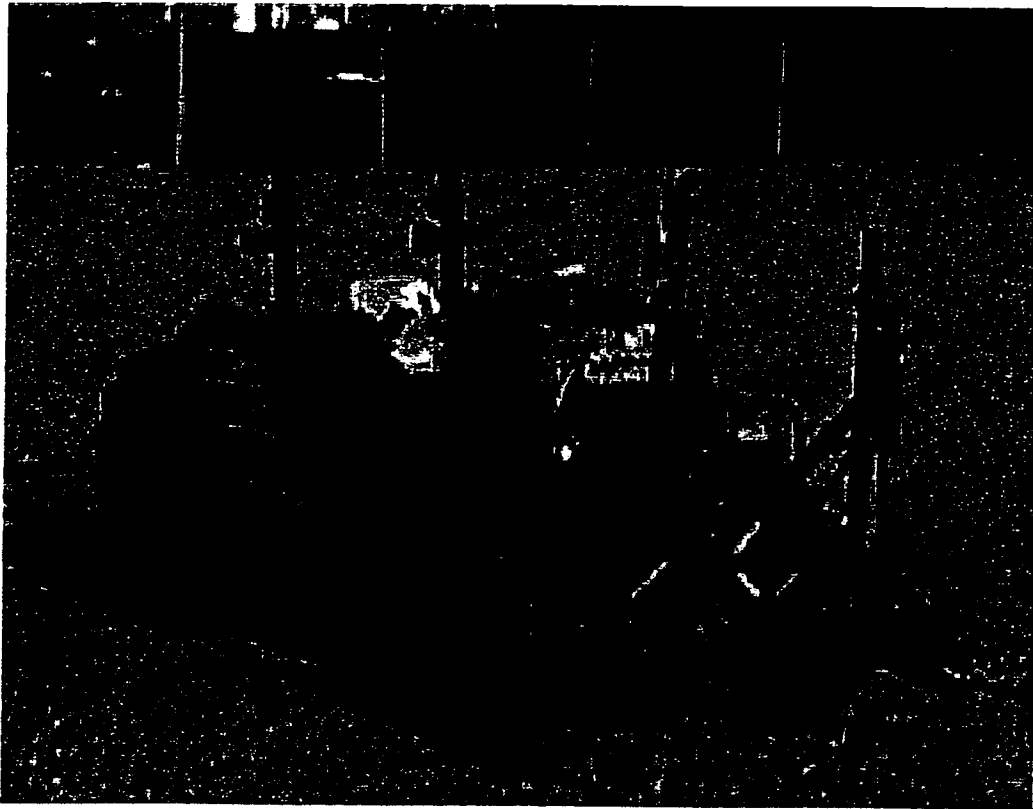


Figure A.6: Formation Driving Master Vehicle Test Tractor

## A.4 Formation Driving Master Vehicle

The master vehicle used for formation driving experiments was a small 4000 series tractor shown in figure A.6. This vehicle was configured with an Integrinautics CDGPS receiver and a radio modem. Due to modem communication restrictions, the reference station would send corrections to the 8400 slave vehicle and they would then be relayed to the master vehicle as described in section 7.1.3. Once a master vehicle position was available it was transmitted to the slave vehicle over the same radio modem. During all experiments, the master vehicle was under manual control.



# Bibliography

- [AH97] Luis Alvarez and Roberto Horowitz. Hybrid Controller Design for Safe Maneuvering in the PATH AHS Architecture. In *Proceedings of the 1997 American Control Conference*, pages 2454–2549. IEEE, 1997.
- [Ano99] Anonymous. Agsystems Pty Ltd: Feasibility Analysis. World Wide Web Page: <http://www.agsystems.com.au/>, 1999.
- [Bel99] Thomas Bell. *Precision Robotic Control of Agricultural Vehilces on Realistic Farm Trajectories*. PhD thesis, Stanford University, Stanford, California 94305, June 1999.
- [Ben91] J. G. Bender. An Overview of Systems Studies of Automated Highway Systems. *IEEE Transactions on Vehicular Technology*, 40(1):82–89, 1991.
- [BIMG98] Itzhack T. Bar-Itzhack, Paul Y. Montgomery, and Joseph C. Garrick. Algorithms for attitude Determination Using the Global Positioning System. *AIAA Journal of Guidance Control and Navigation*, 21(6):846–852, November–December 1998.
- [CDN71] S. K. Clark, R. N. Dodge, and G. H. Nybakken. An Evaluation of String Theory for the Prediction of Dynamic Tire Properties Using Scale Model



Aircraft Tires. Technical Report 05680-18-T, University of Michigan, Tire and Suspension Systems Research Group, 1971.

- [Coh92] Clark Cohen. *Attitude Determination Using GPS*. PhD thesis, Stanford University, Stanford, California 94305, December 1992.
- [EOBP96] G. Elkaim, M. O'Connor, T. Bell, and B. Parkinson. System Identification of a Farm Vehicle Using Carrier-Phase Differential GPS. In *Proceedings of the 9th International Technical Meeting of the Setellite Division of the Institute of Navigation, ION GPS-96*, pages 485 – 494. Institute of Navigation, 1996.
- [EOBP97] G. Elkaim, M. O'Connor, T. Bell, and B. Parkinson. System Identification and Robust Control of Farm Vehicles Using CDGPS. In *Proceedings of the 10th International Technical Meeting of the Setellite Division of the Institute of Navigation, ION GPS-97*, pages 1415 – 1424. Institute of Navigation, 1997.
- [EWP<sup>+</sup>96] Per Enge, Todd Walter, Sam Pullen, Changdon Kee, Yi-Chung Chao, and Yeou-Jyh Tsai. Wide Area Augmentation of the Global Positioning System. *Proceedings of the IEEE*, 84(8):1063–1088, August 1996. Paper Number 0018-9219.
- [FCA99] Mark Farwell, Doug Caldwell, and Mohamed Abousalem. RTK-Based Vehicle Tracking and Unmanned Operation for Agriculture. In *Proceedings of ION-GPS '99*. Institute of Navigation, 1999.

- [For91] B. Forsell. *Radionavigation Systems*. Prentice Hall, New York, New York, 1991.
- [GB96] J. Guinn and R. Boain. Spacecraft Autonomous Formation Flying Earth Orbiters Using GPS. In *AIAA/AAS Astrodynamics Specialists Conference*. American Institute of Aeronautics and Astronautics, July 1996.
- [GG76] M.S. Grewal and K. Glover. Identifiability of Linear and Non-Linear Dynamical Systems. *IEEE Transaction on Automatic Control*, 21(6):833 – 837, December 1976.
- [Gil92] Thomas D. Gillespie. *Fundamentals of Vehicle Dynamics*, pages 335 – 375. Society of Automotive Engineers, Warrendale, Pennsylvania, 1992.
- [Goo82] Richard P. Gooch. Adaptive Pole-Zero Array Processing. In *IEEE 1982 Conference Record of the Sixteenth Asilomar Conference on Circuits, Systems & Computers*, pages 45 – 49, Silver Spring, Maryland, 1982. IEEE.
- [Hay84] S. Haykin. *Introduction To Adaptive Filters*. Macmillan, New York, New York, 1984.
- [HKKP95] Gordon T. Haupt, N. Jeremy Kasdin, George M. Keiser, and Bradford W. Parkinson. Optimal Recursive Iterative Algorithm for Discrete Nonlinear Least-Squares Estimation. *AIAA Journal of Guidance, Control, and Dynamics*, 19(3):643–649, 1995.
- [HMNS91] J. K. Hedrick, D. McMahon, V. Narendran, and D. Swaroop. Longitudinal Vehicle Controller Design for IVHS System. In *Proceedings of*

- the 1991 American Control Conference*, pages 3107–3112. American Automatic Control Council, 1991.
- [HTV94] J.K. Hedrick, M. Tomizuka, and P. Varaiya. Control Issues in Automated Highway Systems. *IEEE Control Systems Magazine*, 14(6):21–32, 1994.
- [JG97] J. S. Roger Jang and Ned Gulley. *MATLAB Fuzzy Logic Toolbox User's Guide*. MathWorks Inc., Natick, Massachusetts, 1997.
- [Joh97] P. Johnson. Boggabilla GPS Boosts Efficiency. *The Land*, 3884, Sept 4 1997.
- [Kan76] G. Kanizsa. Subjective Contours. *Scientific American*, 234:48 – 52, 1976.
- [Kel93] Brian Scott Keller. *On-Line Physical Parameter Identification and Adaptive Control of a Launch Vehicle*. PhD thesis, Stanford University, Stanford, California 94305, March 1993.
- [KF97] Myron Kayton and Walter R. Fried. *Avionics Navigation Systems*. John Wiley and Sons, Inc, New York, New York, 2<sup>nd</sup> edition, 1997.
- [KH97] N. Jeremy Kasdin and Gordon T. Haupt. Second-Order Corrections and Numerical Considerations for the Two-Step optimal Estimator. *AIAA Journal of Guidance, Control, and Dynamics*, 20(2):362–369, 1997.
- [Kos93] Bart Kosko. *Fuzzy Thinking: The New Science of Fuzzy Logic*. Hyperion Books, New York, New York, 1993.
- [Lju87] Lennart Ljung. *System Identification: Theory for the User*. Prentice Hall, Englewood Cliffs, New Jersey, 1987.

- [LSG99] W. S. Lee, D. C. Slaughter, and D. K. Giles. Robotic Weed Control System for Tomatoes. *Precision Agriculture*, 1(1):95–113, January 1999.
- [Mai97] R. Mailer. Innovative Navigation System puts Farmers on the Right Track. *Australian Grain*, 7:3–6, June–July 1997.
- [MHQK98] M. Susan Moran, Daniel C. Hymer, Jiaguo Qi, and Yann Kerr. Radar Imagery for Precision Crop and Soil Management. In P. C. Robert, R. H. Rust, and W. E. Larson, editors, *Proceedings of the 4th International Conference On Precision Agriculture*, pages 1423–1434. American Society of Agronomy, Crop Science Society of America and Soil Science Society of America, July 1998.
- [N<sup>+</sup>97a] N. Noguchi et al. Development of a Tillage Robot Using a Position Sensing System and a Geomagnetic Direction Sensor. In *Proceedings of the 1997 ASAE Annual International Meeting*, Minneapolis, Minnesota, 1997. ASAE.
- [N<sup>+</sup>97b] N. Noguchi et al. Development of an Agricultural Mobil Robot using a Geomagnetic Direction Sensor and Image Sensors. *Journal of Agricultural Engineering Research*, 67:1–15, 1997.
- [Nas97] J. Nason. Boggabilla GPS Cuts Farm Costs. *Queensland Country Life*, August 21 1997.
- [OB82] Russel H. Owen and James E. Bernard. Directional Dynamics of a Tractor-Loader-Backhoe. *Vehicle System Dynamics 11*, pages 251 – 265, 1982.

- [O'C97] Michael L. O'Connor. *Carrier-Phase Differential GPS for Automatic Control of Land Vehicles*. PhD thesis, Stanford University, Stanford, California 94305, December 1997.
- [OPH98] Eric A. Olsen, Chan-Woo Park, and Jonothan P. How. 3D Formation Flight using Differential Carrier-Phase GPS sensors. In *Proceedings of ION GPS-98*. Institute of Navigation, September 1998.
- [Owe82] G. M. Owen. A Tractor Handling Study. *Vehicle System Dynamics*, 11:215 – 240, 1982.
- [Pac72] H. B. Pacejka. Analysis of the Dynamic Response of a Rolling String-Type Tire Model to Lateral Wheel Plane Vibrations. *Vehicle System Dynamics I*, 1972.
- [Par96] Bradford Parkinson. GPS Error Analysis. In Bradford W. Parkinson and James J. Spilker Jr, editors, *Global Positioning System: Theory and Applications*, volume 1, pages 469 – 483. AIAA, Washington D.C., 1996.
- [PE96] Bradford Parkinson and Per Enge. Differential GPS. In Bradford W. Parkinson and James J. Spilker Jr, editors, *Global Positioning System: Theory and Applications*, volume 2, pages 3 – 50. AIAA, Washington D.C., 1996.
- [PJ96] Bradford W. Parkinson and James J. Spilker Jr. *Global Positioning System: Theory and Applications*, volume 1 and 2. AIAA, Washington D.C., 1996.

- [RBBP99] A. Rekow, T. Bell, D. Bevly, and B. Parkinson. On-Line System Identification and Adaptive Steering of Farm Tractors Utilizing CDGPS. *AIAA Journal of Guidance Control and Navigation*, 11(2):671–674, September–October 1999.
- [Rei77] J.G. Reid. Structural Identifiability in Linear Time-Invariant Systems. *IEEE Transaction on Automatic Control*, 22(2):242 – 246, April 1977.
- [RJP98] A. Rekow, V.K. Jones, and B. Parkinson. LMS Identification of Systems with Dynamics and an Output Deadzone. In *1998 American Control Conference*, pages 2770 – 2774. American Automatic Control Council, 1998.
- [Rov87] D. Rovner. *Experiments in Adaptive Control of a Very Flexible One Link Manipulator*. PhD thesis, Stanford University, Stanford, California 94305, August 1987.
- [RS87] J. F. Reid and S. W. Searcy. Vision-Based Guidance of an Agricultural Tractor. *IEEE Control Systems Magazine*, 7:49–43, April 1987.
- [Ste94a] Robert F. Stengel. *Optimal Control and Estimation*, pages 392 – 407. Dover, New York, New York, 1994.
- [Ste94b] Robert F. Stengel. *Optimal Control and Estimation*, pages 343 – 351. Dover, New York, New York, 1994.
- [T<sup>+</sup>85] B. R. Tennes et al. Microcomputers Automate Tractor Steering. *Hydraulics and Pneumatics*, 38:52 – 55, March 1985.

- [TJL87] J.R. Treichler, C.R. Johnson Jr, and M.G. Larimore. *Theory and Design of Adaptive Filters*. John-Wiley, New York, New York, 1987.
- [Tom94] Masayoshi Tomizuka. Advanced Vehicle Control Systems (AVCS) Research for Automatic Highway Systems in California PATH. In *Proceedings of the 1994 Vehicle Navigation and Information Systems Conference*, pages plenary-41-45. IEEE, 1994.
- [TPS98] Claire Tomlin, George Pappas, and Shankar Sastry. Conflict Resolution for Air Traffic Management: A study in Multiagent Hybrid Systems. *IEEE Transactions on Automatic Control*, 43(4):509 –521, April 1998.
- [Var93] P. Varaiya. Smart Cars on Smart Roads: Problems of Control. *IEEE Transactions Automatic Control*, 38(2):195–207, 1993.
- [WB98] E. White and R. Buick. Comparing GPS Guidance with Foam Marker Guidance. In *Proceedings of the 4th International Conference on Precision Agriculture, Minneapolis, MN*. ASA/CSSA/SSSA, 1998.
- [Won93] J. Y. Wong. *Theory of Ground Vehicles*. Wiley, New York, New York, 1993.
- [WS85] B. Widrow and S. Stearns. *Adaptive Signal Processing*, pages 99 – 114. Prentice Hall, Upper Saddle River, New Jersey, 1985.
- [WW96] B. Widrow and E. Walach. *Adaptive Inverse Control*, pages 59 – 84. Prentice Hall, Upper Saddle River, New Jersey, 1996.
- [Zad65] Lofti Zadeh. Fuzzy Sets. *Information and Control*, 8:338–353, 1965.

- [ZC95] K. R. Zimmerman and R. H. Cannon. Experimental Demonstration of GPS for Rendezvous Between Two Prototype Space Vehicles. In *Proceedings of ION GPS-95*. Institute of Navigation, September 1995.